Characterization of the Group B *Streptococcus* Hemolysin and its Role in Intrauterine Infection

Christopher-Mychael Whidbey

A dissertation
submitted in partial fulfillment of the
requirements for the degree of

Doctor of Philosophy

University of Washington
2015

Reading Committee:
Lakshmi Rajagopal, Chair
Ferric C. Fang
David R. Sherman

Program Authorized to Offer Degree:
Pathobiology

University of Washington

Abstract

Characterization of the Group B *Streptococcus* Hemolysin and its Role in Intrauterine Infection

Christopher-Mychael Whidbey

Chair of the Supervisory Committee:

Lakshmi Rajagopal, Ph.D.

Pathobiology Program, Department of Global Health

Intrauterine infection and inflammation are a major cause of perinatal morbidity, including preterm birth. A pathogen associated with intrauterine infection, preterm birth, and perinatal disease is *Streptococcus agalactiae*, or Group B *streptococcus* (GBS). Despite its importance to public health, little is known about the immune response during intrauterine GBS infection and the role of specific GBS virulence factors in this process. One major GBS virulence factor is the β-hemolysin which allows GBS to lyse host cells; however, the hemolysin had never been purified and its molecular nature was undefined. Additionally, the mechanism of hemolysin-mediated cytotoxicity, the host cellular immune response to the hemolysin, and the role of the hemolysin during intrauterine infection were unknown. Gaining insight into the molecular nature of the β-hemolysin and the role it plays in GBS pathogenesis is important to develop new

therapeutic strategies for GBS associated disease. This dissertation describes our efforts to purify and characterize the GBS hemolysin, understand the mechanisms of pigment-mediated host cell lysis, and establish the role of this toxin during intrauterine infection that lead to fetal injury.

The molecule responsible for GBS hemolytic activity had not been identified at the onset of this project. Using genetic and biochemical approaches, we demonstrated that the GBS hemolysin is not a protein toxin, but rather an ornithine rhamnolipid pigment produced by the bacterial *cyl* operon. The GBS pigment is toxic to both red blood cells and amniotic epithelial cells. Overproduction of this pigment allows GBS to traverse human placental membranes. Hyperpigmented GBS strains were identified among clinical isolates from women in preterm birth, supporting the hypothesis that the pigment is important during intrauterine infection.

With purification of this major virulence factor, we were able to investigate how the GBS pigment causes membrane disruption and identify the immune pathways it activates. We found that the GBS pigment induces membrane perturbations in lipid membranes, which leads to ion flux. In red blood cells, this ion flux results in colloidal-osmotic lysis. In macrophages, membrane disruption triggers activation of the NLRP3 inflammasome, leading to activation of caspase 1. Caspase 1 activation by both whole cell GBS and the purified pigment is NLRP3 dependent, and results in secretion of IL-1β and the programmed, proinflammatory cell death known as pyroptosis.

We developed a murine model of intrauterine infection to test the role of the GBS pigment *in vivo.* Infection with hyperpigmented/hyperhemolytic bacteria resulted in intrauterine fetal injury and preterm birth. Intrauterine fetal death in NLRP3 deficient mice was decreased compared to wild-type mice, demonstrating a role for pigment-mediated activation of NLRP3 during

intrauterine infection. Interestingly, even in NLRP3-deficient mice, hyperpigmented GBS caused more fetal death that nonpigmented GBS. These results suggest that both NLRP3 dependent and NLRP3-independent pathways contribute to pathogenesis during intrauterine infection. Together, these data demonstrate that the GBS hemolysin, an ornithine rhamnolipid toxin, plays a key role during intrauterine infection.

Table of Contents

List of Figures

List of Tables

Acknowledgements

No achievement is made alone. I've been blessed to have mentors, friends, and family to help me through the graduate school marathon. To all of my teachers and mentors, thank you for getting me to this point. Thanks to all the past and present members of the Rajagopal lab for teaching me, helping me, working alongside me, and being there for me. To my graduate advisor, Dr. Lakshmi Rajagopal, thank you for being willing to teach and guide me, and to let me try things my own way (even though I was typically wrong in the end).

To my friends and family, I can't express how grateful I am for all you've done along the way. Your love and support mean the world to me. And to Michelle, thank you for being such a wonderful partner. I could not have done this without you.

Chapter 1 – Introduction

Infection associated preterm birth

Improving maternal and child health is a major component of efforts to improve public health worldwide. An important goal is reducing the global incidence of preterm birth. Preterm birth is birth before 37 weeks gestation (compared to 39-40 weeks for term pregnancy), and is the leading cause of neonatal mortality and the second leading cause of mortality in children under 5 years of age (1, 2). An estimated 15 million preterm births occur annually (approximately 11% of all live births) with the greatest incidence in North America and Africa (2, 3). Due to the high incidence and the age group affected, preterm birth poses a substantial economic burden. The cost of preterm birth is estimated at $26 billion in the United States alone, with the global cost likely much higher (4). In order to prevent preterm birth-associated morbidities, a better understanding of the underlying physiology is needed.

Preterm birth is a condition with many possible causes. Some known causes include decidual hemorrhage and vascular damage, disruption of maternal-fetal tolerance, and infection associated inflammation (2, 5, 6). Thus, treatment and prevention of infection could be potential interventions for preterm birth. Infection is a common cause of preterm birth; with an estimated one in four preterm infants born to a mother with bacterial infection of the amniotic fluid (5, 7). These bacteria reach the amniotic fluid from the vaginal tract through a process called ascending infection (5). Ascending infection occurs when resident vaginal bacteria breach the cervical barrier and enter the uterus. In the uterus, bacteria can induce inflammation and/or transverse the placental membranes to enter the amniotic cavity. This leads to infection of the amniotic fluid and fetal tissues. All of these events can contribute to preterm birth. Thus, therapies to prevent

and treat intrauterine infection could help reduce the incidence of preterm birth. In order to develop these therapies, a better understanding of the bacterial and host factors involved in infection-associated preterm birth is crucial.

Group B *streptococcus* and associated disease

One pathogen that causes perinatal disease is *Streptococcus agalactiae* or Group B *streptococcus* (GBS) (5, 6). GBS are Gram-positive bacteria that reside as commensals in the lower gastrointestinal and vaginal tracts but can cause severe disease in neonates. Neonatal infection due to GBS was first described in the 1970s after an increase in incidence, and is categorized based on the age at onset of symptoms (8, 9). Early-onset disease (EOD) due to GBS occurs in infants within the first week of life and is caused by infection acquired either *in utero* via ascending infection or during delivery via aspiration of contaminated vaginal fluids. In contrast, late-onset disease (LOD) is seen in infants between 7 and 90 days of life. While the exact mechanism by which infants with LOD acquire GBS is not established, acquisition from both maternal and nonmaternal sources, such as nosocomial acquisition, has been reported (8, 10, 11). EOD typically manifests as pneumonia or sepsis while LOD often manifests as bacteremia and in severe cases, meningitis (12). Meningitis due to GBS infection is particularly dangerous with a 5-10% mortality rate and approximately 50% of surviving infants having neurological sequelae (13, 14).

Epidemiological data describing neonatal GBS infection are available. A meta-analysis conducted by Edmond *et al.* in 2012 estimated the global incidence of neonatal GBS infection to be approximately 53 cases/100,000 live births (15). This rate varied geographically, with the highest incidence in Africa (127 cases/100,000 live births) and the lowest in the Western Pacific

(15 cases/100,000 live births), although the reason for this difference is unknown. The overall mortality rate reported for neonatal GBS infection was approximately 10%. However, these estimates are limited by the scarcity of data from low- and middle-income countries. The lack of monitoring makes it difficult to estimate the true disease burden and to design effective public health interventions in these areas (16). There are numerous identified risk factors for neonatal GBS infection, although few are robust enough to be clinically useful as indicators (17). Heavy GBS colonization of the lower genital tract is the primary risk factor for EOD. An estimated 10-30% of adult women test positive for GBS colonization by recto-vaginal culture, varying by geographical region and race/ethnicity (15). Other risk factors include African descent, history of previous neonatal GBS infection, chorioamnionitis, and prolonged, premature rupture of membranes. The primary risk factor for LOD is extreme prematurity (18).

In addition to neonatal infection, GBS can also cause intrauterine infection (see Figure 1-1). Intrauterine GBS infection can result in maternal bacteremia, chorioamnionitis (inflammation of the placental membranes), endometritis, or puerperal sepsis. Intrauterine infection can also lead to infection of the fetus *in utero* and is associated with preterm birth, spontaneous abortion, and stillbirth (19, 20). While data describing the incidence of intrauterine GBS infection are not available, a 2008 study found that GBS were present in approximately 20% of cases of midgestation abortion and were highly associated with chorioamnionitis (20).

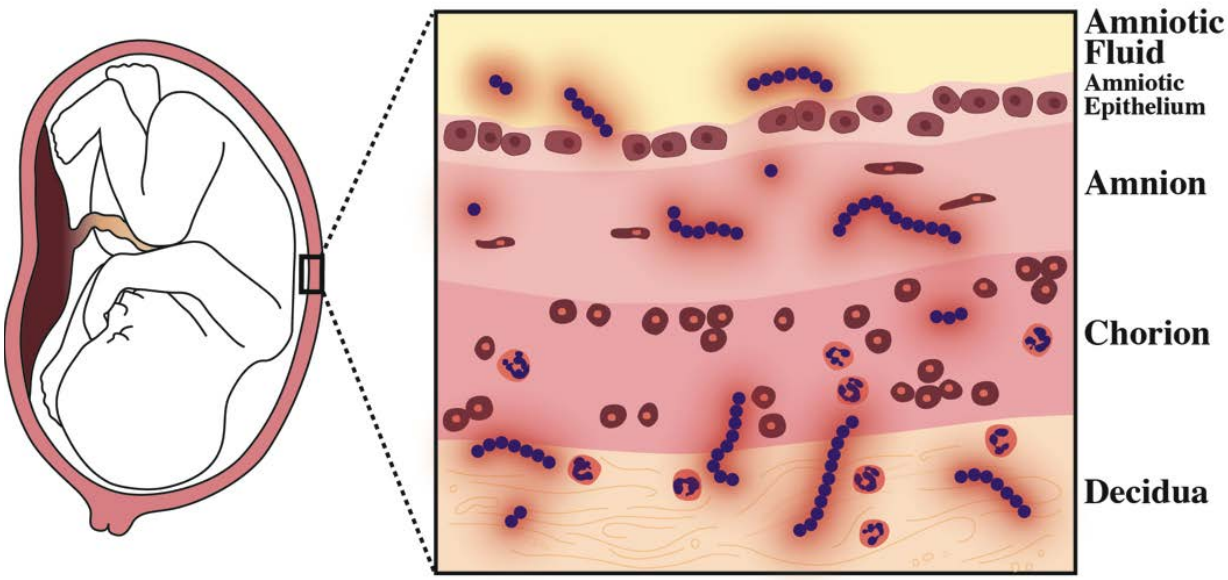

Figure 1-1. Intrauterine infection with Group B streptococci.

During pregnancy, GBS can ascend from the vaginal tract into the uterus to cause intrauterine infection. Intrauterine GBS infection can cause inflammation of the placental membranes (chorioamnionitis). GBS can also transverse the placental membranes (from maternal to fetal: decidua, chorion, amnion, and amniotic epithelium) resulting in infection of the amniotic fluid and fetus. Intrauterine GBS infection is associated with fetal injury, preterm birth, and still birth (19, 20).

Therapeutic strategy for GBS infection

Currently there is no available vaccine to prevent GBS infection, although one candidate vaccine has advanced to Phase III trials. This vaccine candidate targets the polysaccharide capsule of GBS. Ten serotypes of GBS have been described (Ia, Ib, II-IX), and the vaccine candidate is designed to generate immunity to serotypes Ia, Ib, and III. These serotypes are commonly associated with human infections, accounting for 79% of cases (21). However, recent reports of capsular serotype switching generate concern for the long-term efficacy of an anti-capsular vaccine (15, 22). As such, current strategies for prevention and treatment of GBS infection rely on antibiotics.

The current GBS disease prevention standard in the United States, Canada, and many European Union countries is intrapartum antibiotic prophylaxis (IAP) (23). Pregnant women who meet specific criteria are given antibiotics, typically penicillin, during labor and delivery. These criteria include women who are GBS-positive by rectovaginal culture at 35-37 weeks gestation, have GBS bacteriuria during the third trimester of pregnancy, have previously given birth to a child with GBS infection, are presenting with symptoms of infection, or are in preterm-labor. IAP is effective in reducing the incidence of EOD, resulting in an almost 70% decrease (17, 24). However, there are several drawbacks to IAP. First, the widespread use of antibiotics raises concerns for the development of antibiotic-resistant GBS strains. While most clinical isolates of GBS are sensitive to β-lactams, there have been several recent reports of GBS strains with elevated β-lactam resistance (25, 26). Additionally, there have also been reports of strains resistant to the second-line of antibiotics that include clindamycin and erythromycin which are given to women with penicillin allergies (27, 28). Secondly, IAP has only been effective in preventing EOD. Because antibiotics are given during labor and delivery, IAP cannot prevent against LOD due to infection acquired after birth or intrauterine infection acquired prior to onset of labor. Indeed, levels of LOD have remained steady despite the implementation of IAP (29). Finally, women in low- and middle-income nations where labor and delivery typically occur in the home are less likely to have access to facilities capable of determining risk of GBS infection and administering antibiotics during labor and delivery. These limitations of IAP create a major need for new approaches to prevent GBS infection.

GBS hemolytic activity and virulence *in vitro*

To develop new strategies for prevention or treatment of GBS infections, a better understanding of GBS virulence factors is necessary. GBS virulence is associated with bacterial hemolytic/cytolytic activity. Hemolytic strains of GBS are significantly more pathogenic than nonhemolytic GBS strains in models of sepsis, meningitis, and pneumonia (30-34). Hemolytic GBS are cytotoxic to immortalized cell lines such as A549 lung epithelial cells and human brain microvascular endothelial cells, murine macrophages, and human primary neutrophils (34-37). Hemolytic and hyperhemolytic GBS strains were also shown to disrupt epithelial and endothelial barriers such as the blood-brain barrier, leading to bacterial dissemination and disease progression (34, 38).

The GBS hemolysin is also important for activation of the immune system in response to GBS. Hemolytic GBS strains induce significantly higher levels of the proinflammatory cytokines IL-1β, IL-6, IL-8, and TNFα than nonhemolytic strains both *in vitro* and *in vivo* (34, 38, 39). Importantly, these cytokines are associated with the onset of preterm birth (40-44). Thus, preterm birth may be caused by inflammation resulting from GBS hemolysin activity during intrauterine infection. In order to identify inflammatory pathways activated by the hemolysin, purified toxin is necessary. At the onset of this project however, the GBS hemolysin had never been successfully purified. This was a major limitation for studies of GBS pathogenesis (45).

The GBS hemolysin – biochemical studies

Despite many studies demonstrating that GBS hemolytic activity was critical for bacterial virulence, the molecule responsible for this hemolytic activity had never been successfully purified or characterized. Originally, the GBS hemolysin was assumed to be a protein toxin

similar to other exotoxins such as *S. aureus* α-hemolysin (46). Many attempts to purify the GBS hemolysin were unsuccessful as hemolytic activity was lost during purification procedures (46-48). It was shown that hemolytic activity could be extracted from GBS using a high molecular-weight carrier compound such as bovine serum albumin, Tween-20, or starch (47-49). While these studies showed that the GBS hemolysin was a cell surface-associated molecule, removal of the carrier molecule resulted in a loss of hemolytic activity. This made it impossible to track activity through subsequent purification steps and identify the molecule responsible for GBS hemolytic activity.

The GBS hemolysin – genetic studies and the *cyl* operon

Genetic studies were also performed to identify the gene that encodes the GBS hemolysin. Using transposon mutagenesis, Spellerberg *et al.* first identified a twelve-gene operon involved in hemolytic activity, and named it the *cyl* operon (50, 51). The *cyl* operon is conserved in all GBS strains sequenced to date. Disruption of some of the *cyl* genes resulted in non-hemolytic strains, while disruption of others only reduced hemolytic activity (45, 50-52). Interestingly, many of the *cyl* genes were predicted to be homologous to components of fatty acid biosynthesis machinery, while others had no obvious homolog at the nucleotide level (putative functions for the *cyl* genes are assigned and described in Chapter 2 of this work). These transposon studies led to the hypothesis that the *cyl* operon was the genetic basis of GBS hemolytic activity.

Subsequent study of the *cyl* genes demonstrated that the gene *cylE* was necessary for hemolysis in GBS. Pritzlaff *et al.* observed that deletion of *cylE* abolished GBS hemolytic activity (51). Intriguingly, this work also showed that expression of *cylE* in *E. coli* was sufficient to confer hemolytic activity, and it was concluded that *cylE* encoded the GBS hemolysin (51).

However, several observations argued against this conclusion. First, the purified CylE protein from transformed *E. coli* was nonhemolytic, though the authors suggested that this resulted from rapid degradation (51). Second, bioinformatic analysis of the CylE protein did not indicate the presence of a canonical secretion signal or transmembrane domain, making it difficult to understand how the CylE protein could be transported to the GBS cell surface (53). Finally, the presence of the *cylE* gene in an operon and the importance of other *cyl* genes for hemolytic activity suggested that CylE might play a role in hemolysis while not actually being the hemolysin itself ((45, 50, 52, 54), see Chapter 2 for details).

GBS hemolytic activity and pigmentation

Hemolytic activity of GBS has long been associated with production of an orange pigment (36, 47, 55). Production of this pigment can be used to detect the presence of GBS in complex clinical samples using selective and differential media such as Granada media or Carrot Broth (56, 57). Pigmented GBS strains are hemolytic, while nonpigmented strains are nonhemolytic (36, 54). Pigment and hemolysin are also connected at the genetic level. Shortly after the *cyl* operon was characterized for its role in hemolysis, it was shown that disruption of the *cyl* operon abolished both hemolysis and pigment biosynthesis (54). In 2006, Rosa-Fraile *et al*. purified and characterized the structure of the GBS pigment (58). The authors showed that the pigment is an ornithine rhamnolipid containing 12 conjugated double bonds with an ornithine headgroup at the acyl carbon and a rhamnose connected to the carbon adjacent to the ω-carbon (Figure 1-2).

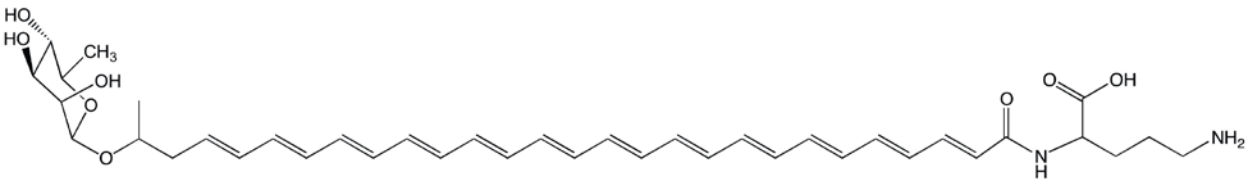

Figure 1-2. Structure of the GBS pigment.

The GBS pigment is an ornithine rhamnolipid (58). It consists of an ornithine headgroup that is acylated at the α-amine with a C28 lipid. This lipid backbone contains 12 conjugated *trans*-double bonds, and is rhamnosylated at the second to last carbon.

The GBS pigment has some similarity to bacterial lipids that possess cytotoxic activity. Specifically, an ornithine lipid produced by *Bordetella pertussis* and a rhamnolipid produced by *Pseudomonas aeruginosa* were shown to lyse red blood cells (59, 60). Antifungal polyenes (lipids containing multiple double bonds) such as amphotericin B can also cause lysis of human cells (61). Because the pigment contains similar moieties to the above lipids and the correlation between pigment and hemolysin, Rosa Fraile *et al.* examined if the GBS pigment was hemolytic (58). They indicated that when they spotted purified pigment on blood agar, no hemolysis was observed, and concluded that the GBS pigment was not the hemolysin (58).

Regulation of the *cyl* operon

Genetic studies also identified regulatory genes that impacted hemolysin production by controlling transcription of the *cyl* operon (62). The best-characterized regulator of the *cyl* operon is a two-component system encoded by *covRS*, also known as *csrRS*. This two-component system controls transcription of approximately 130 genes, many of which are involved in virulence (63). The CovRS system consists of two separate proteins – a transmembrane sensor histidine kinase, CovS, and a DNA-binding response regulator, CovR.

The exact signal sensed by CovS is unknown, although low pH and/or cations such as magnesium have been suggested as potential signals (64-66). Upon activation, the intracellular domain of CovS phosphorylates the response regulator CovR on the aspartic acid located at position 53 (67). Aspartate-phosphorylated CovR then binds to the promoter region of the *cyl* operon, repressing transcription (63, 67). Thus, strains mutated to lack *covR* or *covS* do not repress *cyl* transcription, are hyperhemolytic, and were found to be hypervirulent in a meningitis model (34). CovRS tightly regulates GBS virulence genes, and dysregulation of this system leads to altered virulence (34, 63, 68).

The CovRS system was originally identified as a homolog to a two-component system in Group A streptococcus (GAS) or *Streptococcus pyogenes* (63). The CovRS system in GAS also controls virulence, and like GBS, GAS strains with nonfunctional *covRS* loci are hypervirulent (69, 70). Importantly, previous work identified clinical isolates of GAS that had spontaneous mutations in the *covRS* locus (71, 72). Thus, we hypothesized that GBS strains with *covRS* mutations would be hyperhemolytic and hypervirulent and may cause intrauterine infection. This finding would support the connection between GBS, its hemolysin, and perinatal disease.

Dissertation Summary

At the onset of this project, a major limitation in the understanding of GBS biology was the lack of information about the nature of the GBS hemolysin and its role in intrauterine infection. The goal of this dissertation was to address this limitation in two major aims. The first aim was to identify and characterize the molecule responsible for hemolytic activity of GBS. The second aim was to utilize the purified hemolysin to understand how it causes host cell inflammation and

cytotoxicity and to determine its role in intrauterine GBS infection, fetal injury, and preterm birth.

The results obtained from the first aim are described in Chapter 2. This chapter details my findings that the CylE protein is insufficient for GBS hemolysis, and that the GBS pigment itself is hemolytic/cytolytic. The role of the pigment in penetration of human placental membranes and the identification of hyperhemolytic GBS strains isolated from amniotic fluid and placental membranes of women with preterm labor are also presented in this chapter. The results presented in Chapter 3 address the second aim of this dissertation and demonstrate the mechanism of pigment-induced cytotoxicity, identify immune pathways activated by the GBS hemolysin, and establish the role of the hemolysin in fetal injury and preterm birth. The final chapter provides a summary of my findings, overarching conclusions, and future directions for research concerning the unique toxin produced by GBS and perinatal GBS disease.

Chapter 2 – The β-hemolysin of Group B *streptococcus* is an ornithine rhamnolipid pigment

The following text is from the article: Christopher Whidbey[1], Maria Isabel Harrell[1], Kellie Burnside, Lisa Ngo, Alexis Becraft, Lakshminarayan Iyer, L. Aravind, Jane Hitti, Kristina Adams Waldorf, and Lakshmi Rajagopal. (2013) A hemolytic pigment of Group B Streptococcus allows bacterial penetration of human placenta. **Journal of Experimental Medicine**, 210, 1265-1281. Figure numbers have been updated to conform to the formatting of the dissertation, however the rest of the text remains essentially as published with minor editorial changes.

[1]Equal Contribution

Abstract

Microbial infection of the amniotic fluid is a significant cause of fetal injury, preterm birth and newborn infections**.** Group B streptococcus (GBS) is an important human bacterial pathogen associated with preterm birth, fetal injury and neonatal mortality. Although GBS has been isolated from amniotic fluid of women in preterm labor, mechanisms of *in utero* infection remain unknown. Previous studies indicated that GBS are unable to invade human amniotic epithelial cells, which represent the last barrier to the amniotic cavity and fetus. Here, we show that GBS invades human amniotic epithelial cells and strains lacking the hemolysin repressor CovR/S accelerate amniotic barrier failure and penetrate chorioamniotic membranes in a hemolysin-dependent manner. Clinical GBS isolates obtained from women in preterm labor are hyper-hemolytic and some are associated with *covR/S* mutations. We demonstrate for the first time that hemolytic and cytolytic activity of GBS is due to the ornithine rhamnolipid pigment and not due

to a pore-forming protein toxin. Our studies emphasize the importance of the hemolytic GBS pigment in ascending infection and fetal injury.

Introduction

Preterm birth is a major factor contributing to neonatal disease and accounts for 75% of perinatal mortality worldwide (73). Currently, there is no effective therapy for prevention of human preterm births or stillbirths. Intra-amniotic infection and inflammation are important causes of preterm birth, stillbirth, fetal injury and early onset neonatal sepsis (4, 29, 73-75). Early onset sepsis in human newborns manifests within the first few hours of life, is fulminant and is due to organisms acquired *in utero* with the amniotic fluid and neonatal blood infected with organisms commonly colonizing the lower genital tract such as Group B Streptococcus (GBS) (76-81).

GBS are β-hemolytic, gram-positive bacteria that are a frequent cause of human newborn infections. Morbidities due to GBS infections include delayed development, vision and hearing loss, chronic lung disease, mental retardation and cerebral palsy (82). Despite the success of intrapartum antibiotic prophylaxis to prevent GBS transmission to the neonate during labor and delivery, *in utero* infections that occur earlier in pregnancy leading to stillbirth and preterm birth are not targeted by this approach, and the burden of early onset sepsis in newborn infants remains substantial (77, 83). Additional preventive therapies are urgently needed before the widespread use of antibiotics in pregnant women creates sufficient resistance such that our current antibiotics become ineffective.

A key factor limiting preventive strategies is insufficient knowledge of virulence mechanisms that promote infection of the amniotic cavity. The human placenta is a critical multicellular organ that protects the growing fetus from organisms colonizing the lower genital tract. As the placenta is the most species-specific mammalian organ (84, 85), no animal placenta

recapitulates the exact mechanistic and physical barriers of the human placenta. The widely accepted route of pathogen entry into the human amniotic fluid requires bacterial ascension through the cervix and breach of several placental layers including the decidua, chorion, amnion and amniotic epithelium (73, 86). Although invasion of the amniotic epithelium is critical for pathogen entry into the amniotic cavity, previous studies have indicated that GBS do not invade human amniotic epithelial cells (hAEC), which constitute the amniotic epithelium (87). Consequently, mechanisms and virulence factors that mediate ascending GBS infection from the lower genital tract into the amniotic cavity and fetus are not understood.

Results

Hemolysin promotes GBS invasion of human amniotic epithelial cells

As GBS has been isolated from amniotic fluid of women with intact chorioamniotic membranes (73, 87-89), we investigated mechanisms that promote GBS invasion and breach of amniotic epithelium and chorioamnion. We hypothesized that intra-amniotic GBS infections in patients with intact placental or chorioamniotic membranes (73, 87-89) may be due to elevated virulence factor expression. The two component regulatory system CovR/S was described to repress the expression of many GBS virulence genes including genes of the *cyl* operon containing *cylE* important for the pluripotent toxin known as β-hemolysin/cytolysin (hereafter referred to as hemolysin) (63, 64, 90). To test if increased expression of virulence factors promotes GBS invasion of amniotic epithelium, we compared the ability of WT GBS and the hyper-hemolytic Δ*covR* to adhere to and invade hAEC. To evaluate the role of hemolysin, nonhemolytic GBS lacking the *cylE* gene associated with hemolysin production (51) were

included (Δ*cylE*, Δ*covR*Δ*cylE*). The hemolytic activity of WT, hyper-hemolytic Δ*covR* and non-hemolytic Δ*cylE* strains is shown in Fig. 1A. Primary hAEC were isolated and cultured from normal, term placentas obtained immediately after cesarean delivery from women without labor and adherence and invasion of GBS to hAEC was determined as described (34, 87). Consistent with previous reports (87), we observed that WT GBS adhere to hAEC (Fig. 1B). The presence or absence of CovR or CylE had no significant effect on GBS adherence to hAEC (Fig. 1B, $P > 0.2$). However, in contrast to previous observations (87), we observed that WT GBS invade hAEC (~4% invasion, Fig. 1C). The Δ*cylE* mutant showed significantly decreased invasion when compared to WT (~0.3% invasion, $p=0.008$, Fig. 1C). Consistent with our hypothesis, we observed that the hyper-hemolytic GBSΔ*covR* was significantly more invasive to hAEC when compared to the WT (~80% invasion, $p<0.0001$, Fig.1C). Notably, the increase in hAEC invasion observed with GBSΔ*covR* was abolished in the absence of the gene *cylE* linked to hemolysin expression (see Δ*covR*Δ*cylE* in Fig. 1C). Taken together, these results indicate that hemolysin promotes GBS invasion of human amniotic epithelial cells. Of note, the levels of GBS invasion observed with hAEC and differences between hypoinvasive and hyperinvasive strains are consistent with levels of GBS invasion reported in other cell types, including human brain microvascular endothelial cells and lung epithelial cells (91-93).

Hemolysin induces activation of proinflammatory mediators in human amniotic epithelium

We examined if increased hemolysin in Δ*covR* activates an inflammatory response in human amniotic epithelium. To evaluate changes in expression of inflammatory genes in GBS infected hAEC, qRT-PCR was performed on RNA isolated at 4 hours post-infection using methods

described (34). These results indicate that infection with Δ*covR* caused a significant increase in transcription of cytokines such as IL-6, IL-8, IL-1β, CXCL1 and CCL20 in hAEC compared to cells infected with the isogenic WT (COH1) or uninfected controls (Fig. 2A, *$P=0.03$, **$P=0.007$). Interestingly, the increase in inflammatory gene expression observed with GBSΔ*covR* was abolished in hAEC infected with Δ*covR*Δ*cylE* (Fig. 2A). Luminex bead assays confirmed that secretion of IL-6, IL-8 and IL-1β was higher in Δ*covR* infected hAEC compared to WT GBS or a Δ*covR*Δ*cylE* mutant (Fig. 2B, $P \leq 0.005$).

Hyper-hemolytic GBSΔ*covR* infection increases NF-κB recruitment into the nucleus of hAEC

Microbial toxins have been implicated in activating inflammatory signaling pathways via the nuclear transcription factor NF-κB, which is recruited from the cytoplasm to the nucleus during activation (94). Therefore, we examined whether the increase in pro-inflammatory gene expression observed in hAEC infected with the hyper-hemolytic GBSΔ*covR* was associated with nuclear localization/recruitment of the transcription factor NF-κB. To test this hypothesis, total nuclear and cytoplasmic proteins isolated from infected and uninfected hAEC were resolved on 10% SDS-PAGE and western blots were performed using antibody to NF-κB p65. The results shown in Fig. 2C indicate that infection with a Δ*covR* mutant results in an approximate 2.5-fold increase in recruitment of NF-κB into the nucleus of infected hAEC when compared to WT GBS or uninfected controls. These data confirm that the increase in inflammatory gene expression

observed in Δ*covR* mutant-infected hAEC is associated with increased nuclear recruitment of NF-κB.

Hemolysin promotes GBS breach of the human amniotic epithelial barrier

We next examined if hemolysin accelerates failure of the human amniotic epithelial barrier. Changes in transepithelial electrical resistance were monitored across hAEC monolayers in real-time using electric cell–substrate impedance sensing (ECIS, (95)). Briefly, hAEC monolayers established on gold-plated electrodes in 8-well array slides were infected with GBS WT, isogenic Δ*covR*, Δ*covR*Δ*cylE* or Δ*cylE* mutantsat $1x10^5$ colony forming units (CFU)/well as described (34). Uninfected wells were included as controls. Fig. 2D shows that the decrease in barrier resistance observed in hAEC infected with WT GBS was not observed in hAEC infected with the hemolysin-deficient Δ*cylE* strain. Furthermore, we observed that infection with a Δ*covR* mutant accelerated the decrease in barrier resistance compared to WT (Fig. 2D). Notably, the rapid decrease in barrier resistance due to Δ*covR* was abolished when a Δ*covR*Δ*cylE* mutant was employed (Fig. 2D). These results suggest that increased hemolysin expression enables GBS to breach the barrier function of the amniotic epithelium. We further observed that prolonged exposure of GBS Δ*covR* to hAEC (> 4h) induced cytotoxic effects in contrast to hAEC exposed to GBS WT and Δ*cylE* strains. Collectively, these observations indicated that hemolysin is an important virulence factor that promotes bacterial invasion and immune activation of the amniotic epithelium, leading to secretion of cytokines such as IL-6, IL-8, and IL-1β that have associated with preterm labor and neonatal morbidity (40, 96-99).

Hyper-hemolytic GBS penetrate human placenta/chorioamnion and can be associated with women in preterm labor

Ascending *in utero* infection of GBS from the lower genital tract into the amniotic cavity requires the pathogen to penetrate the chorioamniotic membranes. Thus, we tested the ability of GBS to penetrate intact membranes that were mounted and maintained on a modified transwell system as described (100). Forty-eight hours post-stabilization, intact chorioamniotic membranes *(n=6)* were infected with 10^7 CFU of GBS (WT, Δ*covR*, Δ*covR*Δ*cylE*) on the choriodecidual side of the placenta. Uninfected chorioamnion was included as a control. In parallel, we also examined the ability of GBS to penetrate either chorion or amnion alone, using the transwell model system (for details, see Methods). At 24-hrs post infection, aliquots of media from the lower chamber were analyzed for bacterial CFU. As shown in Fig. 3A, we observed that all GBS strains efficiently penetrated either the amnion or the chorion as $\geq 10^8$ CFU were recovered from the lower chamber of membranes infected with WT or Δ*covR* and Δ*covR*Δ*cylE* derivatives. In contrast, no bacterial CFU were recovered from chorioamnion infected with WT or a Δ*covR*Δ*cylE* mutant (Fig. 3A). Notably, $\geq 10^2$ bacterial CFU were recovered from four of six chorioamniotic membranes infected with GBS Δ*covR* (Fig. 3A, $P = 0.02$). Transverse histological sections of the infected chorioamnion were prepared and stained for bacteria as described (101). Interestingly, bacterial invasion of the chorioamnion including penetration of the amniotic epithelium was observed in chorioamniotic membranes infected with hyper-hemolytic GBS Δ*covR* even when bacteria were not recovered in the lower chamber (Fig. 3B). In contrast, bacteria were primarily seen in the choriodecidual region in chorioamniotic membranes

infected with WT and very few bacteria were observed in membranes infected with a Δ*covR*Δ*cylE* mutant (Fig. 3B). Increased secretion of IL-6 was also observed in media obtained from the lower chamber of chorioamniotic membranes infected with GBS Δ*covR* (Fig. 3C, $P = 0.02$). We were unable to extend the experiments longer than 24 hrs post-GBS infection, as the placental membranes began to destabilize at >75hrs post-cesarean section. Collectively, these data show that while chorioamniotic membranes serve as an effective barrier to prevent GBS trafficking, increased production of hemolysin can facilitate bacterial penetration of chorioamniotic membranes and the amniotic cavity.

We examined if increased hemolytic activity could be observed in GBS isolated from women in preterm labor. To this end, clinical isolates obtained from human amniotic fluid and chorioamnion were examined for their hemolytic properties and potential mutations in the *covR/S* locus. We obtained eight GBS strains that were isolated from six women enrolled in a cohort of women in preterm labor with intact membranes for whom information on outcomes and microbiological cultures of the amniotic fluid, chorioamnion, and cord blood were available ((102), see Table 1). Most of these GBS isolates exhibited increased hemolytic activity and increased transcription of genes in the *cyl* operon such as *cylE* (Figs. 4 A, B). DNA sequencing indicated the presence of mutations in the *covR/S* loci in six isolates obtained from four women (Table 1). GBS isolated from both the amniotic fluid and chorioamnion of one patient in preterm labor had a stop codon mutation in the kinase domain of CovS (CovS220Stop, Table 1). GBS isolated from amniotic fluid and cord blood of another patient in preterm labor had a valine-to-methionine substitution in CovS at position 343; the same mutation was also observed in a GBS isolate obtained from the amniotic fluid of a third patient (Table 1). GBS from amniotic fluid of

another woman in preterm labor had a deletion in the promoter of *covR/S* (Table 1). Of note, two GBS isolates recovered from women in preterm labor had no mutations in the *covR/S* loci. This suggests that increased hemolytic activity and transcription of *cyl* genes (Fig. 4A, B) may be mediated by additional regulators of GBS hemolysin.

To determine if the identified CovR/S mutations affect hemolytic activity of GBS, we generated site directed mutants. As shown in Fig. 4C, GBSΔ*covR* and Δ*covS* strains exhibit increased hemolytic activity when compared to WT, and complementation with plasmids that constitutively express either CovR or CovS restores repression of hemolytic activity to WT levels or greater. However, complementation of Δ*covS* with a plasmid encoding CovS220Stop failed to restore repression of hemolytic activity, and partial complementation was observed with CovSV343M (compare Δ*covS*/pCovS to Δ*covS*/CovS220stop and Δ*covS*/CovSV343M in Fig. 4C). Further studies are necessary to understand the role of this substitution in CovS signaling. Similarly, the presence of the promoter deletion in *covR/S* on the chromosome of WT GBS alleviated CovR repression of hemolysin (Fig. 4C) and is consistent with our previous observations that CovR can positively regulate its own expression (34). These results suggest that the increased hemolytic activity observed in the clinical isolates with CovR/S mutations can, at least in part, be attributed to these mutations. However, as GBS has an open pan-genome (103), the effect of other strain specific regulators cannot be ruled out. We further confirmed that similar to a Δ*covR* mutant, GBS Δ*covS* showed increased invasion and accelerated barrier disruption of hAEC (Figs. 4D-E). Complementation of Δ*covR* or Δ*covS* decreased amniotic epithelial invasion at levels similar to WT (Fig. 4D) as did the complemented Δ*cylE* strain (data not shown). Although we were unable to complement the Δ*covR*Δ*cylE* double mutant due to

instability of the complementing plasmid, introduction of a plasmid encoding CylE to GBS Δ*covR*Δ*cylE* restored hemolytic activity, amniotic epithelial invasion and barrier disruption to levels that were intermediate between WT and Δ*covR* (Figs. 4C-E).

CylE expression is necessary but not sufficient for GBS hemolysis

Our results above add to the large body of literature demonstrating the essential nature of hemolysin to various facets of GBS pathogenesis including pneumonia, sepsis, meningitis (30, 34, 36) and now bacterial penetration of human placenta/chorioamnion. Despite the importance of hemolysin to GBS virulence, its biochemical and molecular nature has remained elusive. Extraction of the GBS hemolysin requires high molecular weight stabilizers such as starch, Tween or BSA (47, 48). Previous studies proposed that the 78kDa protein encoded by the *cylE* gene located in the *cyl* operon (Fig. 5A) is the GBS hemolysin, as deletion of the *cylE* gene abolished hemolytic activity and expression of *cylE* increased hemolysis in *E. coli* (51). However, Pritzaff *et al*. also reported that they could not detect the CylE protein in secreted/extracellular fractions of *E. coli* expressing CylE, nor were able to extract hemolytic activity from bacterial cells using starch, BSA or Tween (51). These observations suggest that increased hemolytic activity in *E. coli* may not be due to the GBS hemolysin. It is also noteworthy that CylE has 43 rare codons that are not efficiently translated in *E. coli* (*i.e*. 24 Arg (AGG, AGA, CGA), 5 Leu (CTA) 11 Ile (ATA) and 3 Pro (CCC)). BLAST searches have revealed no significant homology of CylE to known pore-forming toxins, and the protein does not possess any canonical secretion signal (51, 53). Moreover, SDS-PAGE analysis of cell-free extracts of GBS with hemolytic activity did not reveal the presence of any protein (data not

shown). To further determine whether that *cylE* alone is necessary and sufficient for GBS hemolysis, we constructed a GBS strain that lacked all genes of the *cyl* operon (Δ*cylX-K*, see Fig. 5A for operon). This strain is nonhemolytic and interestingly, complementation with plasmids that constitutively express either CylE or CylABE ((which includes the ABC transporter system CylA/B, (52)) failed to restore hemolytic activity (Fig. 5B). In contrast, these plasmids restored hemolytic activity to a GBS strain lacking only *cylE* (Fig. 5B) but were unable to induce hemolysis in *E. coli* (Fig. 5C). Consistent with these observations, complementation of GBSΔ*covR*Δ*cylE* with pCylE restored hemolytic activity to levels greater than WT (Fig. 4C) due to derepression of the other *cyl* operon genes in the absence of CovR (34, 63, 104). Collectively, these observations indicate that CylE and its putative transporter CylA/B are necessary but not sufficient for GBS hemolytic activity.

The functional basis of GBS hemolytic activity is the ornithine rhamnolipid pigment

Although the hemolytic phenotype of GBS correlates with pigmentation, with non-hemolytic strains being non-pigmented and hemolytic strains a pigmented (51, 54, 105), also see Fig. 5D), this link is not mechanistically understood. The pigment was recently described to be an ornithine rhamnolipid known as granadaene (58). Like hemolytic activity, pigment biosynthesis in GBS requires the 12 gene *cyl* operon ((51, 54). Fig. 5A), and several genes in this operon (*cylD*, *cylG*, *cylI*, *cylK*, *cylZ*, and *acpC*) encode enzymes catalyzing different steps in fatty acid biosynthesis (Fig. 6A). The *cyl* operon also encodes a glycosyltransferase (CylJ), an aminomethyltransferase (CylF), a lipoate carrier (CylX) and an ABC transporter (CylA/B). Sequence profile analysis of CylE revealed an *N*-terminal domain of the acyltransferase

superfamily known to catalyze several amidoligase reactions (Fig. S1). Using these predicted homologies a pathway for GBS pigment biosynthesis that requires most genes of the *cyl* operon is proposed (Fig. 6B).

Based on the tight link between hemolysin and pigment production, the failure of *cylE* or *cylABE* to restore hemolytic activity to GBSΔ*cylX-K*, the absence of protein in hemolytic extracts and observations that disruption of several other *cyl* genes such as *cylD*, *acpC*, *cylZ*, *cylA/B and cylK* abolish hemolytic activity (45, 50-52), we hypothesized that hemolytic activity of GBS may be due to the ornithine rhamnolipid pigment and rather than the CylE protein. To test this hypothesis, we extracted pigment from WT GBS using DMSO containing 0.1% TFA as described (58). Subsequently, the pigment was purified by gel filtration column chromatography designed for selective purification of small molecules (< 5kDa) using a Sephadex LH-20 column and DMSO:0.1% TFA as the mobile phase (58). Although soluble in DMSO:0.1% TFA, the pigment was non-hemolytic in this solvent, as observed previously (58). Because traditional isolation of GBS hemolytic extracts requires a large carrier molecule such as starch (48, 106), we reasoned that addition of starch to the purified pigment may be required for functional activity. Thus, we dissolved purified pigment in DMSO containing 0.1%TFA and 20% starch (DTS). As a control, the pigment extraction procedure was performed on the non-hemolytic and non-pigmented Δ*cylE* strain. We then examined hemolytic activity of purified pigment using two methods that involved lysis of red blood cells. First, two-fold dilutions of pigment were used to examine lysis of human red blood cells using the hemolytic titer assay described previously (105). The results shown in Fig. 7A indicate that the purified pigment possesses hemolytic activity and the effective concentration 50 (EC_{50}; concentration at which 50% of erythrocytes are

lysed) correspond to a pigment concentration of 0.11μM. The control samples that included buffer alone and extracts from the non-hemolytic Δ*cylE* strain were not pigmented and did not possess hemolytic activity (Fig. 7A). Second, varying concentrations of purified pigment were spotted on sheep blood agar (SBA) plates and the results shown in Fig. 7B indicate that lysis of red blood cells is observed in the presence of pigment but not in Δ*cylE* extract or buffer controls. Scanning electron micrographs of human red blood cells revealed that a brief (8 min) exposure to GBS pigment induces dramatic alterations in membrane morphology from the usual disc shape of erythrocytes (see buffer and Δ*cylE* control) to that of echinocytes and spheroechinocytes (Fig. 7C).

The hemolytic activity of the ornithine rhamnolipid is not sensitive to proteinase K

To determine if the hemolytic activity observed with purified pigment could be attributed to a protein toxin, we performed proteinase K digestion of the purified pigment prior to hemolytic assays. For proteinase K digestion, GBS pigment and control Δ*cylE* extract previously dissolved in DTS was lyophilized, resuspended in proteinase K buffer and digested in the presence or absence of proteinase K (see Methods for details). Subsequently hemolytic titer assays were performed on all samples including controls. The results shown in Fig. 7D indicate that pigment treated with proteinase K had similar hemolytic properties compared to pigment not treated with proteinase K ($P \geq 0.9$). We further performed Fourier Transform Ion Cyclotron Resonance Tandem Mass Spectrometry (FTICR-MS/MS) and nuclear magnetic resonance (NMR) on the purified pigment and control Δ*cylE* extract (Figs. S2, S3). A comparison of the MS spectra revealed that peaks at 677.38 *m/z* and a methylated derivative at 691.46 *m/z*, characteristic of the

GBS pigment are uniquely present in purified pigment and not in control Δ*cylE* extract (Fig. S2). ^{1}H NMR and Correlation Spectroscopy (COSY) confirmed the structure of the pigment and its presence in the pigment from WT (Figs. S3 A, B) and not in the Δ*cylE* control (Fig. S3C). Also, SDS-PAGE analysis of purified pigment followed by Ruby staining did not reveal the presence of any protein and LC-MS/MS analysis of tryptic digests of purified pigment only identified peptides corresponding to trypsin and common contaminants in these analyses i.e. keratin (data not shown). Collectively, these results indicate that the hemolytic molecule purified from GBS is not a protein, but rather the ornithine rhamnolipid previously described as granadaene (58, 107).

The GBS pigment is cytotoxic to human amniotic epithelial cells

To determine if the purified pigment has cytotoxic properties attributed to the previously elusive GBS hemolysin, varying concentrations of purified pigment or buffer and Δ*cylE* controls were added to hAEC followed by trypan blue straining. These results indicate that the purified pigment possesses cytolytic properties as evidenced by increased trypan blue staining indicative of dead cells in the presence of pigment but not following treatment with buffer or Δ*cylE* extract controls (Fig. 8A, B, P <0.005). ELISA assays for cytokines indicated that the purified pigment is unable to induce an inflammatory response in hAEC (data not shown). These results are not unexpected since GBS hemolysin/pigment is normallyassociated with the bacterial cell surface and is not secreted. These observations suggest that while the purified pigment may induce pore formation similar to other rhamnolipids (60, 93) and polyenes (61), exposure of host cells to bacterial cell surface-associated hemolysin is required for induction of the inflammatory response.

Discussion

This work provides novel evidence that elevated expression of a virulence factor promotes GBS penetration of the amniotic cavity, a critical step in the pathway to preterm birth and fetal injury. Currently, there is no effective vaccine to prevent maternal-to-infant transmission of GBS. Knowledge of virulence factors associated with preterm birth and neonatal infections will allow for a more informed approach towards strategies for prevention of GBS infections. We have demonstrated that hemolysin promotes GBS invasion of placental cells and that hyper-hemolytic strains are more proficient in disruption of the amniotic barrier and penetration of placental membranes. We predict that environmental changes in the lower genital tract (e.g. neutral pH (65)) may be sensed by sensor kinases such as CovS to alleviate CovR repression, thus triggering an increase in hemolysin expression that mediates ascending GBS infection. Alternatively, mutations in hemolysin regulators such as *covR/S* that potentially arise while GBS is in a commensal niche (e.g. during vaginal colonization) may promote penetration of chorioamnion and invasion of the amniotic cavity. Consistent with this hypothesis, hyper-hemolytic GBS with *covR/S* mutations were isolated from the amniotic fluid, chorioamnion and cord blood of women who delivered preterm. However, GBS strains that had no mutations in the *covR/S* loci were also recovered from women in preterm labor. While repression of hemolysin by the CovR/S two component system has been demonstrated in a number of GBS strains (*e.g.* A909, COH1, NEM316, 515, 2603v/r, NCTC10/84 (63-65, 67, 90, 104, 108)), and *covR/S* and *cyl* genes are conserved among all sequenced GBS strains (103, 109), it is likely that additional strain-specific regulators also influence the expression of this important virulence factor. Regulators such as the sensor kinase Stk1 (67, 90) and an Abi-domain protein Abx1 (108)

influence the expression of *cyl* genes through their interaction with CovR and CovS respectively. As strains lacking Stk1 or Abx1 exhibit decreased hemolytic activity (67, 90, 108), increased hemolytic activity observed in the clinical isolates cannot be attributed to the loss of Stk1 or Abx1 and DNA sequence analysis also did not indicate the presence of mutations in these genes (data not shown). The complexity of hemolysin regulation is emerging and is likely to play a role in GBS infections associated with preterm premature rupture of membranes (PPROM), preterm delivery (PTD) and neonatal sepsis.

For the first time, we have described the biochemical nature of the GBS hemolysin and elucidated the connection between hemolysis and pigmentation. We have shown that CylE is necessary but not sufficient for GBS hemolysis and that the ornithine rhamnolipid pigment is hemolytic and cytotoxic. Although a previous study suggested that the GBS hemolysin is likely to be a protein as hemolytic activity diminished due to protease treatment (46), three proteins including a glycoprotein co-purified with the hemolysin in these prior studies. Given the promiscuity of stabilizers used by the GBS hemolysin (starch, Tween and BSA, (47, 48)), we spectulate that protease digestion of the proteins that co-purified with the GBS pigment/hemolysin may have destabilized the pigment, leading to the erroneous conclusion that the GBS hemolysin is a protein.

Our finding that an ornithine rhamnolipid is the hemolysin has important implications for GBS disease pathogenesis. As the GBS hemolysin/pigment is a surface-associated toxin, we predict that the cytotoxic effects are primarily extracellular but that the toxin also mediates host cell lysis when bacteria are internalized into host cells. These cytotoxic properties contribute to barrier failure, thus promoting bacterial dissemination within the host. Hemolytic GBS also

induce a strong immune response (Figs. 2A-B, 3C), which plays an important role in its pathogenesis. However, specific host immune pathways that respond to this virulence factor remain undefined (34, 92, 105, 110, 111). With the identification, purification and biochemical characterization of the GBS hemolysin as the ornithine rhamnolipid pigment, key mechanisms of host immune activation can now be addressed. Such studies will provide critical insight necessary for preventive strategies against GBS infections. Although vaccines that target surface proteins were shown to provide protection against GBS in mouse models of infection (112), protein based vaccines cannot neutralize the effect of this lipid-toxin. Previous attempts to raise anti-sera to crude extracts of the GBS hemolysin were unsuccessful (113), consistent with the notion that lipids typically do not elicit an antibody response. However, therapeutic measures designed to inhibit biosynthesis of the ornithine rhamnolipid pigment or its function may prove effective.

Although ornithine-containing lipids are widely known in bacteria (114) and a few have hemolytic or hemeagglutinating properties(60, 93, 115), their role in the virulence of bacterial pathogens is not fully appreciated. Orthologs of the *cyl* operon are present in other bacterial species including opportunistic human and insect pathogens such *Bacillus cereus, Bacillus thuringiensis*, *Paenibacillus larvae* and actinobacteria such as *Actinomyces viscosus*, *Kitasatospora setae*, *Arthrobacter* species and *Propionibacterium* species (Fig. 9). In these organisms the core *cyl* operon containing genes for fatty acid and ornithine biosynthesis and their amidoligation are strongly conserved. Also, *P. jensenii* was described to produce a pigment similar to the GBS granadaene (107). Given their ubiquitous nature, our findings have significant implication in the classification of bacteria that encode pigments with hemolytic and cytolytic

properties. In summary, our work shows that GBS virulence and its transition from commensal to invasive niches hinges on its ability to regulate the expression of a key virulence factor which we describe as a hemolytic ornithine lipid.

Materials and Methods

Human Subjects

Written informed patient consent for donation of normal, term placentas immediately after cesarean delivery from women without labor was obtained with approval from the University of Washington Institutional Review Board (protocol # 34004). GBS clinical isolates from amniotic fluid, chorioamnion and/or cord blood were obtained from women enrolled with preterm labor and intact membranes at less than or equal to 34 weeks gestation at the University of Washington Medical Center, Swedish Medical Center and Virginia Mason Medical Center, Seattle, Washington between June 25, 1991 to June 30, 1997. This cohort was previously described (102). The University of Washington Institutional Review Board approved the study protocol #25739 and all participants provided written informed consent. Written informed patient consent for donation of human blood was obtained with approval from the Seattle Children's Research Institute Institutional Review Board (protocol #11117).

Bacterial Isolates

The WT GBS strains used in this study, COH1 and A909, are clinical isolates obtained from infected human newborns. (116, 117). COH1 belongs the hypervirulent MLST-ST17 clone of GBS serotype III associated with severe neonatal infections (118). The Δ*cylE*, Δ*covR*, and Δ*covR*Δ*cylE* mutants were derived from COH1 and A909 using methods described (34, 90). The Δ*covS* mutant was derived using methods described (64). Routine cultures of GBS were grown

in Tryptic Soy Broth (TSB, Difco Laboratories) at 37^0C in 5% CO_2, and routine cultures of *E. coli* were performed in Luria-Bertani Broth (LB, Difco Laboratories) at 37°C. Cell growth was monitored at 600 nm. Antibiotics were added at the following concentrations when necessary: For GBS, erythromycin 1 μg/ml; spectinomycin 300 μg/ml; kanamycin 1000 μg/ml; chloramphenicol 2.5-5μg/ml; For *E. coli*, erythromycin 300 μg/ml; spectinomycin 50 μg/ml; kanamycin 50 μg/ml; chloramphenicol 10μg/ml. Antibiotics and other chemicals were purchased for Sigma-Aldrich, unless otherwise specified. Cell culture medium was purchased from Mediatech Inc. All GBS mutants used in this study had similar growth rates compared to isogenic WT in the medium used for cell culture and *ex vivo* experiments (DMEM containing 1% FCS). Restriction enzymes were purchased from Fermentas, and primers were purchased from Sigma-Aldrich. RNA isolation and qRT-PCR for analysis of GBS gene expression was performed as described previously (34). GBS pictures shown on Red Blood Agar and Granada Media were captured using a Canon EOS Rebel XSi 12.2MP Digital SLR camera with a 18-55mm Zoom Lens, processed using Abobe Photoshop CS2, version 9, and compiled using Deneba Canvas 9 version 9.0.4.

Construction of GBS Δ*cylX-K* and complementing plasmids

Approximately 1 kb of DNA located upstream of *cylX* and 1kb of DNA located downstream of *cylK* were amplified using high fidelity PCR (Invitrogen, USA) and primer pairs dCylopupF and dCylopupR or dCylop dnF and dCylopdnR, respectively. The gene conferring kanamycin (Ω *km-2*) resistance was also amplified using high fidelity PCR from pCIV2 (119) for allelic replacement of *cylX-K*, using primers dCylkanF and dCylkanR. Subsequently, strand overlap extension PCR (120) was performed to introduce the antibiotic resistance gene (Ω *km-2*) between

the flanking regions of *cylX-K* described above. The PCR fragment was then ligated into the temperature-sensitive vector pHY304 (121), and the resulting plasmid was electroporated into GBS WT as described previously (122). Selection and screening for the double crossover mutant was performed as described (122). PCR was used to verify the presence of Ω *km-2* and the absence of *cylX-K*. The genes encoding *cylE, cylABE, covR* and *covS* were amplified using high fidelity PCR using primer pairs CylEF & CylER ; CylABEF & CylABER; CovRF & CovRR; or CovSF & CovSR, respectively. The PCR fragments were digested with restriction enzymes present on the primer sequence/s and then cloned into the multiple cloning site of the GBS complementation vector pDC123 downstream of the constitutive promoter as described previously (122, 123). The complementing plasmids were then electroporated into GBS Δ*cylE*, Δ*cylX-K,* Δ*covS* and Δ*covR* strainsusing methods described (122). Site directed mutants were generated using the Qiagen QuikChange site-directed mutagenesis kit with the complementing pCovS plasmid as the template and primers CovS200F & CovS200R for pCovS220Stop and primers CovSV343MF & CovSV343MR for pCovSV343M. GBS with chromosomal mutations in *covRS* loci was obtained using methods described previously (67). DNA sequencing was performed to confirm the presence of the desired mutations.

Derivation of human amniotic epithelium

Primary hAEC were isolated and cultured from normal, term placentas obtained immediately after cesarean delivery from women without labor as described (124). Briefly, the amnion was peeled from the chorion, and the amnion tissue was washed with PBS and digested with trypsin (Worthington Biochemical Corp.) and DNAse (Sigma) as described (124). Subsequently, the trypsin digestion medium was centrifuged and cell pellets were resuspended in DMEM and

loaded onto pre-prepared discontinuous Percoll (GE Healthcare) gradients (5, 20, 40, and 60%, respectively) before the gradients were centrifuged as described (124). A single band of cells around 20% Percoll concentration was collected, diluted in medium to a density of 10^6 cells/ml and cultured as described (124).

Infection Assays

Three to four independent placentas were used, and all experiments were performed in triplicate. Adherence and invasion of GBS WT COH1 or A909 and isogenic Δ*cylE*, Δ*covR*, Δ*covS* and Δ*covR*Δ*cylE* mutants to hAEC were performed as described (31, 87). Briefly, GBS strains grown to mid-log phase (~10^8 CFU/ml; OD_{600} = 0.3) were washed in PBS, resuspended in DMEM with 10% FBS, and used to infect hAEC monolayers at a multiplicity of infection of 1. For adherence assays, infection was carried out for a period of 2 hrs after which the bacteria were enumerated using methods described (31, 87). For invasion assays, gentamicin (100μg/ml) and penicillin (5μg/ml) was added to each well at 2hrs post infection and the plates were incubated for an additional 2hrs to kill extracellular and surface-adherent bacteria. Subsequently, intracellular bacteria were released using trypsin-EDTA (Gibco) and Triton X-100 and bacteria serially diluted and enumerated as described (31, 87).

Expression of inflammatory mediators

Three independent placentas were used and all experiments were performed in triplicate. Human amniotic epithelial cells (hAEC) were cultured, washed and infected with GBS strains as described above. Subsequently, total RNA was isolated from hAEC monolayers using the RNeasy miniprep kit (Qiagen Inc., Valencia, California, USA) according to the manufacturer's

protocol and digested with DNase I to remove contaminating genomic DNA. Expression of inflammatory mediators in human amniotic epithelium was determined using qRT-PCR as described previously (34). Supernatants from GBS infected hAEC were collected, centrifuged to remove bacteria and Luminex bead assays (Millipore, USA) performed using methods described by the manufacturer to evaluate cytokine levels.

Western blots

Human amniotic epithelial cells were grown to confluence and infected with GBS at a multiplicity of infection of 1 for a period of 4 hrs. Uninfected cells were included as controls. Subsequently, hAEC were washed, digested with trypsin and centrifuged. The NE-PER kit (ThermoScientific/Pierce) was used for stepwise separation and preparation of cytoplasmic and nuclear extracts from infected hAEC as per manufacturer's instructions. Equal amounts (10 μg) of cytoplasmic and nuclear extracts were subjected to 7.5% SDS-PAGE followed by Western blotting. The membrane was blocked in 1:1 Odyssey blocking buffer (Li-Cor Biosciences) in PBS and then incubated at 4°C overnight with a 1:200 dilution of primary NF-κB p65 antibody (Santa Cruz Biotechnology). Secondary antibody Alexa 680 anti-mouse (Life Technologies) was added at a 1:1000 dilution. After several washes, the membrane was visualized with a Odyssey Li-Cor infrared imager (Li-Cor Biosciences, USA).

Barrier integrity analysis

Changes in transepithelial electrical resistance across hAEC monolayers were measured in real time using ECIS (95) with an ECIS ZTheta Instrument and 8W10E+ arrays (Applied BioPhysics, Troy, NY). hAEC monolayers were established on gold plated electrodes in 8 well array slides attached to a computer-operated sensing apparatus to allow measurements in real

time. Monolayers were then infected with the GBS strains at 1 x 10^5 CFU/well, and the system measured the cell membrane capacitance (Cm), resistance from the cell-electrode interaction (α), and barrier function properties of the cell monolayer (Rb). Deconvolution of the overall ECIS signal into these parameters is performed by ECIS software by fitting the mathematical model derived by (125) to the experimental data by least-square optimization procedures. Uninfected wells served as controls for background levels of electrical resistance. Data are represented as a change in resistance as a proportion of the control over time as described previously (34). A representative example of three independent experiments is shown.

***Ex vivo* placental model**

Intact chorioamniotic membranes obtained immediately after normal, cesarean delivery were rinsed in sterile saline and placed over an inverted, upper chamber of a Transwell System (Corning Inc.) from which the original polycarbonate membrane was previously removed as described (100). Sterile silicone rubber rings were used to hold the placental membranes in place. Thus, when the transwell is inserted, the choriodecidua faces the upper chamber and the amniotic epithelium faces the lower chamber, as described (100). Care was taken to during the entire procedure so that there were no tears or rips on the placental membranes mounted on the transwell. The explants were stabilized in medium for a period of 48hrs. Six independent placentas/chorioamniotic membranes were used in these assays. Uninfected placenta was also included as a control in each experiment. For infection of chorioamnion, GBS strains were grown to an $O.D_{600}$ of 0.3, washed twice in PBS, and approximately 10^7 CFU in a final volume of 1ml of DMEM was added to the upper chamber. At 24 hrs post infection, media (DMEM) from the lower chamber was removed and processed for bacterial enumeration and expression of

cytokines. For bacterial enumeration, aliquots of the media were serially diluted and plated on TSA plates. For analysis of inflammatory mediators, aliquots of media were analyzed using ELISA or the Luminex bead assay as described by the manufacturer (R&D Systems or Millipore). For microscopy, infected chorioamniotic membranes were fixed in 10% phosphate-buffered formalin at 4°C overnight and stored in 70% ethanol. The membranes were subsequently embedded in paraffin, sectioned and stained using the Gram-Twort stain as described (101). Images were captured in bright field using the Leica DM4000B Fluorescent upright microscope under 10X and 100X magnifications. The microscope was attached to a Leica DFC310FX camera, and the acquisition software used was the Leica application suite, version 4.0.0. A representative image from experiments with six independent placentas with similar results is shown. As controls for bacterial migration, transwells were also mounted with either chorion alone or amnion alone. Briefly, the amnion was peeled from the chorion, and individual membranes were mounted over the transwell such that their orientation was maintained, i.e. the inner chamber represented the choriodecidual side for chorionic transwells or amniotic mesoderm for amniotic transwells. Infection with GBS strains was performed as described above.

Purification and characterization of the ornithine rhamnolipid pigment

GBS pigment was purified as previously described (58) with some modifications. Briefly, WT GBS were grown at 37°C in New Granada Medium until the broth turned red (48-72 hrs). Bacterial cells were pelleted, washed 3 times with distilled water and twice with DMSO. The cell pellet was then resuspended in DMSO:0.1% TFA overnight to extract the pigment, cell debris was pelleted, and the supernatant containing the pigment was saved. The above process was

repeated until the supernatant obtained from GBS cells was clear. Pigment was then precipitated by addition of 25% NH_4OH to a final concentration of 0.25% as described (107). Precipitated pigment was washed three times with HPLC grade water and twice in DMSO, redissolved in DMSO:0.1%TFA and purified using a Sephadex LH-20 (GE Healthcare) column as described (58, 107). Fractions containing purified pigment were pooled and precipitated with NH_4OH (Scientific Products) as described above, washed three times with HPLC grade water, twice with DMSO and lyophilized. As a control, GBSΔ*cylE* was also grown in New Granada Medium and a pigment extraction protocol was followed as described above. For NMR analysis, purified pigment or control Δ*cylE* samples were resuspended in DMSO-d_6:0.1% *d*-TFA (Sigma). ^{1}H,^{13}C, ^{1}H-COSY NMR experiments were performed at 298K on a Bruker AV-500 NMR Spectrometer. Residual DMSO-d_5 was used to calibrate chemical shifts. For MS experiments, lyophilized pigment or control Δ*cylE* samples were dissolved in DMSO:0.1%TFA and analyzed by Fourier Transform Ion Cyclotron Resonance mass spectrometry on a Bruker AutoFlex APEX Qe 47e instrument. For hemolytic and cytotoxic assays, lyophilized pigment or control Δ*cylE* extract was dissolved in DTS to a final concentration of 1mM. The samples were incubated overnight at room temperature in the dark prior to use.

Hemolytic titer assays were performed using methods described with some modifications (105). Briefly, two fold-serial dilution of purified pigment or control Δ*cylE* extract in DTS was performed in PBS+0.2% glucose in a final volume of 100μl. These samples were then incubated with 100μl heparin-treated human red blood cells (hRBC, 1%) in 96-well plates at 37°C for 1 h, following which the plates were spun for 4 min at 3,000 x g to pellet unlysed hRBC. The supernatants were transferred to a replica-96 well plate, and hemoglobin release was measured

by recording absorbance at 420nm. Positive and negative controls included wells that contained hRBC with 0.1% SDS or PBS, respectively. Solvent control for each pigment concentration was included in the analysis. The effective concentration 50 is the concentration of pigment that produces 50% hemoglobin release compared with the SDS control and was determined using non-linear regression. The experiment was performed in triplicate using three independent preparations of purified pigment.

For proteinase K treatment of the pigment prior to hemolytic assays, pigment and control Δ*cylE* samples in DTS were lyophilized and dissolved in proteinase K buffer (20mM Tris, pH 8.0, 1mM $CaCl_2$). Each sample was divided into two parts and proteinase K added at a final concentration of 0.25mg/ml as described (107) to one of the aliquots before all samples were incubated at 37°C for 1 h. Hemolytic titer assays were then performed on pigment and control samples that were treated with or without proteinase K. Buffer controls were also included. The activity of proteinase K used in these experiments was confirmed by digesting BSA (100μg) with proteinase K (0.25mg/mL) at 37°C for 1 hr followed by 12% SDS-PAGE and SYPRO Ruby staining.

Scanning Electron Microscopy

Erythrocytes from 0.5ml of human blood was centrifuged, washed twice with PBS and resuspended in 5mL PBS. Erythrocytes were then treated with 12.5μM pigment or an equivalent amount of control material (DTS or Δ*cylE* extract) for 8 min at 37^{o}C. Subsequently, the samples were centrifuged at 4^{o}C and the supernatant discarded. The pellet was resuspended in 0.5mL of ½ Karnovsky's Fixative and incubated overnight at room temperature. Samples were then prepared for scanning electron microscopy as previously described (60). Images were captured

using a JEOL 5800 Scanning Electron Microscope equipped with a JEOL Orion Digital Acquisition System. The experiment was performed twice using independent pigment preparations.

Cytotoxicity Assays

Human amniotic epithelial cells (hAEC) cultured in 96-well plates ($1x10^5$ cells/well) for 24hrs were treated with known concentrations of pigment or equivalent amounts of control Δ*cylE* extract or DTS for a period of 4 hrs. Subsequently, the medium was removed, and hAEC were treated with 0.2% trypan blue for 2 min. Cells were washed with PBS and immediately observed and imaged under a Leica DMI6000B inverted microscope with images captured at 10X and 40X magnifications. The microscope was equipped with a Leica DFC310FX camera, and the acquisition software used was the Leica application suite, version 4.0.0. Data are reported as the average and standard deviation of five fields per well.

Statistical Analysis

An unpaired, two tailed Student's *t*-test, Mann-Whitney test, or Wilcoxon's matched pairs rank test was used to estimate differences as appropriate, and *P* value <0.05 was considered significant. A non-linear regression analysis was used to estimate EC_{50} concentration. These tests were performed using GraphPad Prism version 5.0 for Windows, GraphPad Software, USA, www.graphpad.com.

Online supplemental material

Table S1 lists primers used in this study. Fig. S1 shows the alignment of CylE to known N-acyltransferases. Fig. S2 shows the overlay of mass spectra of purified pigment and control

Δ*cylE* extracts. Figs. S3 A & B indicate ^{1}H chemical shifts and ^{1}H-^{1}H COSY NMR of the purified GBS pigment. NMR of control Δ*cylE* extract is shown in Fig. S3C.

Acknowledgements

This work was supported by funding from the National Institutes of Health, Grants R01AI100989 to L. R and K. A. W, R01AI070749 to L.R and K08AI067910 to K. A. W. This work was also supported by funding from the March of Dimes Grant 21-FY08-562 and 21-FY06-77 to K. A.W. Support for K.B was provided by the NIH training grant (5 T32 HD007233-29, PI: Lisa Frenkel). Support for C.W was provided by the NIH training grant (T32 AI07509, PI: Lee Ann Campbell). L. M. I and L. A. are supported by intramural funds from NLM, National Institutes of Health. The Cuyamaca Foundation also provided support for this work. We are grateful to the human subjects who participated in these studies. The study on women in preterm labor from where GBS clinical isolates were obtained was funded by R01AI31871. We thank Dr. Victor Nizet for the GBS Δ*cylE* strain, Dr. David Eschenbach for his input, Dr. Sophia Lannon and Evangelyn Nwakapora for assistance in placenta collection, Dr. Kang Sun for helping with derivation of hAEC, Kathy Agnew for isolation of GBS clinical isolates, Dr. Lisa Cox for help with microscopy, and Nyugen Thao-Binh Tran, Jessica Klein and Hannah Miller for technical assistance. The authors are grateful to Christian Renken (Applied Biophysics) for assistance with ECIS. We thank Dr. Paul Miller and Dale Whittington for assistance with NMR and MS analyses, respectively. We also thank Dr. Toni Kline for her expertise with interpretation of the NMR. Histology was performed using the Histology and Imaging Core at the University of Washington.

The authors have no conflicting financial interests.

Figures

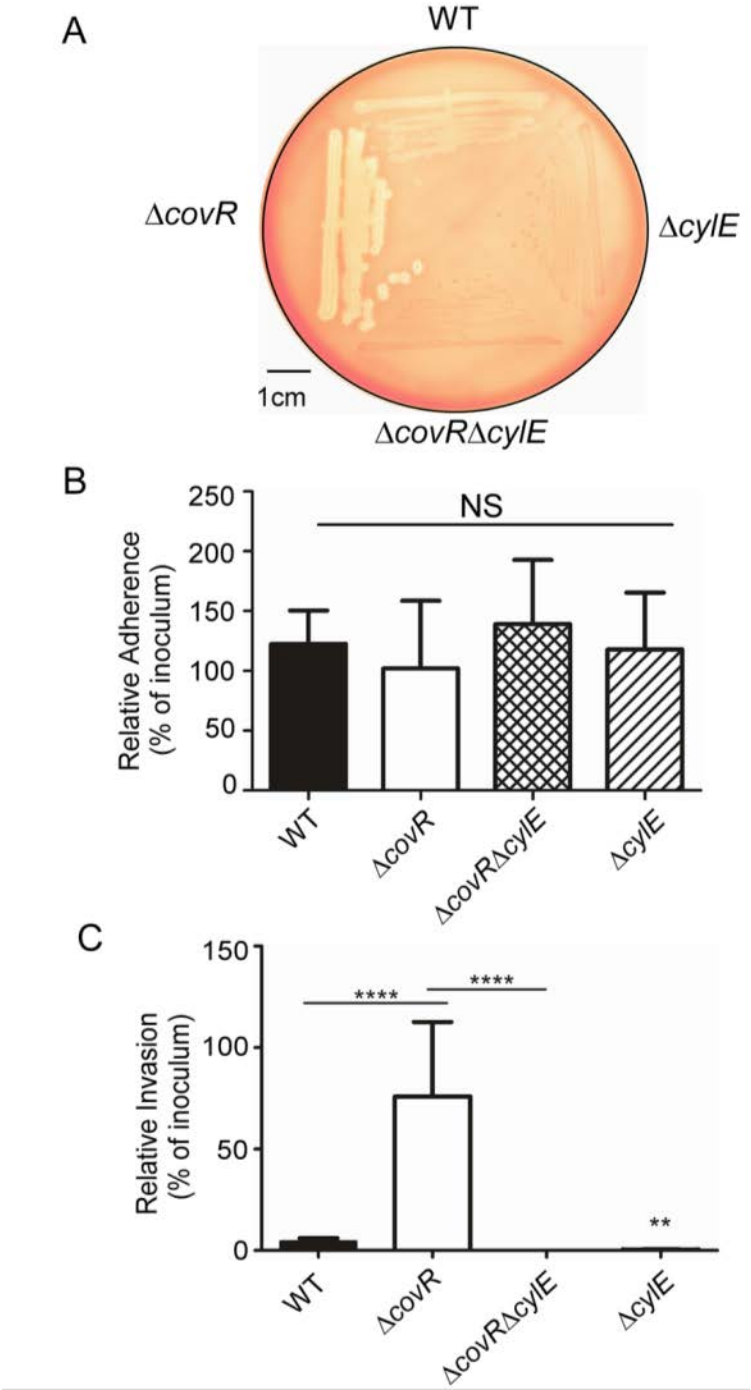

Figure 2-1. Hemolysin promotes GBS invasion of human amniotic epithelial cells.

(A) Hemolytic activity shown by the zone of clearing around the colonies on sheep blood agar of GBS WT, Δ*covR* and isogenic mutants. A representative image from one of three independent experimental replicates is shown.
(B-C) Primary hAEC were isolated from chorioamniotic membranes and adherence and invasion of GBS WT, isogenic Δ*covR*, Δ*covR*Δ*cylE*, Δ*cylE* mutants were compared. Percent adherence (b) and invasion (c) is normalized to that of the initial inoculum. Data shown are the average and standard deviation (SD) obtained from hAEC that were isolated from four independent placentas, each experiment was performed in triplicate (*P* >0.2 =NS, ****$P<0.0001$, **$P=0.008$, Student's *t* test, error bars ± SD).

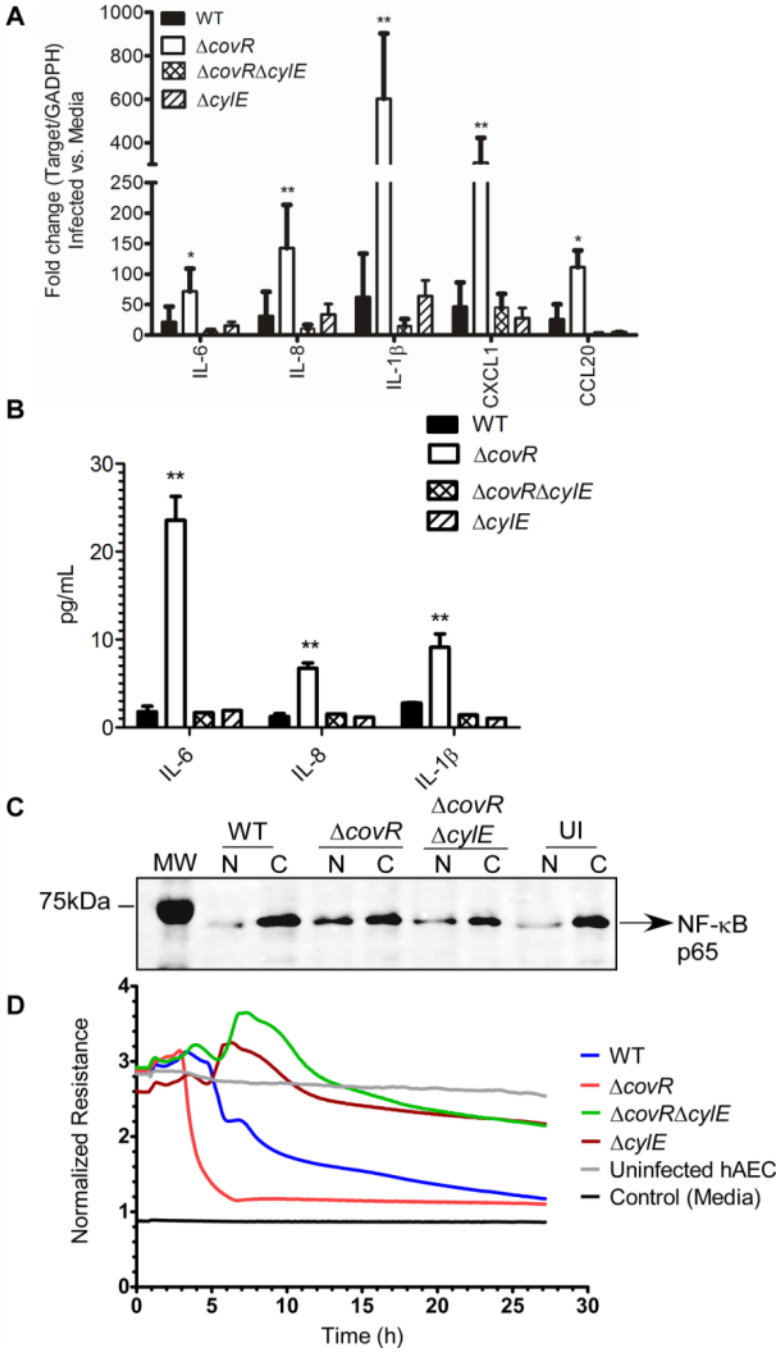

Figure 2-2. Hemolysin increases expression of inflammatory mediators and induces barrier disruption in amniotic epithelial cells.

(A) qRT-PCR was performed of indicated cytokines/chemokines on RNA isolated from hAEC infected with either WT GBS COH1 or isogenic Δ*covR*, Δ*covR*Δ*cylE* and Δ*cylE* mutants at 4 hours post-infection. Data shown are the average and SD obtained from hAEC that were isolated from three independent placentas, performed in triplicate (*n=3*, ***P* =0.007, * *P* =0.03, Student's *t* test, error bars ± SD). **(B)** Luminex bead assays were performed on supernatants of hAEC infected with WT GBS or isogenic Δ*covR*, Δ*covR*Δ*cylE* and Δ*cylE* mutants at 4 hours post-infection The experiment was performed using hAEC that were isolated from three independent placentas, performed in triplicate (*n=3*, ***P* <0.005, Student's *t* test, error bars ± SD). **(C)** Western blots were performed on nuclear (N) and cytoplasmic (C) proteins from GBS infected hAEC using antibody to NF-κB. Uninfected (UI) hAEC were included as controls. MW = molecular weight marker. A representative image from one of three independent experimental replicates is shown. **(D)** Barrier resistance of hAEC was monitored in real time using ECIS. A representative image from one of three independent experimental replicates is shown.

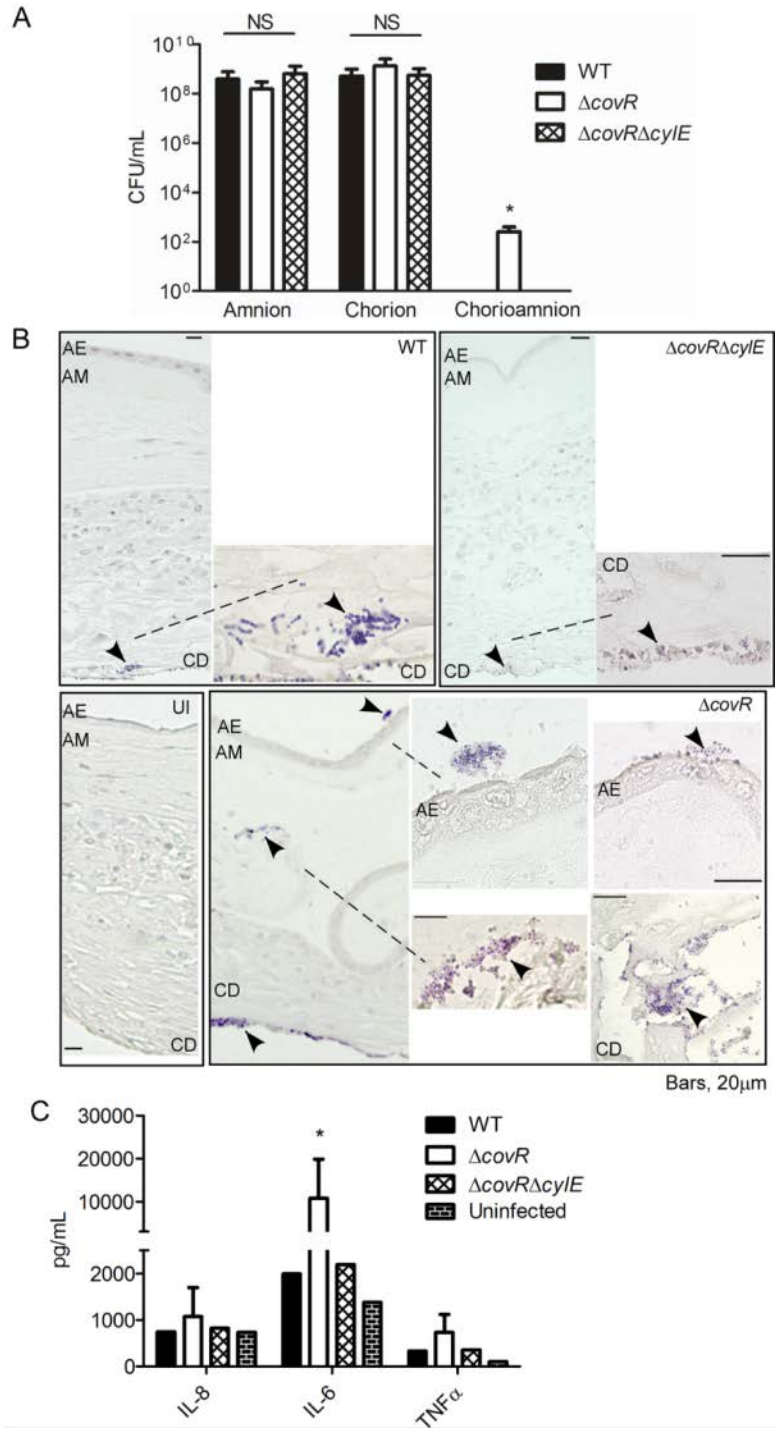

Figure 2-3. Hyper-hemolytic GBS penetrate human chorioamnion.

Intact chorioamniotic membranes as well as either chorion alone or amnion alone *(n=6)* were mounted on a transwell system and infected with either WT GBS COH1 or isogenic Δ*covR* and Δ*covR*Δ*cylE* strains for a period of 24 hrs. Aliquots of the media from the lower chamber were analyzed for CFU and cytokines expression (see A-C below). **(A)** GBS penetration of the chorion, amnion or chorioamniotic membranes (*n=6*, $P > 0.3$ =NS, $*P = 0.02$, Mann Whitney test, error bars ± SD). **(B)** Infected chorioamniotic membranes *(n=6)* were fixed, embedded, sectioned and stained using Gram-Tworts stain. A representative placenta where bacteria were not recovered from the lower chamber for any GBS strain is shown. AE =amniotic epithelium; AM= amniotic mesoderm; CD= choriodecidua, UI = uninfected chorioamnion. Arrows represent gram positive bacteria, dashed line shows region under higher magnification. **(C)** ELISA assays on media obtained from the lower chamber of chorioamniotic membranes infected with GBS WT, Δ*covR* and Δ*covR*Δ*cylE* (*n=6*, $*P = 0.02$, Mann-Whitney test, error bars ± SD).

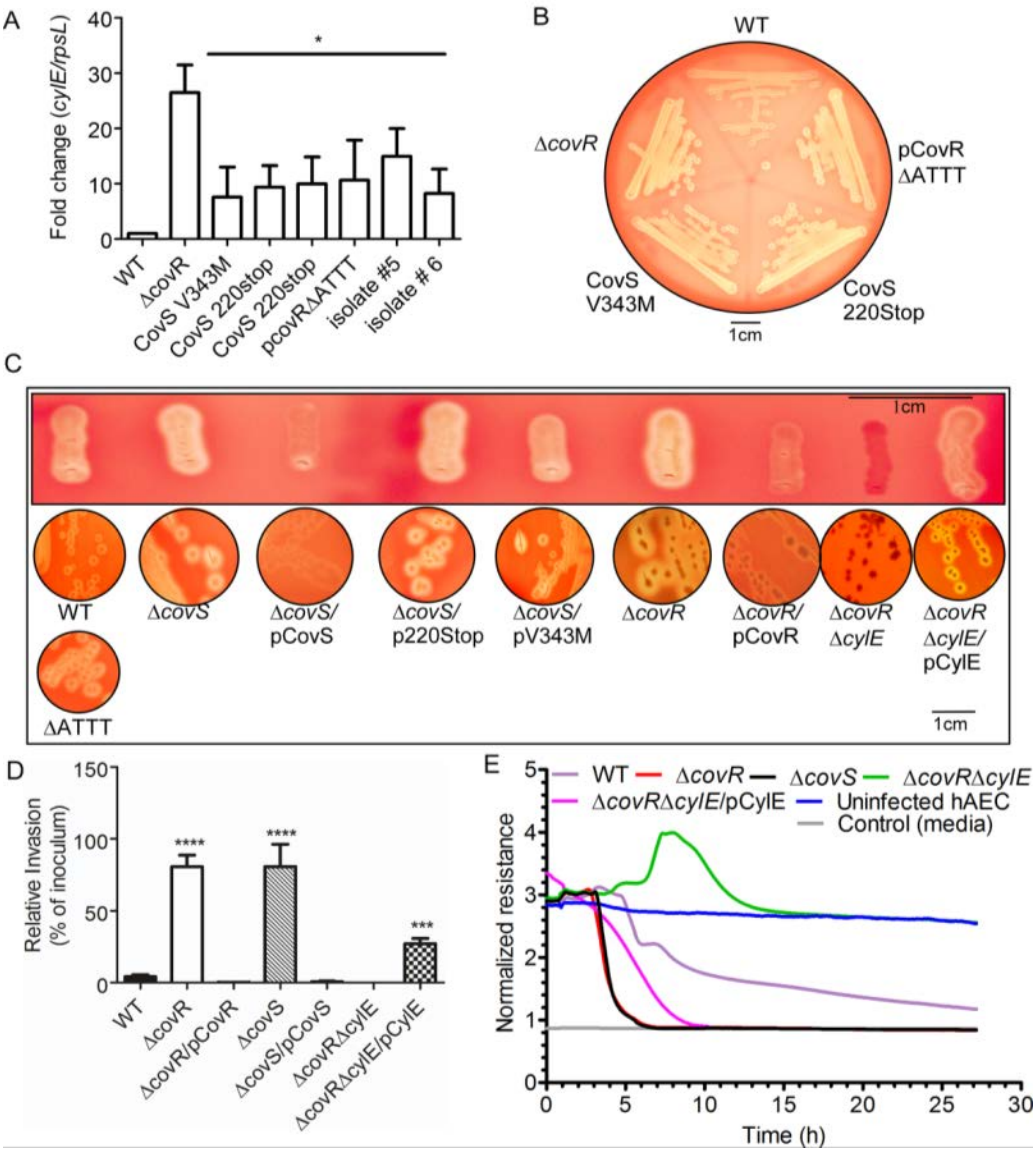

Figure 2-4. GBS clinical isolates from women in preterm labor exhibit increased hemolysis and some are associated with *covR/S* mutations.

(A) qRT-PCR on RNA isolated from log phase GBS ($O.D_{600nm}$ =0.3). Data are normalized to relative expression of the house-keeping gene *rpsL* and are the average and SD from five independent biological replicates performed in triplicate (*n=5*, **P* = 0.03, Wilcoxon matched-pairs rank test). **(B)** Hemolytic activity of GBS clinical isolates associated with preterm labor. A representative image from one of three independent experimental replicates is shown. **(C)** Single colonies were patched and streaked on blood agar. Hemolysis of GBS WT, Δ*covS*, Δ*covR*, and complementing clones including plasmids encoding CovS220stop and CovSV343M. Hemolysis of GBS with the pCovR promoter deletion compared to WT. Complementation of GBS Δ*covR*Δ*cylE* with pCylE on hemolytic activity. A representative image from one of three

independent experimental replicates is shown. **(D)** Invasiveness of GBS Δ*covS* to hAEC compared to WT and Δ*covR*. Complementation of Δ*covS* and Δ*covR* on amniotic invasion and effect of pCylE on amniotic epithelial invasion of Δ*covR*Δ*cylE*. Data shown are the average and SD obtained using hAEC from three independent placentas, performed in triplicate (*n=3*, ****$P<0.0001$, ***$P=0.0006$, Student's *t* test, error bars ± SD). **(E)** Barrier disruption of amniotic epithelium by GBS WT, Δ*covS*, Δ*covR* and Δ*covR*Δ*cylE*. Complementation of GBS Δ*covR*Δ*cylE* with pCylE on amniotic barrier disruption. A representative image from one of three independent experimental replicates is shown.

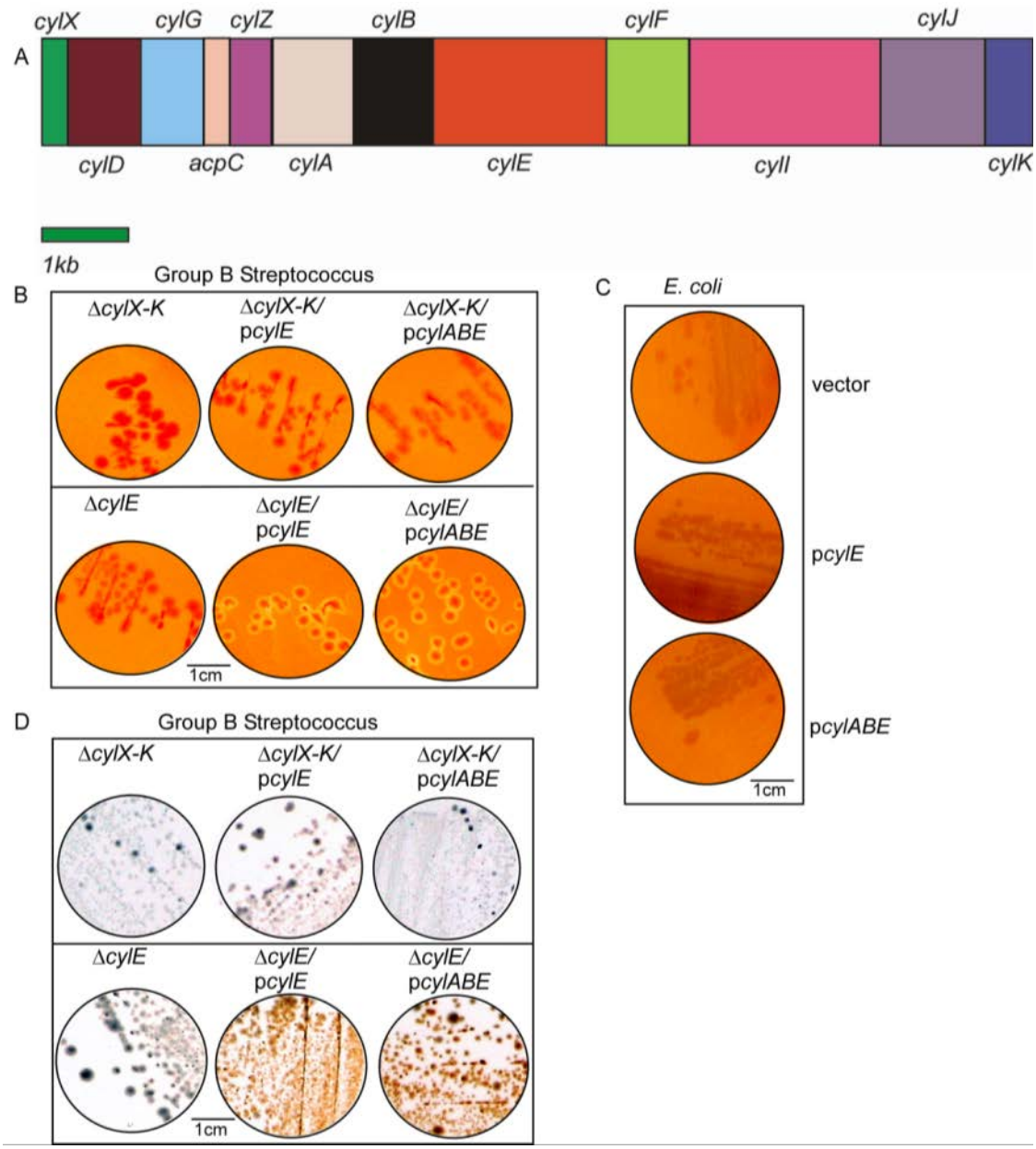

Figure 2-5. CylE is necessary but not sufficient for GBS hemolysis.

(**A**) The GBS *cyl* operon encoding genes *cylX-K* is shown. **(B-C)** Complementation of the non-hemolytic GBSΔ*cylE* and Δ*cylX-K* with plasmids encoding CylE or CylE along with the ABC transporter CylA/B on hemolytic activity. A representative image from one of three independent experimental replicates is shown. **(D)** Hemolytic and non-hemolytic GBS strains on Granada medium. A representative image from one of three independent experimental replicates is shown.

A

Gene	Predicted Function	Gene	Predicted Function
cylX	Acetyl CoA carboxylase	*cylB*	ABC transport
cylD	Malonyl-CoA-ACP transacylase	*cylE*	N-acyltransferase
cylG	3-ketoacyl-ACP reductase	*cylF*	Aminomethyltransferase
acpC	Acyl carrier protein	*cylI*	3-ketoacyl-ACP synthase
cylZ	β-hydroxy-ACP dehydratase	*cylJ*	Glycosyltransferase
cylA	ABC transport	*cylK*	Phosphopantetheinyl transferase

B

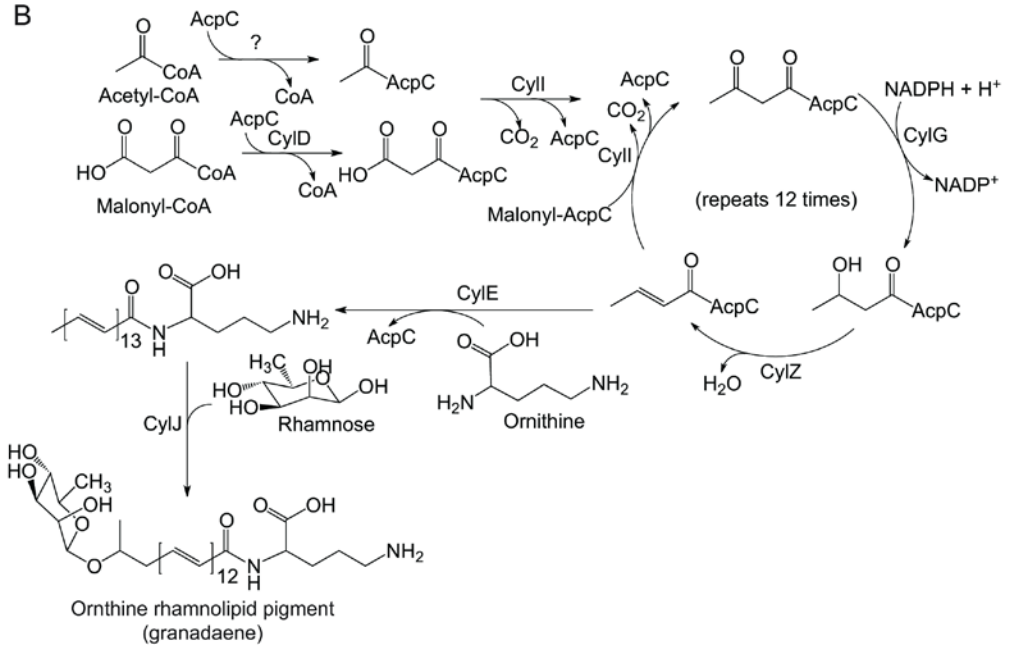

Figure 2-6. Proposed biosynthetic pathway for the GBS pigment, granadaene.

(A-B) Predicted functions of the *cyl* operon proteins and proposed biosynthetic pathway for synthesis of the GBS pigment utilizing acetyl-CoA, malonyl-CoA, ornithine, and rhamnose. CylD conjugates the elongating malonyl CoA units to the acyl carrier protein (ACP) AcpC. CylI links the malonyl CoA to an initial fatty acid-ACP complex, beginning the fatty acid biosynthesis like pathway. CylG reduces the 3-keto group to a hydroxyl group, which is further reduced to an alkene by CylZ. The *cyl* operon lacks an enoyl-ACP reductase thereby eliminating the final reduction of the alkene to an alkane. The unsaturated fatty acid serves as a substrate for further elongation by CylI, accounting for the large degree of unsaturation in the pigment. After 13 total rounds of elongation, the fatty acid is conjugated to ornithine by CylE, and glycosylated by CylJ. CylX, CylF and CylK likely function upstream or downstream of this pathway. CylX is homologous to a component of the acetyl-CoA carboxylase, which generates malonyl-CoA. CylF is an aminomethyltransferase, likely involved in production of the methylated derivative seen in the mass spectrum (Fig. S2). CylK is a putative phosphopantetheinyl transferase, which is involved in the activation of acyl carrier proteins. While GBS has a separate fatty acid biosynthesis (*fab*) operon, deletion of genes in the *cyl* operon (Δ*cylX-K*, Fig. 5B) abolishes pigment biosynthesis suggesting that the *fab* and *cyl* operons are not functionally redundant.

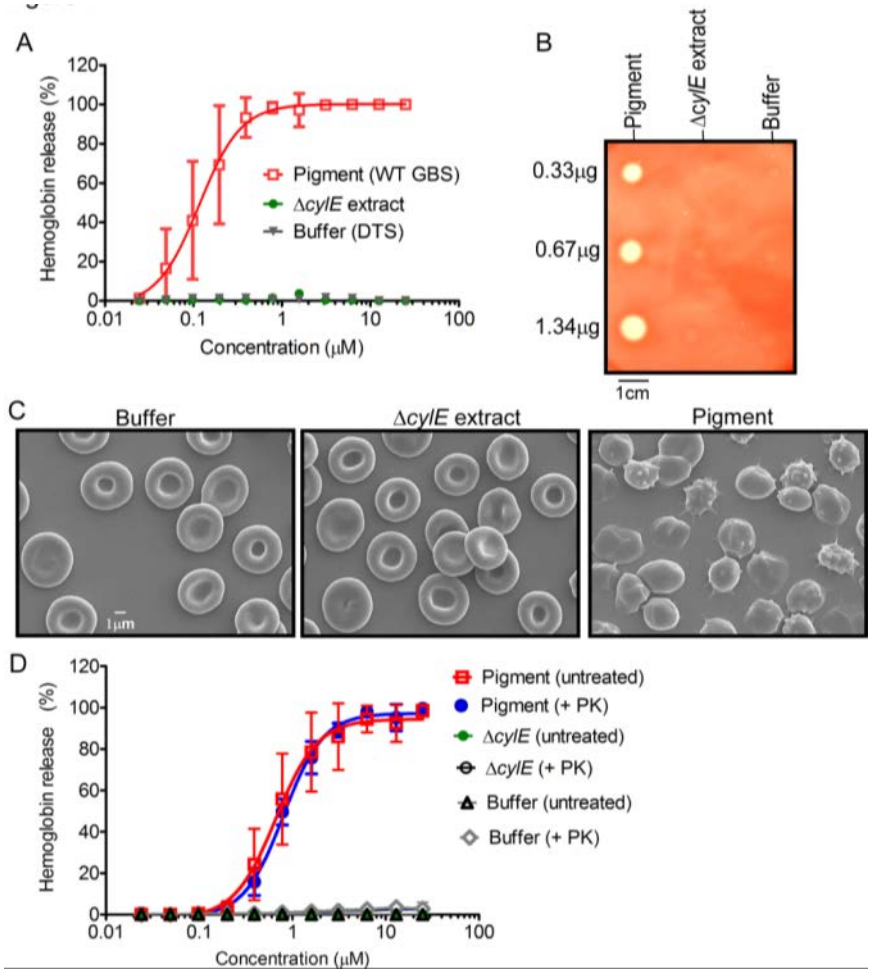

Figure 2-7. The functional basis of GBS hemolytic activity is the pigment.

(A) Pigment was added to human red blood cells (hRBC) in 2-fold serial dilutions from 25μM to 0.024μM. As controls, equivalent amounts of sample from Δ*cylE* or DTS were added to hRBC. The data shown are the average and SD from three independent pigment preparations, performed in triplicate (*n=3*, *P* <0.0001 Student's *t* test, error bars ± SD). **(B)** Varying amounts of purified GBS pigment (0.33μg, 0.66μg, 1.34μg) was spotted on sheep blood agar plates and incubated overnight at 37°C. Equivalent amounts (2, 1 and 0.5μl) of purified extract from GBSΔ*cylE* and DTS were spotted as controls. A representative image from one of three independent experimental replicates is shown. **(C)** Scanning electron micrographs showing human red blood cell membrane morphology after a brief (8 min) exposure to GBS pigment (12.5μM) or an equal amount of control (buffer or Δ*cylE* extract). The experiment was performed twice using independent pigment preparations. **(D)** For proteinase K (PK) treatment of pigment prior to hemolytic assays, pigment and control Δ*cylE* samples in DTS were lyophilized and digested in the presence and absence of proteinase K. The data shown are the average and SD from three independent pigment preparations, performed in triplicate (*n=3*, *P* ≥ 0.9 Student's *t* test, error bars ± SD).

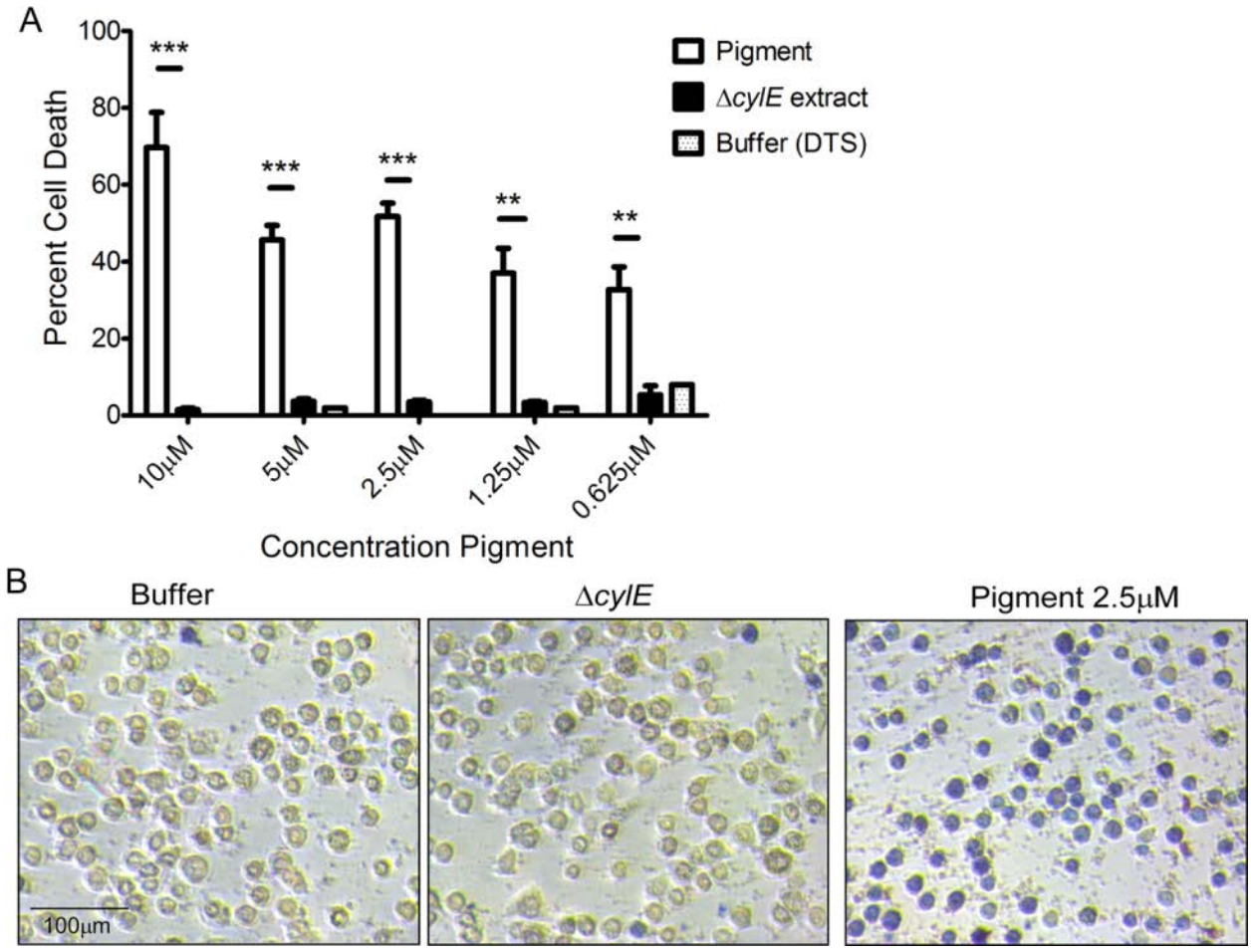

Figure 2-8. The GBS pigment is cytotoxic to human amniotic epithelial cells.

Various concentrations of GBS pigment or an equal amount of control (Δ*cylE* or DTS) were added to hAEC for 4hrs followed by trypan blue staining. The experiment was performed twice in triplicate using independent pigment samples and hAECs. **(A)** Percent cell death represented as the average and SD of five randomly selected fields (n = 500 cells, ** p< 0.005; *** p< 0.001, Student's t test, error bars ± SD). **(B)** Sample field showing GBS pigment cytotoxicity at 2.5 μM compared to an equivalent amount of controls.

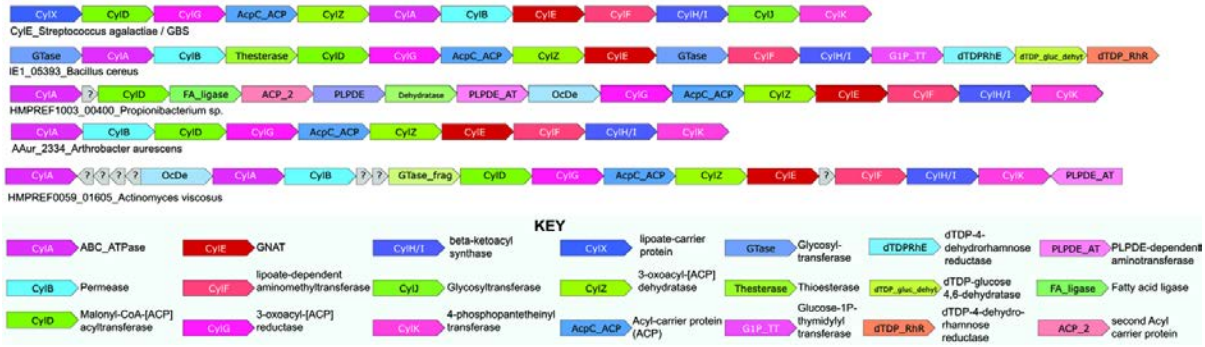

Figure 2-9. The rhamnolipid biosynthetic Cyl operon is conserved in several bacteria.

Genes within operons are shown as box arrows with the arrowhead pointing in the 5' to the 3' direction of the coding strand. Bacteria representing a subset of the species containing the Cyl operon are shown (for a detailed list, also see CylE homologues in Fig. S1). Gene and species names are indicated below the operons and gene-name abbreviations are expanded in the key provided below.

Table 2-1. GBS clinical isolates associated with preterm labor and mutations in *covR/S* locus.

Isolate number[a]	Source	Mutation in *covR/S* loci[b]	Gestational Age at Birth[c]
1	Amniotic fluid	Deletion of adenine residue at position 658 in *covS* resulting in truncation of CovS at amino acid 220 (CovS 220Stop)	30 weeks
	Chorioamnion	Same as above *i.e*. CovS 220Stop	
2	Amniotic fluid	Deletion of 4 nucleotides 'ATTT' spanning -110 to -107 upstream to the ATG start codon in the promoter region of *covR/S*	34 weeks
3	Amniotic fluid	Substitution of adenine instead of guanine resulting in amino acid substitution from valine to methionine in CovS (CovS V343M)	26 weeks
	Blood	CovS V343M	
4	Chorioamnion	CovS V343M	36 weeks
5	Chorioamnion	None	36 weeks
6	Chorioamnion	None	28 weeks

[a] In some patients, GBS were isolated from two different locations, both these isolates had the same mutation in *covR/S.*

[b]Only non-synonymous changes are reported.

[c] All women enrolled in the study had preterm labor with intact membranes at less than or equal to 34 weeks gestation.

Supplementary Information

Supplemental Figures

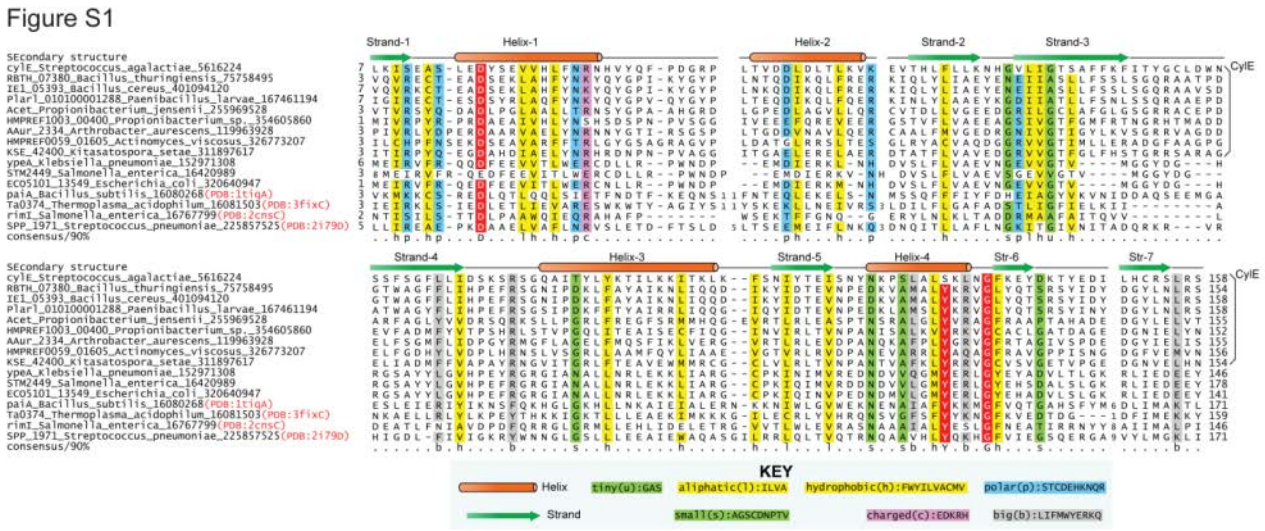

Figure 2-S1. Alignment of CylE to known N-acyltransferases.

Iterative sequence searches of GBS or *Streptococcus agalactiae* CylE using PSI-BLAST identified a number of homologues within the *N*-acyltransferase superfamily and these sequences were aligned using Kalign. Secondary structure predictions show similar progression of secondary structure elements as known *N*-acyltransferases, further supporting the conclusion that CylE is an *N*-acyltransferase. Bracket denotes CylE homologues in organisms that also have genes of the *cyl* operon.

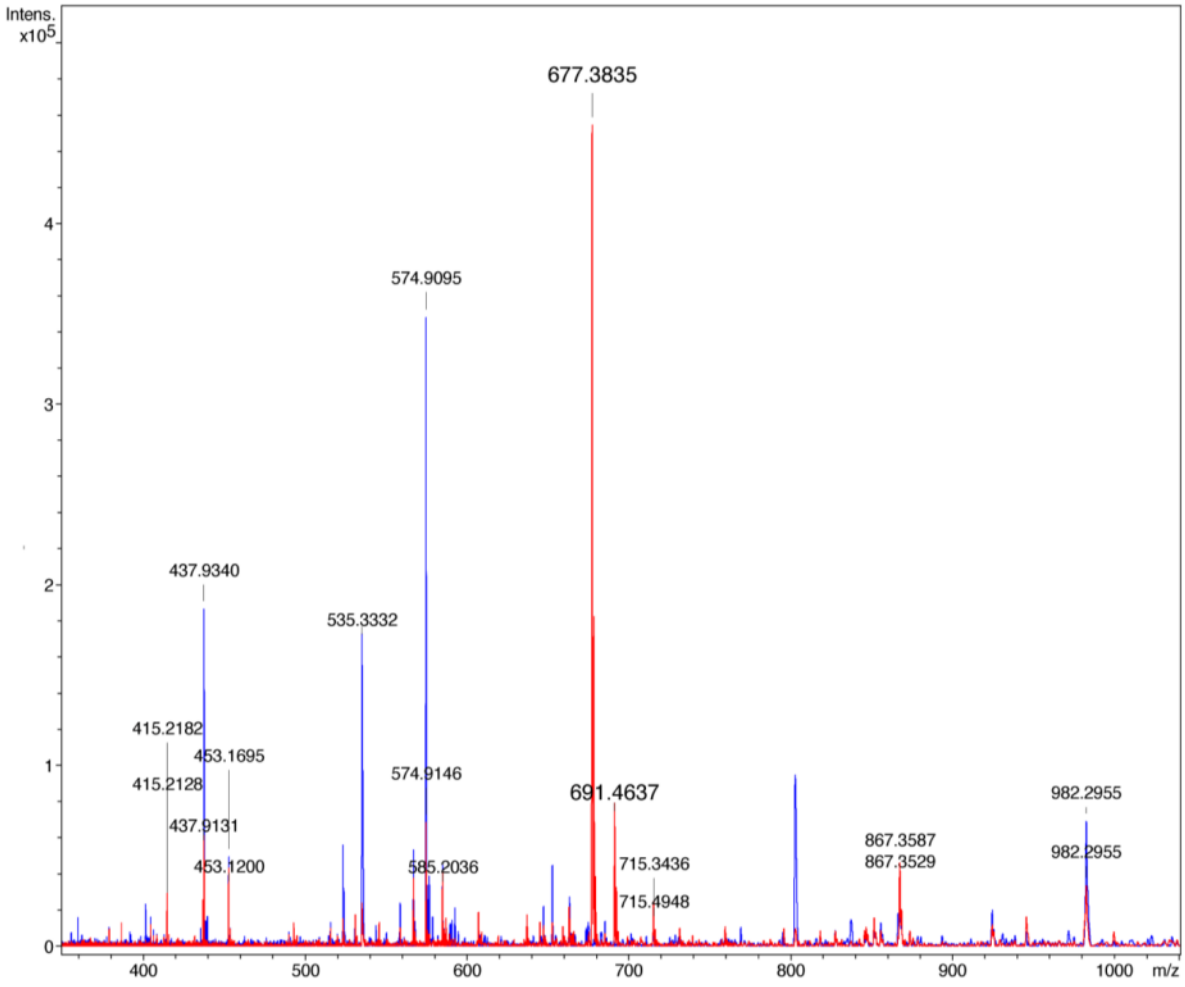

Figure 2-S2. Mass spectrometry confirms that the purified pigment with hemolytic activity is the GBS pigment previously identified as granadaene.

Purified pigment from wild type GBS dissolved in DMSO with 0.1% TFA was analyzed by Fourier Transform Ion Cyclotron Resonance mass spectrometry (FTICR-MS) and the spectrum is shown in red. The peak at 677.3835 *m/z* corresponds to the full length pigment, and the peak at 691.4637 *m/z* corresponds to a methylated derivative. To control for possible contaminants, extraction was also performed on the non-hemolytic and non-pigmented sample from the Δ*cylE* strain (spectrum overlaid in blue). A comparison between the MS spectra revealed that the 677.3835 *m/z* and 691.4637 *m/z* are unique to the pigmented sample. Data shown are representative spectra from experiments performed on three independent pigment preparations and controls.

A

Position	^{1}H (ppm)	$^1J_{H,H}$ (Hz)	Position	^{1}H (ppm)	$^1J_{H,H}$ (Hz)
2	6.12 (*br. s*)		5'	2.80 (*br. s*)	
3-23	6.0-7.4		NH	8.36 (*d*)	8.1
24	6.15 (*m*)		NH_2	7.68 (*br. s*)	
25	5.77 (*dd*)	14.9, 7.5	1"	4.66 (*s*)	
26	2.29 (*m*)		2"	3.54 (*m*)	
27	3.72 (*m*)		3"	3.41 (*dd*)	9.4, 3.1
28	1.07 (*d*)	6.2	4"	3.19 (*t*)	9.2
2'	4.31 (*m*)		5"	3.45 (*dd*)	9.4, 6.4
3'	1.59 (*m*)		6"	1.12 (*d*)	6.2
4'	1.51 (*m*)				

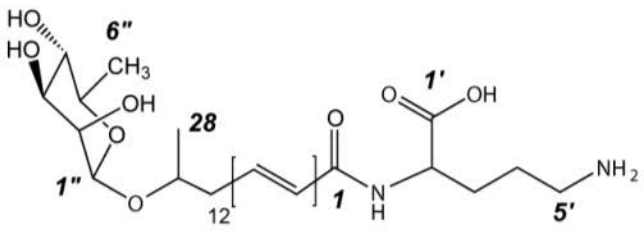

B

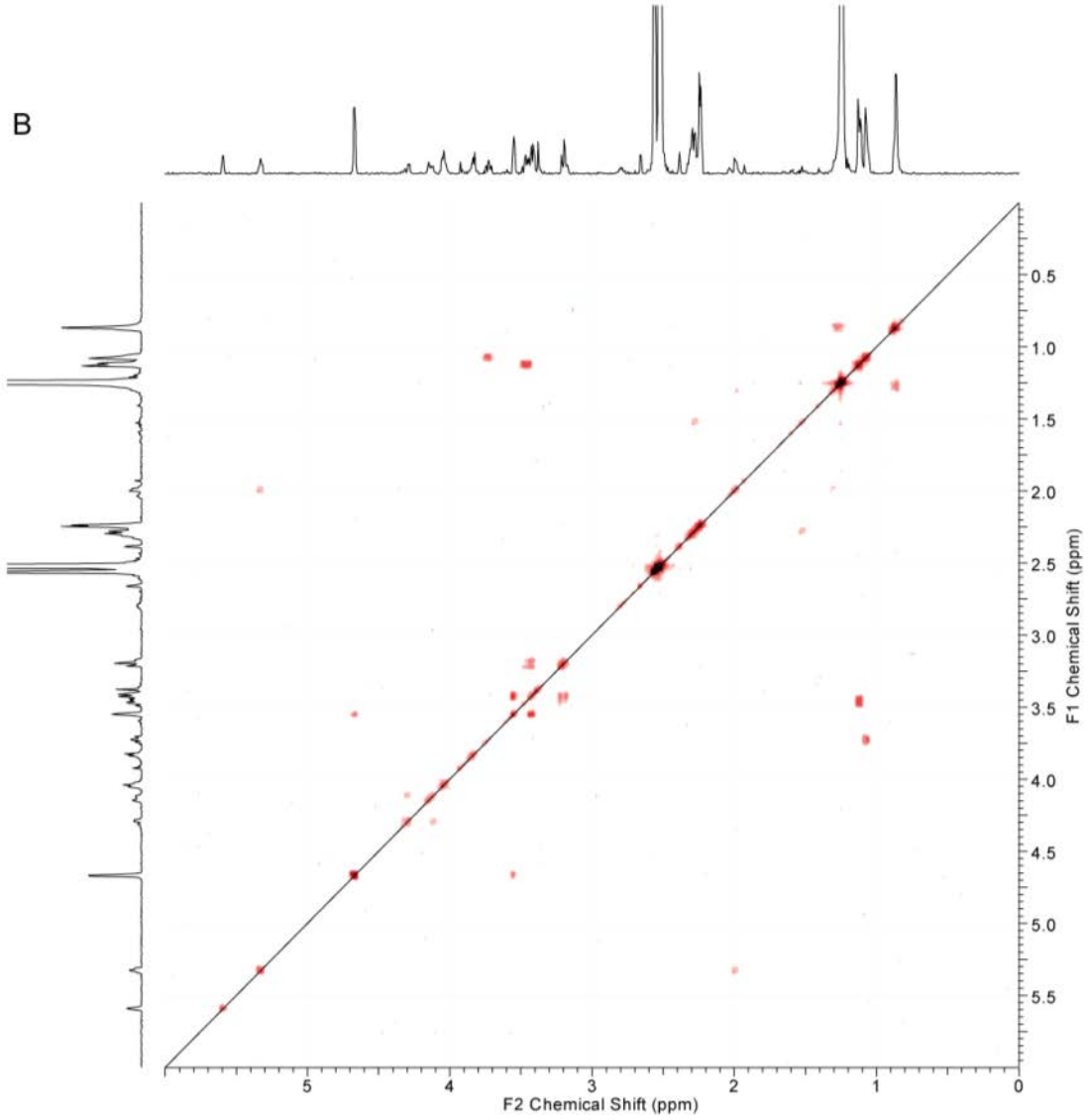

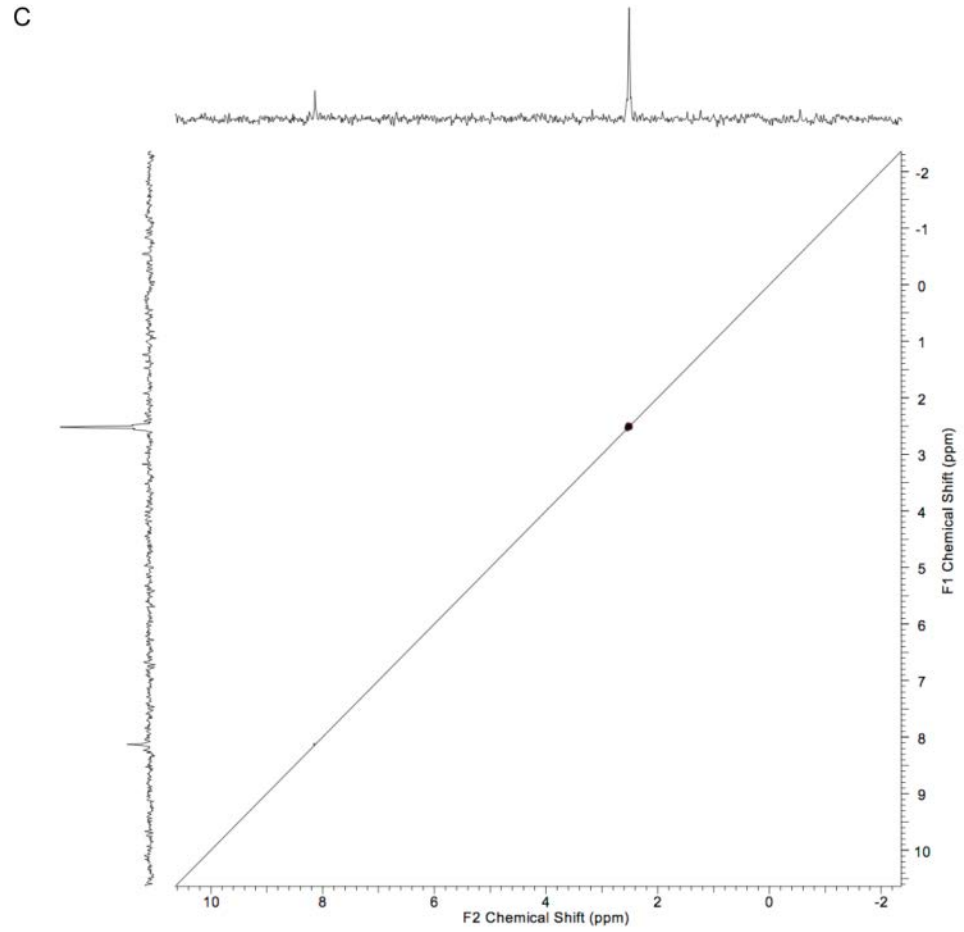

Figure 2-S3. ^{1}H chemical shifts (A) and ^{1}H-^{1}H COSY NMR (B) of the purified GBS pigment.

The pigment from WT GBS or control extract from Δ*cylE* were dissolved in DMSO-d_6: 0.1% *d*-TFA and analyzed by ^{1}H NMR and Correlation Spectroscopy (COSY) at 298K on a Bruker AV-500 instrument. NMR was performed on two independent pigment preparations and controls**. (A)** ^{1}H shift assignments are listed - the broad peak from 6.4 to 6.8 ppm corresponds to the olefinic hydrogens present in the polyene; peaks at 7.68, 4.31, 1.62, 1.51, and 2.8 ppm correspond to hydrogens present in ornithine, while peaks at 4.66, 3.54, 3.41, 3.19, 3.46, and 1.12 ppm correspond to hydrogens on the rhamnose. Pigment structure is shown on the right. **(B)** The C27 hydrogen shift (3.73 ppm) corresponds to the ether linkage between rhamnose and C27. Likewise, the C2' hydrogen shift (4.31 ppm) suggests that ornithine is linked to the polyene by an amide bond at the alpha carbon (C2'). Collectively, these results indicate that the hemolytic molecule purified from GBS is the ornithine rhamnolipid previously described as granadaene (58, 107). **(C)** COSY analysis of the Δ*cylE* extract only shows peaks corresponding to residual DMSO (2.52 ppm) and TFA (8.13 ppm).

Supplementary Tables

Table 2-S1. Primers used in this study (listed 5'-3)

CylEF	TAGCGAATTCAGGAGGATGAAAGATGATAATAAATTAAAG
CylER	TAGCGAATTCATGAAAGATGATAATAAATTAAAG
CylABEF	AAAAAAGAATTCAGGAGGATATACATATGGAAATTAAACTCAAAAATATTGG
CylABER	TTTTTTGGATCCCTGTTCTCAATGTATTATAAATAGTATTC
dCylopupF	AAAAAATCTAGAAAGCTGGACCGTGCC
dCylopupR	CACTGTTCCTTGCATATTATCACCTTCAAC
dcylkanF	GTTGAAGGTGATAATATGCAAGGAACAGTG
dcylkanR	GGAACAACATGTTGCGAGTTGCGGATGTACTTCAG
dCylopdnF	CTGAAGTACATCCGCAACTCGCAACATGTTGTTCC
dCylopdnR	TTTTTTCTCGAGCAGTTTCACTTTTGACAACC
*qRTcylE*L	GGAAGTTACCCGATTGAGCA
*qRTcylE*R	TGCCAGGAGGAGAATAGGAA
*rps*LF	TGCCCTTCGTAAATTTGCTC
*rps*LR	AACGTACCCCTGGAAGGTCT
IL6F	GGA GAC TTG CCT GGT GAA AA
IL6R	CAG GGG TGG TTA TTG CAT CT
IL8F	AGC TCT GTG TGA AGG TGC AG
IL8R	AAT TTC TGT GTT GGC GCA GT
CXCL1F	CTC TTC CGC TCC TCT CAC AG
CXCL1R	GGG GAC TTC ACG TTC ACA CT
CCL20F	GCG CAA ATC CAA AAC AGA CT

CCL20R	CAA GTC CAG TGA GGC ACA AA
IL1bF	TGGGCCTCAAAGGAAAGA
IL1bR	GGTGCTGATGTACCAGTT
GAPDHF	GAA GGT GAA GGT CGG AGT CAA CG
GAPDHR	TCC TGG AAG ATG GTG ATG GGA T
CovR F	GCGCGGAGCTCTTGTTAAGTAAAGAATAAG
CovR R	GCGCGAGGATCCTTTATTTTTCACGAATCAC
CovS F	GCGCGCGAGCTCTATTCAAACTGTTCGCGGAAT
CovS R	GCGCGCGGATCCTTTATATTTCTTTAGTTTCTT
CovS220F	GTGCTACTAAGCGTATTGTTCGTCCGGTTAAAATTTACACGAC
CovS220R	GTCGTGTAAATTTTAACCGGACGAACAATACGCTTAGTAGCAC
CovSV343MF	CTTGGAACTTCATCAAGATGAAATGACAGATTTATCAAGCTC
CovSV343MR	GAGCTTGATAAATCTGTCATTTCATCTTGATGAAGTTCCAAG
CovR/S F	AAAAAA GGATCC GAGCTCGTTGATCAGGATTTGGTC
CovR/S R	TTTTTTGGTACCACTAAAAGAGGCAATTCTTCCAAACG

Chapter 3 – A streptoccocal lipid toxin induces membrane permeabilization and pyroptosis leading to fetal injury

The following text is from the article: Christopher Whidbey, Jay Vornhagen[1], Claire Gendrin[1], Erica Boldenow[1], Jenny Mae Samson[1], Kenji Doering, Lisa Ngo, Ejiofor A.D. Ezekwe Jr., Jens H Gundlach, Michal A. Elovitz, Denny Liggitt, Joseph A Duncan , Kristina Adams Waldorf, and Lakshmi Rajagopal. (2015) A streptococcal lipid toxin induces membrane permeabilization and pyroptosis leading to fetal injury. **EMBO Molecular Medicine**, *in press*. Figure numbers have been updated to conform to the formatting of the dissertation, however the rest of the text remains essentially as accepted with minor editorial changes.

[1]Equal Contribution

Abstract

Group B *Streptococcus* (GBS) are Gram-positive bacteria that cause infections *in utero* and in newborns. We recently showed that the GBS pigment is hemolytic and increased pigment production promotes bacterial penetration of human placenta. However, mechanisms utilized by the hemolytic pigment to induce host cell lysis and the consequence on fetal injury are not known. Here, we show that the GBS pigment induces membrane permeability in artificial lipid bilayers and host cells. Membrane defects induced by the GBS pigment triggers K^+ efflux leading to osmotic lysis of red blood cells or pyroptosis in human macrophages. Macrophages lacking the NLRP3 inflammasome recovered from pigment-induced cell damage. In a murine model of *in utero* infection, hyperpigmented GBS strains induced fetal injury in both an NLRP3 inflammasome-dependent and -independent manner. These results demonstrate that the dual mechanism of action of the bacterial pigment/lipid toxin leading to hemolysis or pyroptosis

exacerbates fetal injury and suggest that preventing both activities of the hemolytic lipid can reduce GBS fetal injury and preterm birth.

Introduction

Preterm birth and early onset neonatal infections are estimated to cause approximately 1.4 million neonatal deaths annually (83). Currently, there is no effective therapy for prevention of *in utero* infections, preterm births and stillbirths. An important pathogen that causes perinatal and neonatal infections is Group B *streptococcus* (GBS) or *Streptococcus agalactiae*. GBS are β-hemolytic, Gram-positive bacteria that are typically found as recto-vaginal colonizers in healthy adult women (1, 2). However, ascending *in utero* GBS infection increases the risk of preterm, premature rupture of membranes (PPROM), fetal injury, and preterm birth (126). As ascending infections cannot be treated by intrapartum antibiotic prophylaxis, new strategies are needed to more effectively treat and prevent *in utero* infections and early onset GBS disease. To develop such strategies, it is paramount to gain a better understanding of GBS virulence factors and how they impact the host immune response.

An important virulence determinant of GBS is the toxin known as β-hemolysin/cytolysin (hereafter referred to as the hemolysin). This toxin is responsible for the characteristic zone of β-hemolysis exhibited by GBS, and hemolytic strains are associated with virulence (36, 39, 127). Also, hyperhemolytic GBS such as those deficient in the two component system CovR/S (due to absence of repression of the hemolysin biosynthesis operon) are significantly more pathogenic, while nonhemolytic GBS are severely attenuated (34, 128). Despite these advances, studies aimed at understanding the mechanism of action of the GBS hemolysin were confounded by difficulties associated with purifying the toxin. Although previously suggested to be a protein toxin (46, 51), we recently showed that the molecule responsible for hemolytic activity of GBS is the ornithine rhamnopolyene lipid/ pigment (129) also known as granadaene (58). With the

identification of the GBS hemolysin as a lipid, understanding how the toxin itself contributes to inflammation, cytotoxicity and preterm birth is critical for development of neutralizing strategies against the lipid toxin. Previous studies that were performed with hemolytic extracts of GBS had contaminating proteins (46); consequently, the exact mechanisms of pigment-induced cytotoxicity is unclear.

Mechanisms that promote ascending GBS infection and the immune responses invoked during this process also remain poorly defined. Studies using pregnant animal models have shown that intrauterine inflammation caused by bacterial infection triggers disruption of placental membranes leading to fetal injury and preterm birth (130-132). A study using intraperitoneal injection of heat-killed GBS showed that a pan-caspase inhibitor was able to delay, but not prevent, preterm birth in a murine model (130). Although hemolytic GBS strains have been described to activate the NLRP3 inflammasome in murine dendritic cells and macrophages (39, 133), whether the hemolytic pigment/lipid toxin is sufficient for inflammasome activation and whether this leads to pyroptosis is not known. Recently, when exogenous GBS RNA was transfected into murine macrophages, the NLRP3 inflammasome was described to associate with GBS RNA but inflammasome activation required the presence of hemolytic GBS (133). However, the relevance of these findings to GBS infection *in vitro* and *in vivo* is unclear. Because NLRP3 activation occurs only in the presence of hemolytic GBS (39, 133), we aimed to understand how the purified GBS pigment activates the inflammasome, induces cell death and leads to fetal injury.

Here, we demonstrate that the purified GBS pigment/lipid toxin induces membrane permeabilization and the efflux of intracellular potassium, which triggers osmotic lysis in red

blood cells and NLRP3 inflammasome and caspase 1 activation leading to pyroptosis in macrophages. In a pregnant mouse model of intrauterine infection, hyperhemolytic/hyperpigmented GBS strains increased the incidence of preterm birth and *in utero* fetal death (IUFD) in both an NLRP3 inflammasome-dependent and -independent manner. Collectively, these findings provide novel insight into how a bacterial lipid toxin/pigment mediates cell death and demonstrates its relevance to bacterial infection and preterm birth.

Results

The GBS lipid toxin lyses red blood cells using a colloidal-osmotic mechanism

Previous work from our group demonstrated that hyperhemolytic GBS strains penetrate the human placenta and can be associated with women in preterm labor (129). We further showed that hemolytic activity of GBS is due to the ornithine rhamnolipid pigment (see structure in Fig. 1A, (58)) and not due to any protein toxin (129). Despite these findings, the mechanism of how the hemolytic pigment/lipid toxin causes hemolysis, cytolysis, and inflammation-mediated cell death was not known. To understand how the pigment/lipid toxin lyses host cells, we first examined pigment-mediated lysis of human red blood cells (RBC). We hypothesized that the pigment may lyse RBC either by the mechanism of direct lysis wherein the lipid itself dissolves the membrane as observed with detergents or by the mechanism of colloidal-osmotic lysis wherein the lipid forms pores or causes membrane perturbations and lysis occurs via osmotic pressure. To determine how the GBS pigment induces cell lysis, we first measured the kinetics of both K^+ and hemoglobin (Hb) release from RBCs treated with 400nM pigment. As a control, an equal amount of extract from a nonhemolytic strain of GBS (Δ*cylE*) was included. The results

shown in Fig. 1B indicate that while the pigment induces the release of both K^+ and Hb from RBCs, efflux of the smaller K^+ ion was faster than efflux of the larger Hb, as measured by time to 50% release (Fig 1B; 4.8 min vs. 8.4 min; $p < 0.0001$, extra sum-of-squares F test). These results suggest that the pigment induces membrane permeabilization that allows K^+ ions to efflux, followed by the release of Hb. The slight lag in release of Hb versus K^+ suggests a colloidal-osmotic mechanism of lysis by the GBS pigment, rather than rapid dissolution of the membrane by direct lysis wherein no lag is expected between K^+ and Hb. A similar lag between K^+ and Hb release was observed during hemolysis mediated by *Staphylococcus aureus* α-toxin (Fig. S1, see A), whereas 100% release of both K^+ and Hb occurred instantly with direct lysis mediated by Triton X 100 (Fig. S1, see B).

We also performed protection assays with osmoprotectants of various sizes ranging from a hydrodynamic radius of 0.40 nm (PEG200) to 1.6 nm (PEG3000). To this end, human RBC were pre-treated with the GBS pigment for two minutes and the RBC were pelleted to remove any unincorporated pigment. Pigment-treated RBCs were then resuspended in PBS or PBS containing 30 mM osmoprotectant, and hemolytic activity was measured (for details, see Materials and Methods). The results shown in Fig. 1C indicate that smaller osmoprotectants such as PEG200 and PEG400 did not protect RBC from pigment-mediated hemolysis whereas complete protection from hemolysis was observed in the presence of the larger osmoprotectants such as PEG1500 and PEG3000. In comparison, minimal protection was observed with SDS, which causes direct and instant lysis of RBCs (Fig. S2).

The GBS hemolytic lipid induces membrane permeabilization of artificial lipid bilayers

To determine if membrane permeability observed with the GBS pigment requires the active cellular response of host cells, we tested the ability of the pigment to disrupt artificial lipid bilayers using model black lipid membranes (BLMs). BLMs mimic membrane lipid bilayers but lack the active cellular responses of host cells. To test our hypothesis, BLMs composed of 1,2-diphytanoyl-sn-glycero-3-phosphocholine (DPhPC) were established across an aperture separating two chambers of a U-tube as previously described (134). A voltage was applied, and current was measured between the two chambers; an increase in current corresponds to a compromise in membrane integrity. We observed that treatment of BLMs with pigment resulted in an increase in measured current, while treatment with the control Δ*cylE* extract resulted in no change (data from 2μM are shown in Fig. 1D, and data from 75nM are shown in Fig. S3). Interestingly, jumps were erratic in both frequency and magnitude. The initial compromised bilayer area was on the order of 1 nm^2. Subsequently, the size of the compromise in the bilayer fluctuated frequently before the bilayer finally ruptured at either 120 sec (Fig. 1D) or 345 sec (Fig. S3), depending on pigment concentration. The increase in conductance observed in the lipid bilayers due to the GBS pigment is not consistent with either the formation of discrete protein pores, which is usually marked by well-defined jumps in membrane conductance, or detergent mediated bilayer solubilization which is marked by a rapid increase in conductance followed by spontaneous disappearance of the entire membrane (Fig. S3). Rather, the changes in conductance fluctuations are consistent with the pigment intercalating into and perforating the bilayer. This appears to be a dynamic process in which channel conductance appears and disappears. Taken together, these data demonstrate that the membrane permeability observed in

pigment-treated cells occurs independently of a cellular response and is unique in its mode of action by neither conforming to a typical pore-forming protein toxin nor inducing instant lysis as observed with detergents.

Purified GBS lipid toxin/pigment is sufficient for induction of IL-1β release and cytolysis.

To understand how the hemolytic pigment triggers host cell death, we examined the proinflammatory and cytotoxic properties elicited by the purified hemolytic pigment. In these experiments, we also included GBS strains with differences in hemolytic activity such as GBS WT A909, isogenic hyperhemolytic/hyperpigmented strain Δ*covR* (lacking the two component regulator CovR/S that represses biosynthesis of the hemolytic pigment) and nonhemolytic Δ*cylE*, Δ*covR*Δ*cylE* strains that were derived from WT and Δ*covR* but lack the *cylE* gene required for pigment biosynthesis (for details, see (129)). Given that macrophages are important for defense against GBS infections, we utilized macrophages derived from M-CSF-treated human peripheral blood mononuclear cells (PBMC) as well as differentiated THP-1 cells as models of human macrophage like cells. Human PBMC and THP-1-derived macrophages were treated with GBS WT, hyperhemolytic Δ*covR*, and nonhemolytic Δ*cylE* and Δ*covR*Δ*cylE* at a multiplicity of infection (MOI) of 1 for four hrs, and cytotoxicity was measured by LDH release. The results shown in Figs. 2A and 3A show that LDH release indicative of cell death was significantly higher in macrophages treated with hyperhemolytic GBS when compared to nonhemolytic strains. We also observed that hyperhemolytic GBS induced significantly more IL-1β release when compared to the isogenic nonhemolytic strains (Figs. 2B and 3B).

To determine the contribution of the pigment/lipid toxin to the proinflammatory and cytotoxic nature of GBS, the human PBMC and THP-1-derived macrophages were incubated with various concentrations of purified pigment or control Δ*cylE* extract for four hrs, and cytotoxicity was measured as the loss of metabolic activity as measured by a redox dye, Alamar Blue. Cytotoxicity due to GBS pigment was dose-dependent, and 50% cell death was observed at approximately 1-2 μM (Figs. 2C and 3C), which is noticeably higher than the EC_{50} for RBC (< 0.1 μM, Fig. 1C). This observation is likely due to the membrane turnover that occurs in macrophages and not in RBCs, as has been observed with other bacterial exotoxins (135).

To identify the pathways activated by the purified GBS pigment/lipid toxin, we measured cytokine levels in the supernatants of pigment-treated macrophages. Interestingly, levels of IL-1β were significantly increased in pigment-treated PBMC and THP-1 cells compared to control Δ*cylE* extract-treated cells (Figs. 2D and 3D). Consistent with the above observations, IL-18 levels were also increased in pigment-treated THP-1 macrophages but other pro-inflammatory cytokines such as TNFα, IL-6, and IFN–γ were not significantly increased (Fig. S4). Taken together, these data show that the purified hemolytic GBS pigment is proinflammatory and cytotoxic.

Pigment-induced cytotoxicity and immune response is NLRP3 inflammasome dependent.

The increase in secretion of IL-1β and IL-18 observed in human macrophages treated with GBS pigment suggests that the pigment can trigger activation of the inflammasome. The inflammasome is a cytosolic complex which mediates cleavage of pro-caspase 1 to active caspase 1, which in turn cleaves pro-IL-1β and pro-IL-18 into their active forms. One major

inflammasome comprises the NLR (nucleotide binding, leucine-rich repeat containing) protein known as NLRP3, which associates with the adaptor ASC (Apoptosis-associated Speck-like protein containing the caspase recruitment domain, CARD) (136). To determine if the GBS pigment/lipid toxin activates NLRP3, we exposed previously characterized THP-1 human macrophage cell lines that were constitutively knocked down for expression of NLRP3 or the adapter protein ASC ((137), Fig. S5) to GBS strains (WT, isogenic Δ*covR*, Δ*cylE*, Δ*covR*Δ*cylE*) or purified pigment. As controls, THP-1 macrophages transfected with empty vector or an shRNA of scrambled ASC sequence were included. The results shown in Fig. 4A indicate that GBS induced significant cell death in macrophages containing the NLRP3 inflammasome in a hemolysin-dependent manner. Notably, cell death was significantly decreased in macrophage cell lines knocked down for expression of NLRP3 or ASC (Fig. 4A). Similarly, hemolytic and hyperhemolytic GBS strains induced increased IL-1β secretion in macrophages in an NLRP3 inflammasome dependent manner (Fig. 4B). Consistent with these observations, we observed that increasing concentrations of the purified GBS hemolytic pigment induced cell death and IL-1β secretion in an NLRP3 inflammasome-dependent manner (Figs. 4C, D). These results demonstrate that in macrophages, the GBS hemolytic pigment primarily induces an NLRP3 inflammasome-dependent, programmed cell death. The cell death observed in NLRP3-deficient macrophages with hyperpigmented GBSΔ*covR* (25-40 %, see THP-1/shASC, THP-1/shNLRP3 in Fig. 4A) could not be prevented by the addition of osmoprotectants such as PEG1500 or by the caspase 3/7 inhibitor Z-DEVD-FMK (Fig. S6). Also, levels of IL-1β released by THP-1/shASC and THP-1/shNLRP3 cells exposed to GBS Δ*covR* were not significantly different from cells exposed to GBS WT, Δ*cylE* or Δ*covR*Δ*cylE* strains (Fig. 4B). Based on these

observations, we suggest that the residual cell death observed in inflammasome-deficient cells due to hyperpigmented GBS can be attributed to an inflammasome- and caspase 3/7-independent pathway, as suggested previously for rat neuronal cells (138).

The GBS pigment induces membrane permeabilization and loss of intracellular potassium independent of the NLRP3 inflammasome.

A known activator of the NLRP3 inflammasome is the efflux of intracellular potassium that occurs upon membrane permeabilization (139). Given that the GBS pigment is able to induce membrane disruptions in RBC and even in artificial lipid bilayers (Fig. 1C, D), we hypothesized that intercalation of the GBS pigment into host cells such as human macrophages should trigger membrane permeabilization and the efflux of intracellular potassium, irrespective of the presence or absence of the inflammasome. To test this hypothesis, we measured membrane disruption and quantified intracellular potassium levels in NLRP3-proficient and -deficient macrophages that were treated with the GBS pigment. To examine membrane permeabilization, we exposed NLRP3-proficient and -deficient macrophages to GBS pigment (1μM) or controls for 20 min and measured uptake of a membrane impermeable dye, propidium iodide (see Materials and Methods for details). The results shown in Figs. 5A and B indicate that increased fluorescence is seen in both NLRP3-proficient and -deficient macrophages treated with GBS pigment (1μM) when compared to controls (Δ*cylE* extract). These data indicate that the GBS pigment induces membrane permeability in host cells independent of the inflammasome. To further confirm this, we utilized ion-coupled plasma atomic emission spectroscopy (ICP-AES) as described (139) to measure levels of intracellular potassium in NLRP3 proficient and deficient macrophages that

were exposed to GBS pigment or to controls over time (0, 30, 60, 120, 180 and 240 min). These results demonstrate that intracellular potassium levels dramatically decreased within 30 minin NLRP3-proficient macrophages (THP-1/scrambled, Fig. 5C) and in NLRP3-deficient macrophages (THP-1/shNLRP3, Fig. 5D) that were exposed to the GBS pigment (1μM), demonstrating that both pigment-mediated membrane disruption and potassium efflux occurs independently of NLRP3 inflammasome activation and even cell death. Notably, NLRP3-deficient macrophages appear to be able to recover from the initial K^+ efflux (see 120, 180 and 240 min. in Fig. 5D). In contrast, cells proficient for NLRP3 undergo cell death and do not significantly recover (Fig. 5C). To determine if K^+ efflux is important for pigment-induced cell death, we performed cytolysis assays of THP-1 cells exposed to the GBS pigment in the presence of excess extracellular potassium (final concentration 50 mM) compared to culture media containing 5mM potassium. The results shown in Fig. 5E indicate that addition of extracellular potassium partially protected the cells from GBS pigment-mediated cytolysis, further supporting a role of K^+ efflux and NLRP3 activation in cytolysis.

The GBS pigment induces caspase 1-dependent pyroptosis.

Activation of the NLRP3 inflammasome by K^+ efflux leads to activation of caspase 1 (26, 27, 139, 140). To determine if the GBS pigment-mediated K^+ efflux induced caspase 1 activation, we utilized a membrane-permeable, caspase 1-specific FLICA reagent (Fluorochrome-Labeled Inhibitors of CAspases, 660-YVAD-FMK; Immunochemistry Technologies) that binds to active caspase 1. We observed that in macrophages expressing NLRP3, pigment treatment resulted in more FLICA+ cells when compared to pigment treatment of macrophages that were knocked

down for NLRP3 expression (Fig. 6A). Collectively, these results show that the GBS pigment triggers potassium efflux and NLRP3 inflammasome-mediated caspase 1 activation. Active caspase 1 can trigger the proinflammatory, programmed cell death known as pyroptosis, a type of cell death that has been increasingly associated with bacterial pathogenesis (141). To determine if the GBS pigment induces cell death by pyroptosis, we utilized the caspase 1-specific inhibitor Z-YVAD-FMK. We observed that when THP-1 macrophages were pre-treated with the caspase 1-specific inhibitor, they were significantly more resistant to pigment-mediated cell death (Fig. 6B) whereas protection from pigment mediated cell death was not observed with the caspase 3/7 inhibitor Z-DEVD-FMK or vehicle only (Fig. 6B). Also, increasing the concentration of the caspase 1-specific inhibitor Z-YVAD-FMK provided dose-dependent protection from pigment-mediated cell death, and complete protection was seen at 200 μM Z-YVAD-FMK (Fig. S7). The requirement of K^+ efflux, NLRP3, ASC, caspase 1 and the ensuing proinflammatory response demonstrates that GBS utilizes a hemolytic pigment/lipid toxin to induce pyroptosis.

The GBS pigment causes fetal injury by NLRP3 inflammasome-dependent and -independent mechanisms.

Previous work from our group demonstrated that hyperhemolytic GBS strains with mutations in *covRS* are more proficient in penetration of human placenta and have been isolated from chorioamniotic membranes and amniotic fluid obtained from women in preterm labor (129). To determine if hyperhemolytic GBS strains induce fetal injury and preterm birth, we adapted a murine model of *E. coli* induced *in utero* infection (142) to GBS. We chose the intrauterine

model of inoculation rather than a vaginal model of inoculation to minimize discrepancies that can be attributed to differences in mouse vaginal persistence (68). To this end, on day E14.5 (day 14.5 of embryonic development) of pregnancy, either WT GBS, the hyperpigmented Δ*covR* strain, or the nonhemolytic Δ*covR*Δ*cylE* strain was infused into the right horn of the uterus between the first (P1) and second (P2) fetal sacs most proximal to the cervix as described ((142, 143), also see Fig. 7A). Mice were monitored for 72 hrs for signs of preterm birth (*i.e.*, at least 1 pup in cage). At either 72 hrs or at the onset of delivery (whichever occurred first), fetal survival rates were determined, and tissue was collected to assess bacterial load. Preterm birth (*i.e.*, at least 1 pup in cage) was observed in three of six mice infected with Δ*covR*, in one of six infected with WT GBS, and in none of the six mice infected with the nonhemolytic Δ*covR*Δ*cylE* strain (preterm delivery rate was 50%, 16% and 0%, respectively). We also observed significantly higher fetal death rates in mice infected with hemolytic GBS, *i.e.*, WT or the hyperpigmented Δ*covR* strain compared to the nonhemolytic Δ*covR*Δ*cylE* strain (Fig. 7B). Bacteria were recovered from all fetuses present in the uterus and there was no significant difference in bacterial load between fetuses of mice infected with the three GBS strains (data not shown). H&E staining of infected uterine tissue showed that while only a few mononuclear cells are present in the Δ*covR*Δ*cylE* sample, increased presence of inflammatory cells and necrotic debris is seen in the Δ*covR* sample (Fig. 7C). The frequency of fetal death between hemolytic strains of GBS such as WT and Δ*covR* was not significantly different and may likely be due to decreased repression of hemolysin/pigment biosynthetic genes by CovR/S *in utero*, as suggested previously (65, 144).

To determine if hemolysis and/or activation of the NLRP3 inflammasome is important for fetal injury and preterm birth caused by hyperhemolytic GBS strains, we utilized pregnant homozygous NLRP3 knock-out (NLRP3KO) mice (145, 146) in the *in utero* model of infection described above. We compared the frequency of preterm birth and fetal death in pregnant WT C57BL6 and NLRP3KO mice that were infected *in utero* with either the hyperhemolytic GBS Δ*covR* strain or an isogenic nonhemolytic GBS Δ*covR*Δ*cylE* strain. Notably, preterm delivery was observed in three of six WT C57BL6 mice infected with Δ*covR* and not in any other groups, *i.e.*, WT C57BL/6 mice infected with a Δ*covR*Δ*cylE* strainor NLRP3KO mice infected with either Δ*covR* or Δ*covR*Δ*cylE* strains. The results shown in Fig. 7D indicate that GBS infection mediated fetal death can be associated with production of the hemolytic pigment (compare Δ*covR* and Δ*covR*Δ*cylE* in WT C57BL/6 mice) and the presence of the NLRP3 inflammasome (compare Δ*covR* in WT C57BL/6 and NLRP3KO mice). Fetal death was also significantly higher in NLRP3KO mice infected with the Δ*covR* strain compared to NLRP3KO mice infected with the Δ*covR*Δ*cylE* strain. These results indicate that the hemolytic/membrane-disrupting nature of the pigment (without NLRP3 inflammasome activation) is also likely to contribute to fetal injury. Both hemolytic and nonhemolytic GBS were able to penetrate all fetuses located throughout the uterus in both WT and NLRP3KO mice (Fig. 7E) indicating that decreased fetal death observed in the inflammasome-deficient mice or due to non-hemolytic/non-pigmented GBS strains cannot be attributed to decreased bacterial dissemination. Of note, fetal death observed in NLRP3KO mice due to nonhemolytic GBS is not significantly different when compared to WT C57BL/6 mice ($p > 0.3$, Fig. 7D) or CD-1 mice ($p = 1$ compare Fig. 7D to Fig. 7B). IL-1β levels were significantly higher in WT C57BL/6 mice infected with the Δ*covR*

mutant compared to NLRP3KO mice infected with the Δ*covR* mutant or WT mice infected with the Δ*covR*Δ*cylE* mutant (Fig. 7F). As IL-1β levels were not significantly different between NLRP3KO mice infected with the Δ*covR* or Δ*covR*Δ*cylE* strains, these results suggest that the GBS pigment is primarily responsible for NLRP3 inflammasome *in vivo*. IL-1β levels in WT C57BL6 mice infected with the Δ*covR*Δ*cylE* strain were higher than NLRP3KO mice infected with the same strain, suggesting that additional factors besides the pigment also activate the NLRP3 inflammasome, but interestingly this did not correlate with increased fetal death. Collectively, our results indicate that production of the hemolytic pigment contributes to GBS infection-associated fetal injury in both an NLRP3 inflammasome-dependent and -independent manner and establishes the hemolytic pigment as a critical mediator of GBS fetal injury.

Discussion

This study demonstrates how the GBS hemolytic pigment/lipid toxin causes cell death, triggers inflammation and promotes fetal injury. Although the hemolytic nature of GBS was described almost a century ago (147) and has long been associated with virulence of the pathogen (30, 34, 36, 38, 51), mechanistic insight into this potent virulence factor was lacking. We recently showed that the molecular basis of hemolytic activity in GBS is the pigment/lipid toxin (129). In the current study, we utilized artificial lipid bilayers, RBCs and macrophages to understand how a bacterial pigment/lipid toxin disrupts these host cells. The trans-membrane conductance observed in artificial lipid bilayers suggests that the pigment/lipid toxin does not induce the formation of large, multimeric pores (commonly observed with protein toxins) but rather induces membrane permeabilization by forming variably-sized membrane defects similar

to those previously observed with the cyclic antimicrobial peptide Gramicidin S (148). The predicted length of the polyene moiety of the GBS pigment is approximately 32 Å (determined using a molecular model generated by the National Cancer Institute's Online SMILES Translator and modeled using PyMol), which is similar to the average thickness of the plasma membrane at 30-40 Å (149). Thus, we predict that insertion of the GBS hemolytic pigment may span the host cell membrane, with the rhamnose and ornithine moieties acting as polar headgroups. Insertion of the GBS pigment into RBC membranes triggers membrane disruption leading to colloidal-osmotic lysis (see proposed model in Fig. 8).

Unlike RBCs, most host cells have the capability to turn-over their plasma membrane which can confer some protection against membrane-disrupting bacterial toxins (135). Although such a defense mechanism may prevent the toxin from directly killing the cell, the initial membrane disruption can activate immune pathways such as the NLRP3 inflammasome. Our data demonstrate that this is the case for the GBS hemolytic pigment. After intercalating into the plasma membrane, the GBS pigment triggers membrane permeability leading to ion flux. In the presence of TLR signaling (150), this initiates activation of the NLRP3 inflammasome leading to caspase-1 activation, increased IL-1β and IL-18 secretion and the form of programmed cell death known as pyroptosis (see proposed model in Fig. 8). We demonstrate that the GBS pigment is sufficient for inflammasome activation. Previous work indicated that hemolytic GBS strains activate the NLRP3 inflammasome in mouse dendritic cells (39), RNA has been recently implicated in hemolysin-mediated NLRP3 activation (133). However, the extraction and isolation procedures followed for purification of the GBS pigment (58, 129) is expected to remove any contaminating nucleic acid. In addition, we did not observe the presence of nucleic

acid in purified pigment samples that were analyzed directly or following RT-PCR on ethidium bromide-stained agarose gels (Fig. S8). NMR data of purified pigment (129) did not reveal the presence of imino protons characteristic of RNA (151). Also, we did not detect any protein on pigment samples analyzed on Sypro Ruby stained SDS-PAGE (Fig. S8). As the purified GBS pigment, which is devoid of nucleic acids, activates the NLRP3 inflammasome and induces pyroptosis, these results suggest that GBS pigment can induce pyroptosis in the absence of RNA. These conclusions are also supported by our observations that inactive pigment (pigment lacking the carrier molecule starch) is not hemolytic and does not activate the NLRP3 inflammasome or induce pyroptosis (Fig. S9). These data also indicate that background absorbance values from the pigment do not confound analysis of cell death or cytokines.

Activation of the inflammasome likely leads to a more robust immune response that facilitates pathogen clearance. Indeed, the presence of the NLRP3 inflammasome was shown to be critical for bacterial clearance in a murine model of GBS sepsis (39). In such a model, activation of the inflammasome was clearly beneficial to the host. However, activation of a robust inflammatory response can be detrimental during pregnancy, leading to tissue damage and perinatal complications. While increased IL-1β has been associated with chorioamnionitis, fetal injury and preterm birth (42, 152, 153), mechanistic insight into microbial factors that trigger inflammasome activation and the consequence on fetal injury and preterm birth was not previously known. Furthermore, a large number of studies on preterm birth have utilized either purified PAMPs that trigger TLRs such as LPS or peptidoglycan (152, 154, 155), heat killed bacteria (130, 156) or direct infusion of cytokines into amniotic fluid (42, 157) to ascribe the role of cytokines and other host factors in infection-associated preterm birth. However, these

strategies fail to completely recapitulate the events that occur during bacterial infections *in utero*. In a murine model of *in utero* GBS infection, we observed that hemolytic and hyperhemolytic strains induce preterm birth and cause significantly more fetal death than nonhemolytic strains, similar to recent observations in a vaginal model of ascending GBS infection (158). Our results comparing pregnant WT and NLRP3-deficient mice suggest that pigment-mediated activation of the NLRP3 inflammasome enhances GBS infection-associated fetal injury. Thus, contrary to the benefits of inflammasome activation during systemic GBS infection, inflammasome activation appears to be detrimental during pregnancy. The balance between these two requirements – the necessity of inflammation to protect the mother from infection and the necessity of an anti-inflammatory environment to promote fetal survival – is critical to maternal and child health.

Our studies also reveal that GBS pigment-mediated fetal injury is observed even in the absence of the NLRP3 inflammasome. These data indicate that the hemolytic nature of the pigment is also likely to contribute to fetal injury. This can be expected as the pigment more efficiently lyses RBC (EC_{50} < 0.1 μM) when compared to IL-1β induction (0.25 μM) or pyroptosis (1–2 μM). It is also likely that inflammasome and caspase 3/7 independent mechanisms contribute to GBS infection-associated fetal injury. Taken together, these data suggest that prevention of fetal injury and preterm birth caused by infection of hyperhemolytic GBS strains cannot solely be achieved by inhibition of the inflammasome or by caspase inhibitors. Rather, the generation of analogues or vaccines that prevent pigment-mediated hemolysis and pyroptosis may be necessary for prevention of GBS-associated host injury and preterm birth. Although our studies comparing GBS-induced fetal death in NLRP3KO and WT C57BL/6J mice were performed using the hyperpigmented GBS Δ*covR* and isogenic

nonpigmented Δ*covR*Δ*cylE* strains, we have previously shown that the hypervirulent phenotype of GBSΔ*covR* in a murine model of systemic infection (34) and for penetration of human placenta (129) are reversed when the gene *cylE* required for hemolytic pigment production (51, 129) is deleted from the GBS Δ*covR* mutant (34, 129). Furthermore, deletion of *cylE* in GBS Δ*covR* did not restore the expression of CAMP factor, a CovR-activated gene (34). Nevertheless, CovR/S is a global regulator in GBS, and the possibility that hemolysin-independent CovR/S-regulated genes contribute to our observations cannot be excluded.

Given the potent biological activity of the pigment, it is necessary for pathogens such as GBS, which typically exist as commensals in the lower genital tract, to repress pigment expression to minimize host injury. It is likely that under certain conditions of environmental stress (*e.g.*, changes in pH (65, 144)), GBS utilizes signaling systems such as CovR/S to derepress expression of pigment genes leading to barrier disruption and ascending infection. Understanding how pathogen-encoded lipid toxins mediate host cell lysis and contribute to infection and inflammation will be critical for developing preventive measures. This is relevant beyond GBS, as opportunistic pathogens such as *Bacillus cereus* contain genes homologous to those encoding the GBS hemolytic pigment/ lipid toxin (129), and other rhamnolipid toxins are produced by pathogens such as *Pseudomonas aeruginosa* and *Burkholderia pseudomallei* (115, 159). It is also likely that other pathogens encode yet to be discovered hemolytic and cytolytic lipid toxins. In summary, we show that the GBS hemolytic pigment functions as a double-edged sword causing colloidal osmotic lysis or NLRP3 inflammasome activation and pyroptosis, which together exacerbate fetal injury and preterm birth. These findings emphasize the importance of cytotoxic

lipids in fetal injury and have important implications for prevention of GBS pigment-mediated fetal injury and preterm births.

Materials and Methods

Ethics Statement

Written informed patient consent for donation of human blood was obtained with approval from the Seattle Children's Research Institute Institutional Review Board (protocol # 11117) as per the principles in the WMA Declaration of Helsinki and Dept. of Health and Human Services Belmont Report. Children under the age of 18 were not recruited for donation of human blood.

All animal experiments were approved by the Seattle Children's Research Institutional Animal Care and Use Committee (protocols #13907 and #13311) and performed in strict accordance with the recommendations in the Guide for the Care and Use of Laboratory Animals of the National Institutes of Health (8^{th} Edition). All surgery was performed under anesthesia, and every effort was made to minimize suffering and animal use.

Materials, bacterial strains, and cell lines

All chemicals were purchased from Sigma Aldrich, unless otherwise noted. Cell culture medium was purchased from Fisher Scientific. The WT GBS strains A909 and COH1 used in this study are clinical isolates obtained from infected human newborns (116, 117), The GBS Δ*cylE*, Δ*covR*, and Δ*covR*Δ*cylE* mutants were previously derived from A909 and COH1 (34, 51, 90, 129). Routine cultures of GBS were grown in tryptic soy broth (TSB, Difco Laboratories) at 37^{o}C in 5% CO_2. WT THP-1s were kindly provided by Dr. Ferric C Fang. THP-1 cells stably transfected with shRNA to NLRP3 (C CIAS1), ASC or scrambled controls used in this study

have been previously described (137, 160). THP-1 cells were routinely cultured in RPMI with 10% fetal bovine serum as described (137, 160).

Purification of the GBS pigment

GBS pigment was purified as previously described (129). Briefly, pigment was extracted from WT GBS A909 using DMSO:0.1% TFA, precipitated using NH_4OH and column-purified using a Sephadex LH-20 (GE Healthcare) column as described (58, 107, 129). Fractions containing purified pigment were pooled, precipitated with NH_4OH, washed three times with HPLC grade water, twice with DMSO and lyophilized as described (129). As a control, the pigment extraction protocol was performed on the GBSΔ*cylE* strain and the extract used as a control in all experiments. The purified pigment was tested for the presence of pigment using mass spectrometry and NMR with Δ*cylE* extract as a negative control as described previously (129). Samples of pigment were also analyzed on protein and agarose gels to confirm the lack of DNA, RNA and protein contaminants. For hemolytic and cytotoxic assays, lyophilized pigment or control Δ*cylE* extract was dissolved in DMSO containing 0.1%TFA and 20% Starch (Difco; DTS) to a final concentration of 200 μM. The samples were incubated overnight at room temperature in the dark prior to use.

Hemolysis assays

Hemolysis assays with purified GBS pigment were performed using human RBCs as described previously (129). For osmotic protection assays, RBCs were pre-incubated with purified pigment for 2 minutes at room temperature. Cells were then pelleted by centrifugation and the supernatant extracted to remove unintercalated pigment. The RBCs were then resuspended in PBS or PBS containing a 30mM solution of osmoprotectant with hydrodynamic

radius 0.40 nm (PEG200), 0.56 nm (PEG400), 0.89 nm (PEG1000), 1.1 nm (PEG1500), or 1.6 nm (PEG3000) (107, 161)), and incubated for 1 hr at 37°C. Because SDS-mediated lysis occurred instantly which prevented preincubation with RBC, SDS was added to the resuspended RBCs which was then incubated for 1 hr.

Hemoglobin and potassium efflux kinetics

To measure the kinetics of hemoglobin and potassium release, human blood was centrifuged and washed three times in potassium-free PBS and resuspended to 2% RBCs in potassium-free PBS. RBCs were diluted 1:1 with potassium free PBS in a beaker and continuously stirred on a magnetic stir plate. At time 0, either 400 nM GBS pigment or an equivalent amount of control Δ*cylE* extract or 0.47 μM *Staphylococcus aureus* α-toxin (Calbiochem) were added. The concentration of free potassium in the supernatant at each time point was measured using an ion-specific electrode as per manufacturer's protocol (Cole Parmer Combination Ion Specific Electrode, EW-27504-26). Hemoglobin release was measured by centrifuging a 120 μL aliquot of the mix for 2 min at 1200*g* and measuring the absorbance of the supernatant at 420 nm. Percent release was calculated using the formula Percent Release = (value-minimum)/(maximum-minimum) x 100, where the minimum was the value at $t = 0$, and the maximum was the value obtained via lysis with Triton X-100 (60). A sigmoidal nonlinear regression was performed using Prism software (GraphPad) to determine the time to 50% release.

Conductance measurements through lipid bilayers

The single-channel conductance of the GBS pigment was analyzed on a custom-made lipid bilayer apparatus described previously (134). To test how the pigment alters membrane stability, we used lipid bilayers or black lipid membranes (BLMs) composed of 1,2-diphytanoyl-sn-

glycero-3-phosphocholine (DPhPC; Avanti Polar Lipids) as the model. Lipid bilayers or BLMs were generated as previously described (134). Briefly, the reaction vessel was a Teflon block with two wells connected by a "U-tube." One end of this U-tube was closed except for a 20μm aperture which was painted with DPhPC dissolved in hexadecane. The wells and tube were filled with buffer (0.3 M KCl, 10 mM HEPES, pH 7.4 ± 0.05) and a pipette was used to blow and retract a 10 μl air bubble atop the lipid-painted aperture, producing the BLM as a barrier between the two chambers of the tube. Voltage (180 mV) was applied to the system, and current was measured with a patch clamp amplifier (Axon 200B). Pigment (2 μM or 75 nM) or control Δ*cylE* extract was added to one chamber, and changes in current were monitored for 10 min. As controls, BLMs were incubated with either the pore forming toxin MspA (0.51 nM; (134)) or the detergent sodium dodecyl sulfate (350 μM).

Derivation of primary macrophages from human blood

Peripheral blood mononuclear cells (PBMCs) were isolated using methods previously described (162). Briefly, 60 mL of blood was collected from independent healthy human donors into heparinized tubes. The human blood was diluted 1:1 with PBS, and leukocytes were isolated using UNI-SEP maxi tubes (NOVAmed) following manufacturer's instructions. Briefly, UNI-SEP maxi tubes were spun at 1000g for 20 min and the mononuclear cell layer retrieved using a pipette. The isolated cells were then washed with RPMI 1640 and selection for CD14+ cells was performed using the MACS magnetic separation columns (Miltenyi Biotec) as per manufacturer's instructions. Subsequently, the CD14+ cells were seeded in 96-well tissue culture plates at $1x10^5$ cells/well in 100 μL RPMI 1640 supplemented with 10% FBS containing 100 IU/mL penicillin, 100 μg/mL streptomycin, and 20 ng/mL macrophage colony stimulating factor

(M-CSF)-1 (Life Technologies). The tissue culture medium was replaced on day 5 and on day 7, PBMC-derived macrophages were directly infected with GBS strains or primed with LPS (100 ng/mL) for 3 hrs before exposure to purified pigment (see below).

Derivation of macrophages from THP-1 monocytic cells

For treatment of THP-1-derived macrophages with GBS or pigment, undifferentiated THP-1 monocytes were resuspended in medium containing 100 nM phorbol 12-myristate 13-acetate (PMA) and seeded at 10^5 cells/well into 96-well plates as described (7, 163). After 2 d of incubation, medium was replaced with PMA-free medium, incubated overnight and exposed to either GBS strains or purified pigment as described below.

Cytolysis assays

PBMC-derived macrophages and THP-1-derived macrophages as above were used to measure the cytolytic activity of the GBS strains or purified GBS pigment. For bacterial infection, PBMC- and THP-1-derived macrophages were infected with mid-log phase GBS ($O.D_{600nm}$=0.3) at an MOI (multiplicity of infection) of 1 for 4 hrs. Cytolysis was measured by LDH release (LDH kit, Clontech) as per manufacturer's instructions. For pigment-mediated cytolysis, cells were washed 4 times with PBS and treated with serum-free medium containing GBS pigment (0.125 – 4 μM). DTS alone or Δ*cylE* extract were used as controls. After 4 hrs of incubation, supernatants were removed for cytokine analysis and the media was replaced with TC medium containing serum and Alamar Blue (Life Technologies). After 2 hrs of incubation, the fluorescence in each well was measured as per manufacturer's protocol using a BioTek Plate Reader.

For both bacterial- and pigment-mediated cytolysis, percent of dead cells was calculated by normalizing to untreated cells (0% killing) or cells treated with 1% Triton-X 100 (100% killing).

For experiments with the caspase 1 inhibitor, 50-200 μM Z-YVAD-FMK (R&D Systems), 100μM Z-DEVD-FMK (Cayman Chemical), or an equivalent amount of control DMSO were added to THP-1 cells, 1 hr prior to addition of pigment or controls.

Measurement of cytokine production

Supernatants from the cytolysis assays (see above) were used for cytokine analysis by either Luminex assay (Affymetrix) or ELISA (IL-1β: R&D Systems; IL-18: MBL) per the manufacturer's instructions.

Measurements of caspase-1 activation and membrane permeabilization

Activation of caspase 1 and changes in membrane permeability due to GBS pigment was measured using flow cytometry (LSRII, BD Biosciences). Briefly, THP-1 cells grown on non-TC treated plates were washed and resuspended to 5-10 x 10^5 cells/mL in TC medium lacking serum. For membrane permeabilization assays, uptake of the membrane-impermeable dye propidium iodide (PI, Life Technologies) was measured. Briefly, THP-1 cells were treated for 30 min with 1 μM pigment or an equal volume of control Δ*cylE* extract. PI was added in the last 10 min of incubation and uptake measured by flow cytometry as per manufacturer's instructions. PI+ populations were identified compared to an untreated sample. Data are representative of two independent experiments with independent preparations of pigment. For caspase 1 activation assays, cells were incubated with 1 μM pigment or an equal volume of control Δ*cylE* extract for 1 hr. 660-YVAD-FMK (Immunochemistry Technologies) was then added, and incubation continued for another hour. Caspase 1 activation was measured by flow cytometry as per

manufacturer's instructions. FLICA+ populations were identified, and percent FLICA+ cells were calculated. Data shown are representative of three independent experiments with independent preparations of pigment. Data were collected with the FACSDiva software and were analyzed using the FlowJo software system.

Quantification of intracellular potassium concentration

Intracellular potassium concentration was measured by ion-coupled plasma atomic emission spectroscopy (ICP-AES) as previously described (139). Briefly, THP-1 cells in 12-well plates (10^6 cells/well, seeded in 1 mL) were treated as described above with 1μM pigment. At various time points (0, 30, 60, 120, 180, 240 min), supernatant was removed and wells washed with 1 mL potassium-free PBS. Subsequently, 1 mL of 3% HNO_3 was added to the wells to release intracellular potassium, and incubated for 30 min. 1 mL of HPLC-grade water was then added, and samples were analyzed by ICP-AES (Perkin Elmer Optima 8300). Percent intracellular potassium was calculated relative to an untreated sample.

Murine model of intrauterine GBS infection

Wild type CD-1, C57BL/6-J, or NLRP3-deficient mice (145, 146) were used. Mice were obtained from Jackson Laboratories or Charles River Laboratory, USA and were housed at the Seattle Children's Research Institute Vivarium in accordance with the Guide for the Care and Use of Laboratory Animals of the National Institutes of Health (8th Edition). Mice at 6-10 wks of age were bred in-house for time-mated pregnancy. During mating, a female was paired individually with a male. Infected pregnant mice were housed individually. Intrauterine infections of pregnant female mice were performed as previously described (142, 143) with a few modifications. Briefly, on E14.5 of pregnancy, dams were anesthetized using isoflurane, and

a midline laparotomy was performed to expose uterine horns as described previously (142, 143). Bupivacaine (1-2 mg/kg) was infused along the incision site to provide local anesthesia. Dams were infected with 100 μL of $10^6 – 10^7$ CFU of GBS into the right uterine horn between the first (P1) and second (P2) fetal sacs most proximal to the cervix (also see Fig. 7A). After inoculation, sterile saline was applied to the exposed uterus, and the uterus was returned to the abdomen. The muscle and skin layers were closed using absorbable suture as described (142, 143) and dams were returned to their cage and with monitoring every 12 hrs for signs of preterm delivery. Three days post-infection or at the onset of preterm birth (vaginal bleeding and pups in cage), animals were placed under deep isoflurane anesthesia and repeat laparotomy was performed. Preterm birth was defined as delivery of at least one pup before this time point. *In utero* fetal death (IUFD) was identified by white discoloration and fetal resorption, and % Fetal Death was calculated using the formula: (# of dead fetuses)/(Total # of fetuses) x 100. Fisher's exact test was used to compare statistical differences in fetal death by comparing the number of dead and the number of live fetuses obtained from 6 pregnant mice in each group. The bacterial load in the fetuses (combined CFU obtained from placenta and entire body of each fetus) was enumerated using serial dilution and plating of homogenized tissues. Cytokine IL-1β levels were measured in supernatants of homogenized tissues from placenta and fetus using Luminex assays. Portions of the right uterine horn were processed for histology as described previously (129). All experiments are accurately reported as ARRIVE guidelines.

Statistical Analysis

Student's *t*-test, Mann-Whitney test, Bonferroni's multiple comparison test following ANOVA, or Fisher's exact test were used to estimate differences as appropriate, and *p*-value

<0.05 was considered significant. A non-linear regression analysis followed by an extra sum-of-squares F test was used to estimate and compare time to 50% release and *p* value <0.05 was considered significant. These tests were performed using GraphPad Prism version 5.0 for Windows, GraphPad Software, USA, www.graphpad.com. All *in vitro* experiments were performed a minimum of three independent times in triplicate and analyzed for significance without predetermined assumptions. Based on the expectation that GBS infection will cause fetal injury, animal studies were performed with an *n=6* per group to provide an estimated statistical power ranging from 67% to 82% depending upon standard deviation at an alpha level of 5% (~ 95% confidence level). Animals were randomly paired for pregnancy and infection. No bias was introduced for infection, *i.e.*, animals were not pre-chosen for infection with a particular GBS strain. Analysis of fetal death was performed in an unbiased manner. Histology sections were scored in a blinded fashion.

Acknowledgements

We thank Dr. Ferric C. Fang for providing THP-1 macrophages and Dr. Jenny P-Y Ting for providing the shRNA-transfected THP-1 macrophages. We thank Dr. Ida Washington for assistance with the murine model of intrauterine infection and Dr. Adrienne Roehrich for her assistance with ICP-AES. We are grateful to Drs. Brad Cookson, Ferric C. Fang, Joseph Mougous and David Sherman for helpful discussions. We are grateful to the human subjects who participated in this study. We thank members of the Rajagopal and Gundlach laboratories for technical assistance and input. We also thank Joyce Karlinsey and Jeffrey Myers for their assistance.

This work was supported by funding from the National Institutes of Health, Grants R01AI100989 to L.R and K. A. W, R56AI070749, R01AI112619 and R21AI109222 to L.R., R01AI088255 and Burroughs Wellcome Fund Career Award for Medical Scientists to J.A. D.

C.W and J. V were supported by the NIH training grant (T32 AI07509, PI: Lee Ann Campbell). C.W was also supported by UW GO-MAP Fellowship and J. M. S was supported by UW PREP NIH NIGMS 5R25 GM086304. The content is solely the responsibility of the authors and does not necessarily represent the official views of the National Institutes of Health.

Author Contributions

C.W., J. V., C.G., E.B., J.M.S., K.D., L.N, E.A.D. E., performed the experiments, J. A. D and J. H. G provided reagents, C.W., J. V., C.G., E.B., J.M.S., K.D., L.N., E.A.D. E., J.H.G., M.A.E., D. L., J.A.D., K.A.W., and L. R designed the research, analyzed the results and wrote the paper.

Conflict of Interest

The authors declare no competing financial interests.

Figures

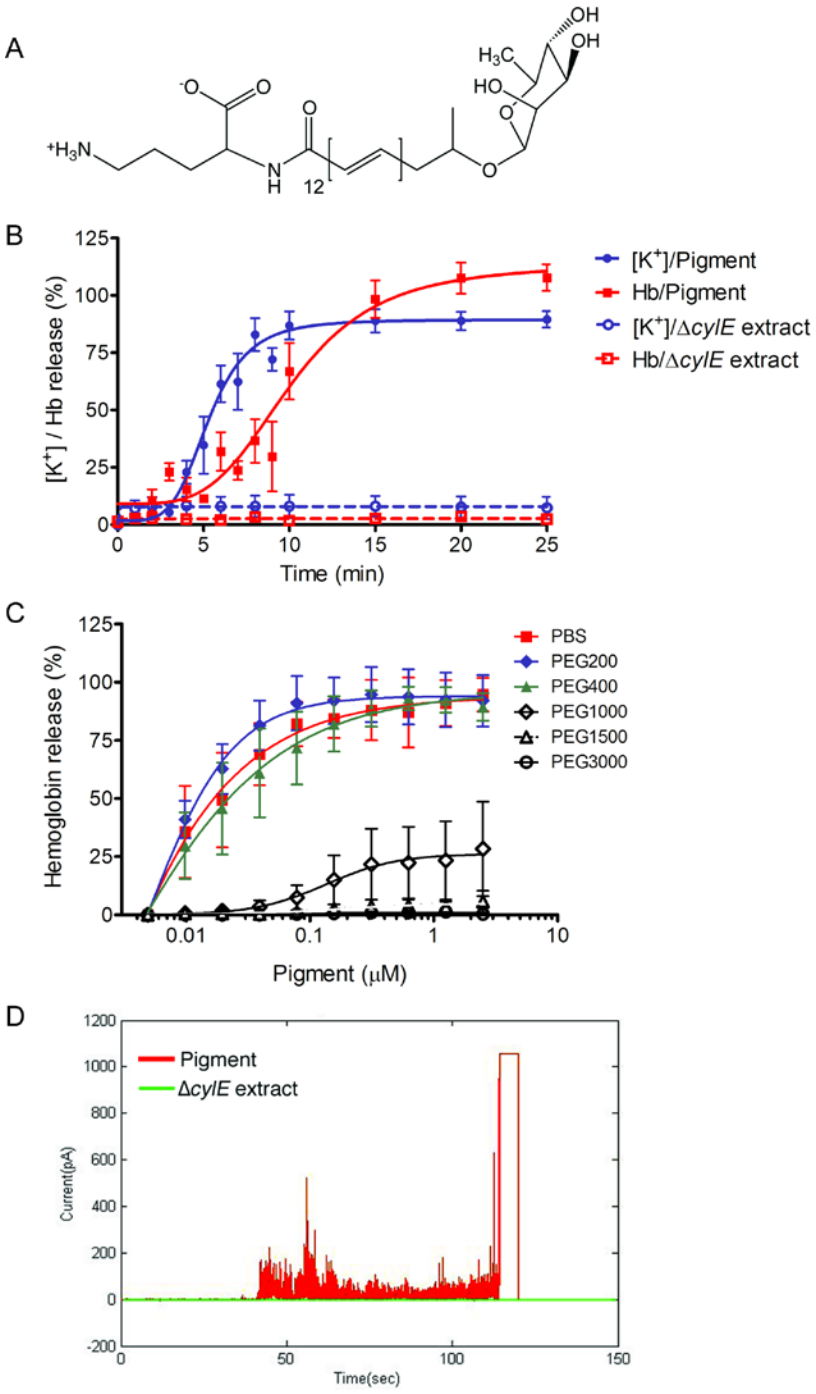

Figure 3-1. Colloidal-osmotic lysis and membrane permeabilization caused by the GBS pigment/lipid toxin.

(A) The GBS pigment, also known as granadaene, is an ornithine rhamnopolyene (58).
(B) Human red blood cells (RBC) were incubated with 400 nM pigment or control Δ*cylE* extract and kinetics of K^+ and Hb release was monitored. Data shown are the average and SEM of six independent experiments. The time to 50% K^+ and 50% Hb release with pigment was 4.8 min and 8.4 min, respectively; $n=6$, $p < 0.0001$, extra sum-of-squares F test, error bars ± SEM.
(C) Role of osmoprotectants in pigment treated RBC. Human RBC were pre-incubated with GBS pigment for 2 minutes at RT, centrifuged, and resuspended in the presence and absence of 30 mM osmoprotectant with hydrodynamic radius of 0.40 nm (PEG200), 0.56 nm (PEG400), 0.89 nm (PEG1000), 1.1 nm (PEG1500), or 1.6 nm (PEG3000) respectively. Release of Hb was measured after 1 hour incubation at 37°C. Data shown are the average and SEM of three independent experiments; error bars ± SEM.
(D) Characteristics of membrane permeabilization by the GBS pigment in artificial lipid bilayers. Lipid bilayers were generated using diphytanoylphosphatidylcholine (DPhPC) and treated with either 2 μM pigment or equivalent amount of the control Δ*cylE* extract. In the pigment treated sample, channel conductance indicating disruption of the membrane is seen within 45 seconds. Erratic and non-discrete fluctuations in current are observed, suggesting the formation of multiple small, membrane defects. The bilayer eventually breaks at 120 seconds. In lipid bilayers treated with the control Δ*cylE* extract, the mean ionic current trace remains constant at 0 pA, showing no membrane disruption. Data shown are representative of three independent experiments.

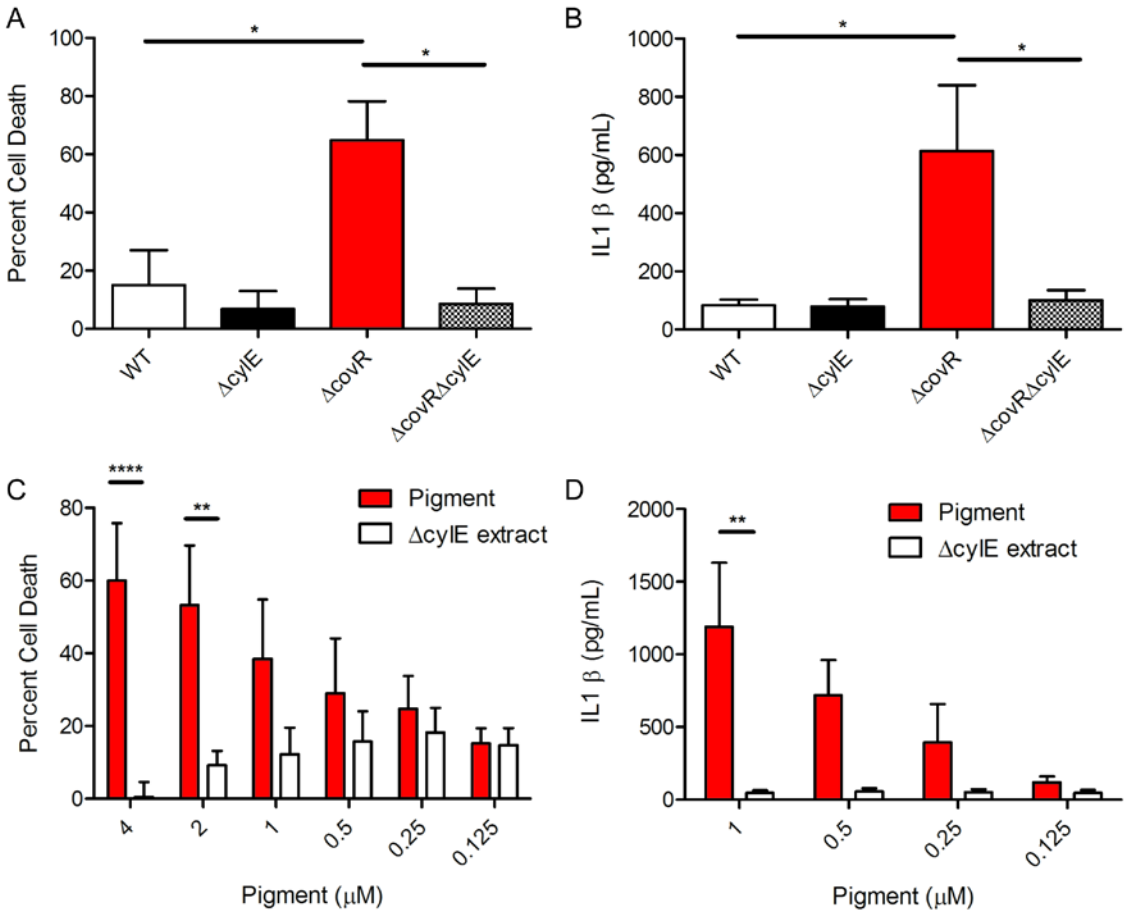

Figure 3-2. The GBS pigment toxin/lipid toxin is proinflammatory and cytotoxic to primary human macrophages.

(A, B) PBMC derived macrophages were treated with GBS WT, Δ*cylE*, Δ*covR*, or Δ*covR*Δ*cylE* at an MOI of 1 and incubated for four hours. Cytotoxicity was measured by LDH release (A) and IL1β release in supernatants was measured by ELISA (B). Data shown are the average of four independent experiments performed in triplicate, error bars ± SEM. Significance was determined using Bonferroni's multiple comparison test following ANOVA. (A) *n=4*, **p* = 0.021 for WT vs. Δ*covR*; **p* = 0.01 for Δ*covR* vs. Δ*covR*Δ*cylE*. (B) *n=4*, **p* = 0.031 for WT vs. Δ*covR*; **p* = 0.036 for Δ*covR* vs. Δ*covR*Δ*cylE*. (C, D) PBMC derived macrophages primed with 100 ng/mL LPS for three hours were incubated with various concentrations of GBS pigment or control Δ*cylE* extract for four hours. Cytotoxicity was measured by alamar blue assay (C) and IL1β release from pigment or Δ*cylE* extract treated cells was measured by Luminex assay (D). Data shown are the average of four independent experiments performed in triplicate, error bars ± SEM. Significance was determined using Bonferroni's multiple comparison test following ANOVA. (C) *n=4*, *****p* < 0.0001, ***p* = 0.002. (D) *n=4*, ***p* = 0.005.

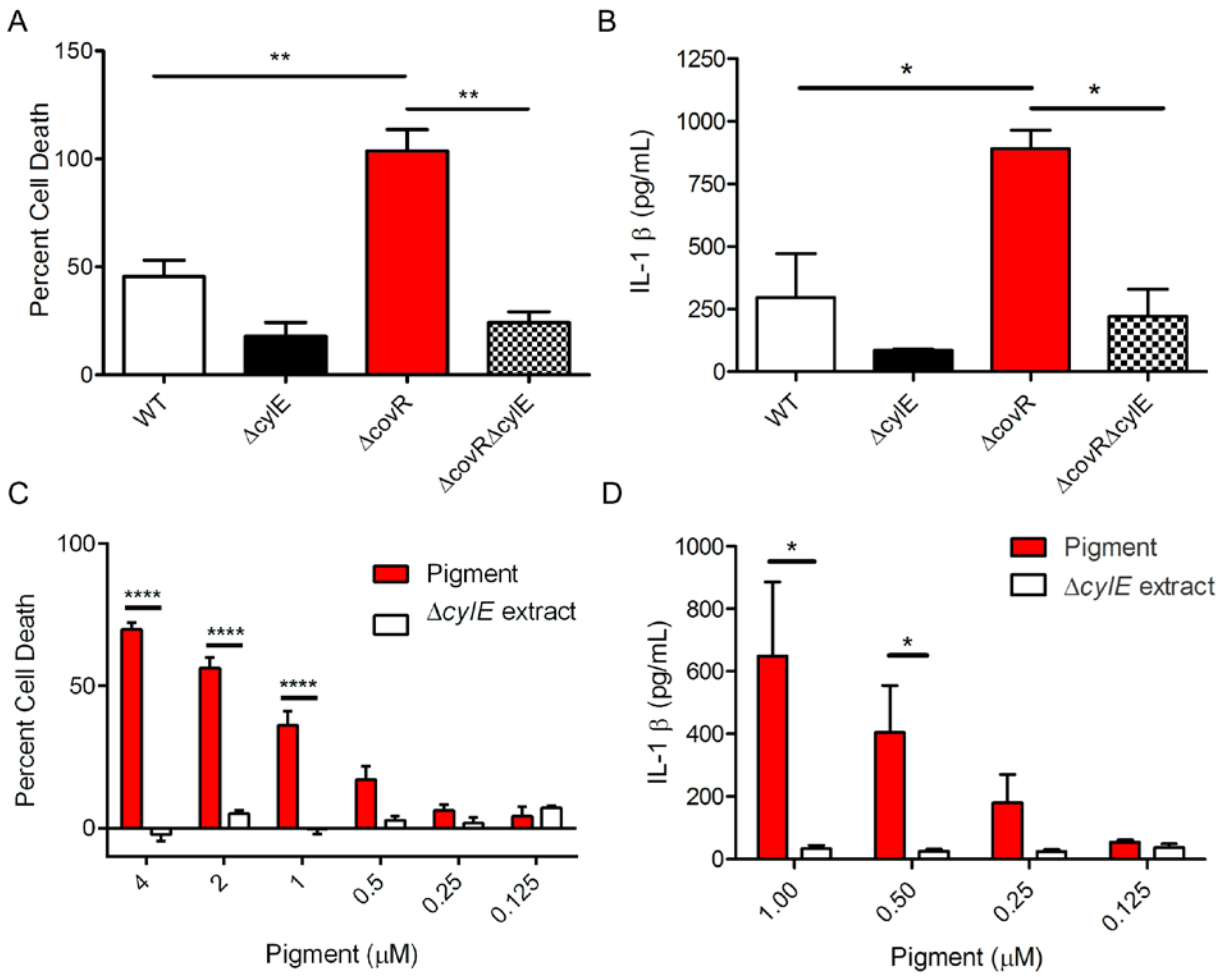

Figure 3-3. The GBS pigment toxin/lipid toxin is proinflammatory and cytotoxic to immortalized THP-1 monocyte derived macrophages.

(A, B) WT THP-1 macrophages were treated with GBS WT, Δ*cylE*, Δ*covR*, or Δ*covR*Δ*cylE* at an MOI of 1 and incubated for four hours. Cytotoxicity was measured by LDH release (A) and IL1β release in supernatants was measured by Luminex assay (B); data shown are three independent experiments performed in triplicate, error bars ± SEM. Significance was determined using Bonferroni's multiple comparison test following ANOVA. (A) *n=3*, ***p* = 0.0080 for WT vs. Δ*covR*; ***p* = 0.0016 for Δ*covR* vs. Δ*covR*Δ*cylE*. (B) *n=3*, **p* = 0.03 for WT vs. Δ*covR*; **p* = 0.02 for Δ*covR* vs. Δ*covR*Δ*cylE*. (C, D) WT THP-1 macrophages were incubated with various concentrations of GBS pigment or control Δ*cylE* extract for four hours. Cytotoxicity was measured by alamar blue assay (C) and IL1β release from pigment or Δ*cylE* extract treated cells was measured by luminex assay (D). Data shown are three independent experiments performed in triplicate, error bars ± SEM. Significance was determined using Bonferroni's multiple comparison test following ANOVA. (C) *n=3*, *****p* < 0.0001. (D) *n=3*, **p* = 0.01.

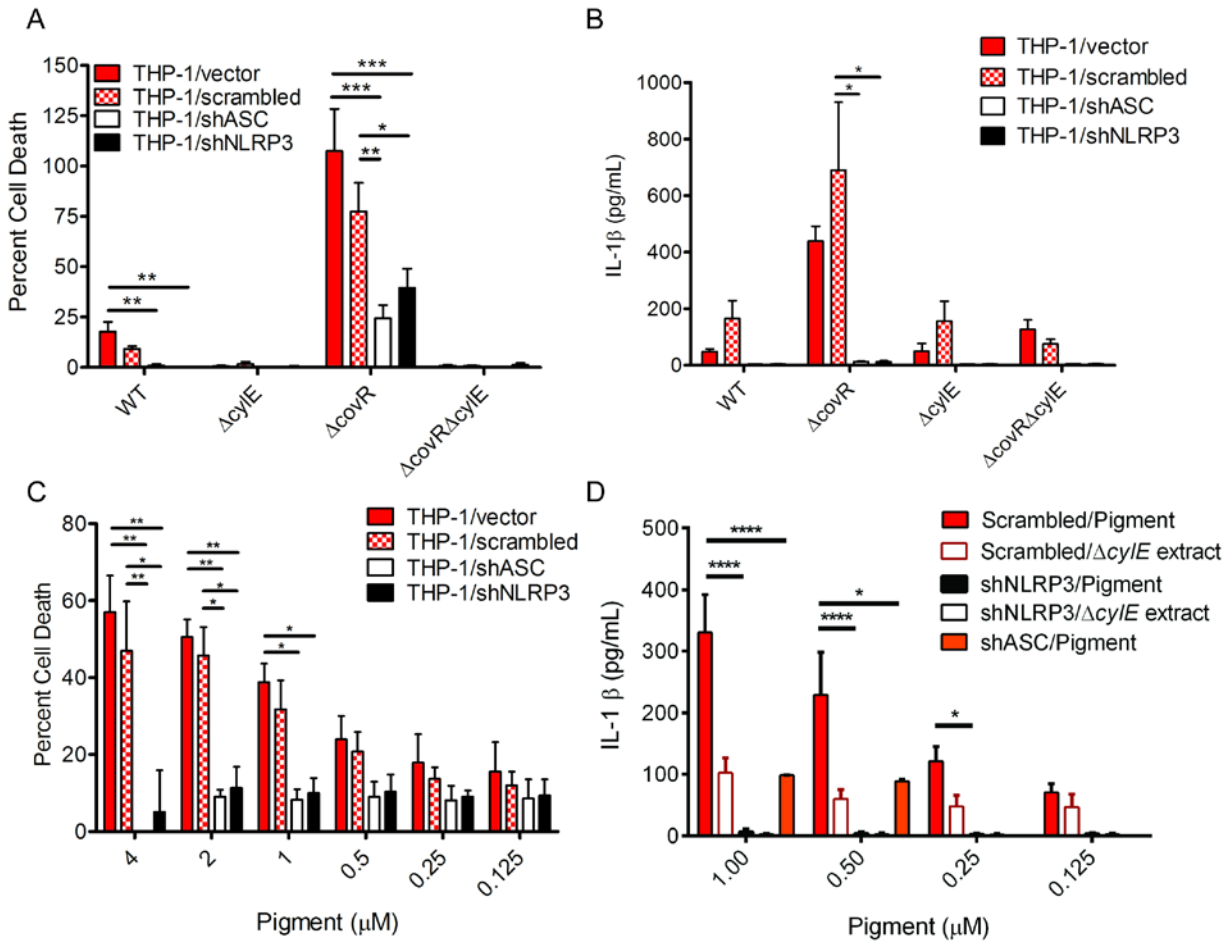

Figure 3-4. The GBS pigment induces NLRP3 inflammasome-dependent cell death in human macrophages.

(A, B). THP-1 macrophages transfected with empty vector, scrambled control, shASC, or shNLRP3 were treated with GBS WT, Δ*cylE*, Δ*covR*, or Δ*covR*Δ*cylE* at an MOI of 1 and incubated for four hours. Cytotoxicity was measured by LDH release (A) and IL1β release in supernatants was measured by Luminex assay (B). Data shown are three independent experiments performed in triplicate and were analyzed using Bonferroni's multiple comparison test following ANOVA, error bars ± SEM. (A) *n=3*, for WT: ** $p = 0.001$ (vector vs. shNLRP3), ** $p = 0.0016$ (vector vs. shASC); for Δ*covR* : ***$p = 0.0008$ (vector vs. shNLRP3), *** $p = 0.0001$ (vector vs. shASC), *$p = 0.047$ (scrambled vs. shNLRP3), ** $p = 0.0054$ (scrambled vs. shASC). Data obtained from THP-1/vector was not significantly different from THP-1/scrambled, $p = 0.18$. (B) *n=3*, *$p = 0.025$. Data obtained from THP-1/vector was not significantly different from THP-1/scrambled, $p = 0.89$. (C, D) The shRNA THP-1 macrophages were incubated with various concentrations of GBS pigment or Δ*cylE* extract for four hours. Cytotoxicity was measured by alamar blue assay (C) and IL1β release in supernatants was

measured by Luminex assay (D). Pigment-mediated cytotoxicity is dependent on the NLRP3 inflammasome components, suggesting that pigment is inducing a programmed cell death. Data shown is the average of at least three independent experiments performed in triplicate and were analyzed using Bonferroni's multiple comparison test following ANOVA, error bars ± SEM.
(C) *n=3,* for 4 μM pigment: ** $p = 0.0063$ (vector vs. shNLRP3), ** $p = 0.0035$ (vector vs. shASC), * $p = 0.01$ (scrambled vs. shNLRP3), ** $p = 0.009$ (scrambled vs. shASC); for 2 μM pigment: ** $p = 0.0088$ (vector vs. shNLRP3), ** $p = 0.0066$ (vector vs. shASC), * $p = 0.01$ (scrambled vs. shNLRP3 or shASC); for 1 μM pigment: * $p = 0.02$ (vector vs. shNLRP3), * $p = 0.01$ (vector vs. shASC). Data obtained from THP-1/vector was not significantly different from THP-1/scrambled, $p = 0.99$. (D) *n=3,* **** $p < 0.0001$, * $p = 0.015$.

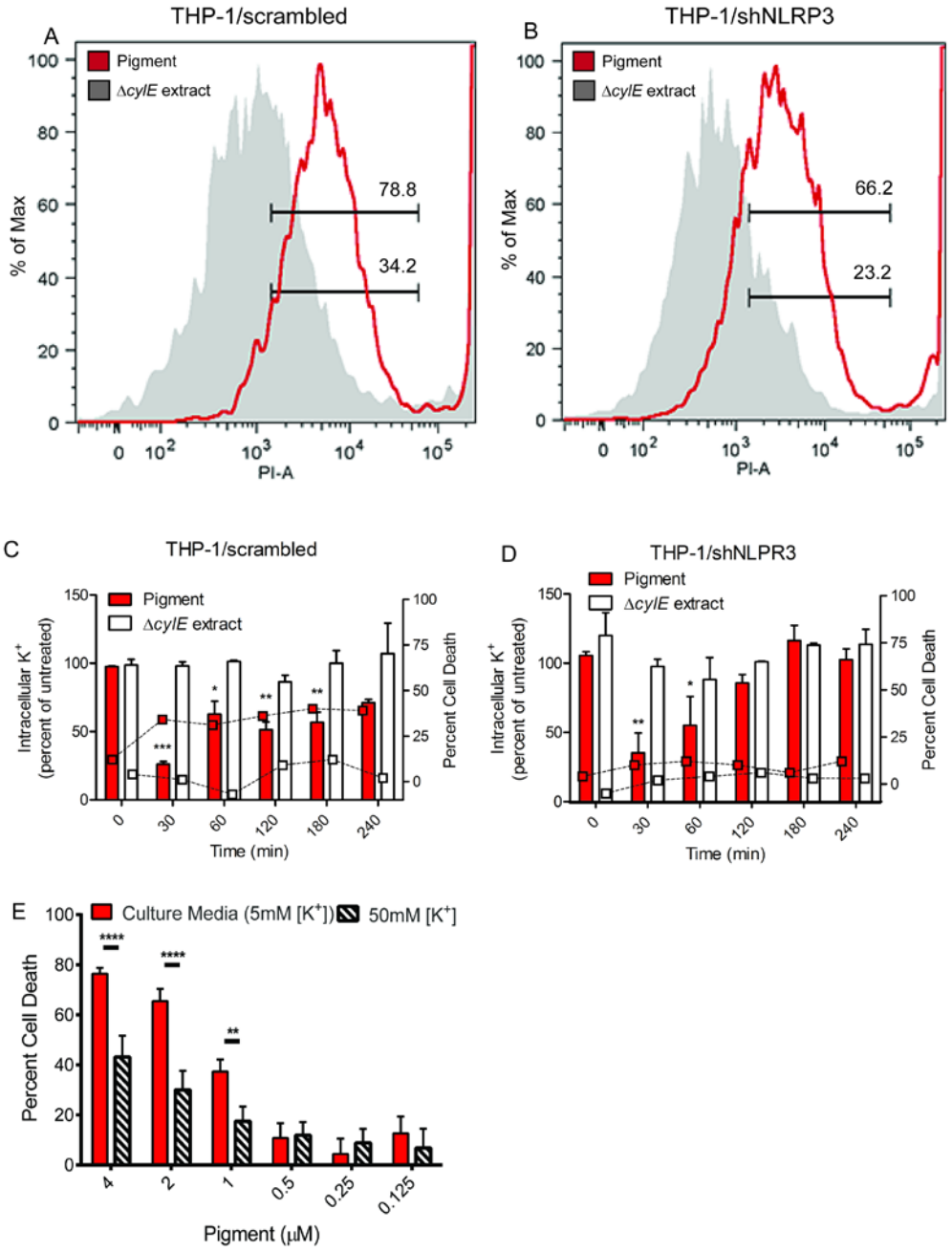

Figure 3-5. GBS pigment induces membrane permeabilization and K^+ efflux independent of the NLRP3 inflammasome.

(A, B) THP-1 macrophages proficient for NLRP3 (transfected with scrambled control, see A) or deficient for NLRP3 (shNLRP3, see B) were treated with 1 μM pigment or Δ*cylE* extract for 20 minutes, and propidium iodide (PI) was added during the final 10 minutes. PI uptake was measured by flow cytometry and data shown are representative of two independent experiments.

(C, D) Intracellular potassium concentration was measured by ICP-AES. THP-1 macrophages transfected with the scrambled control (C) or shNLRP3 (D) were treated with GBS pigment (1 μM) or equivalent amount of the Δ*cylE* extract. At various time points, cells were lysed and intracellular [K^+] was measured relative to untreated cells (see bars and left Y axis), and percent cell death was quantified by Alamar Blue (see squares, dotted connecting lines and right Y axis). Both NLRP3-proficient and -deficient macrophages initially lose intracellular K^+ due to GBS pigment (compare t = 0 min to t = 30 min) but the NLRP3 deficient cells (shNLRP3) are able to recover while the scrambled control do not, demonstrating that initial K^+ loss occurs independent of NLRP3. Data are average of three independent experiments performed with independent pigment preparations in triplicate and were analyzed using Dunnett's multiple comparison test following ANOVA; all data were compared to control at t =0, error bars ± SEM. (C) $n=3$, *** p = 0.0002, *p = 0.019, **p = 0.0032 for 120 min, **p = 0.0072 for 180min. (D) $n=3$, ** p = 0.0043, *p = 0.031.

(E) WT THP-1 macrophages were incubated with pigment in media containing either 5 mM or 50 mM potassium chloride, and cytotoxicity was measured by alamar blue assay. The addition of potassium chloride is able to protect the macrophages from cytolysis, demonstrating that K^+ efflux is essential for this process. Data shown are three independent experiments performed in triplicate and were analyzed using Bonferroni's multiple comparison test following ANOVA, error bars ± SEM ($n=3$, ****p < 0.0001, **p = 0.0036).

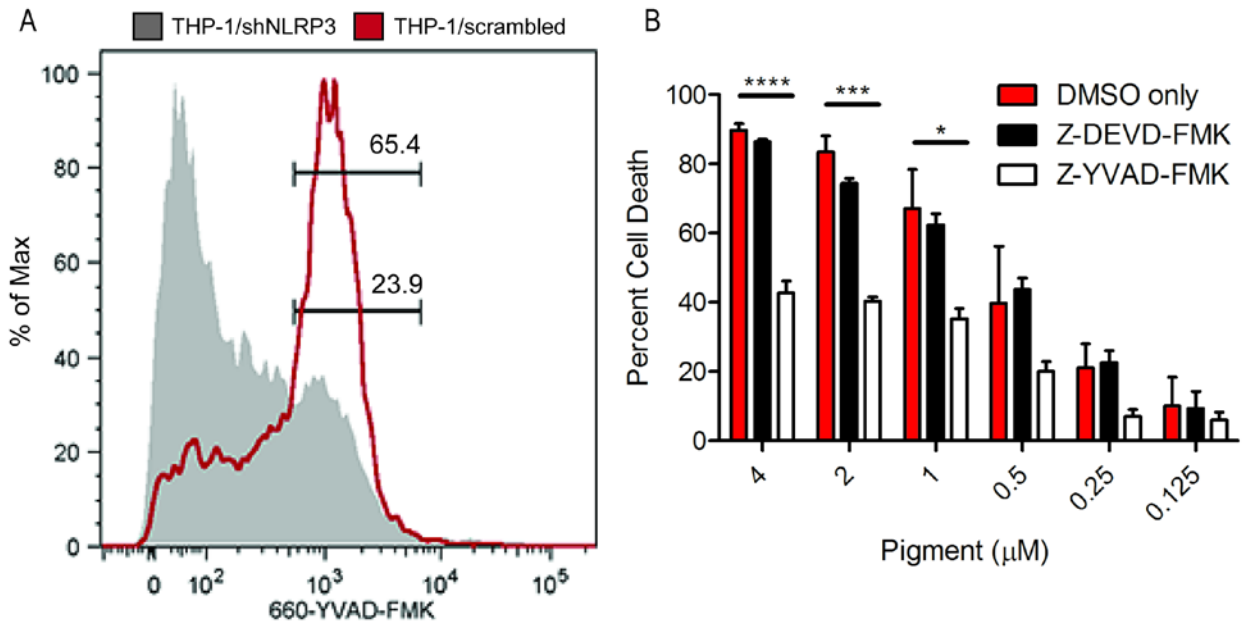

Figure 3-6. The GBS hemolytic pigment/lipid toxin induces caspase 1 activation and pyroptosis.

(A) THP-1 macrophages were treated with GBS pigment and caspase 1 activation measured by flow cytometry using a FLICA reagent. Pigment treatment of the scrambled shRNA control cell line induces more caspase 1 activation compared to the shNLRP3 cell line, demonstrating that the pigment activates caspase 1 exclusively through the NLRP3 inflammasome. Results are representative of three independent experiments.
(B) WT THP-1 macrophages were treated with the caspase 1 inhibitor Z-YVAD-FMK, the caspase 3/7 inhibitor Z-DEVD-FMK or DMSO only prior to treatment with the GBS pigment. YVAD is able to significantly decrease cytotoxicity in cells treated with GBS pigment, demonstrating that caspase 1 is required for GBS pigment-mediated cell death, characteristic of pyroptosis, while DEVD had no effect. Data are average of three independent experiments, error bars ± SEM. Significance was determined using Bonferroni's multiple comparison test following ANOVA ($n=3$, ****$p < 0.0001$, ***$p = 0.0002$. *$p = 0.014$).

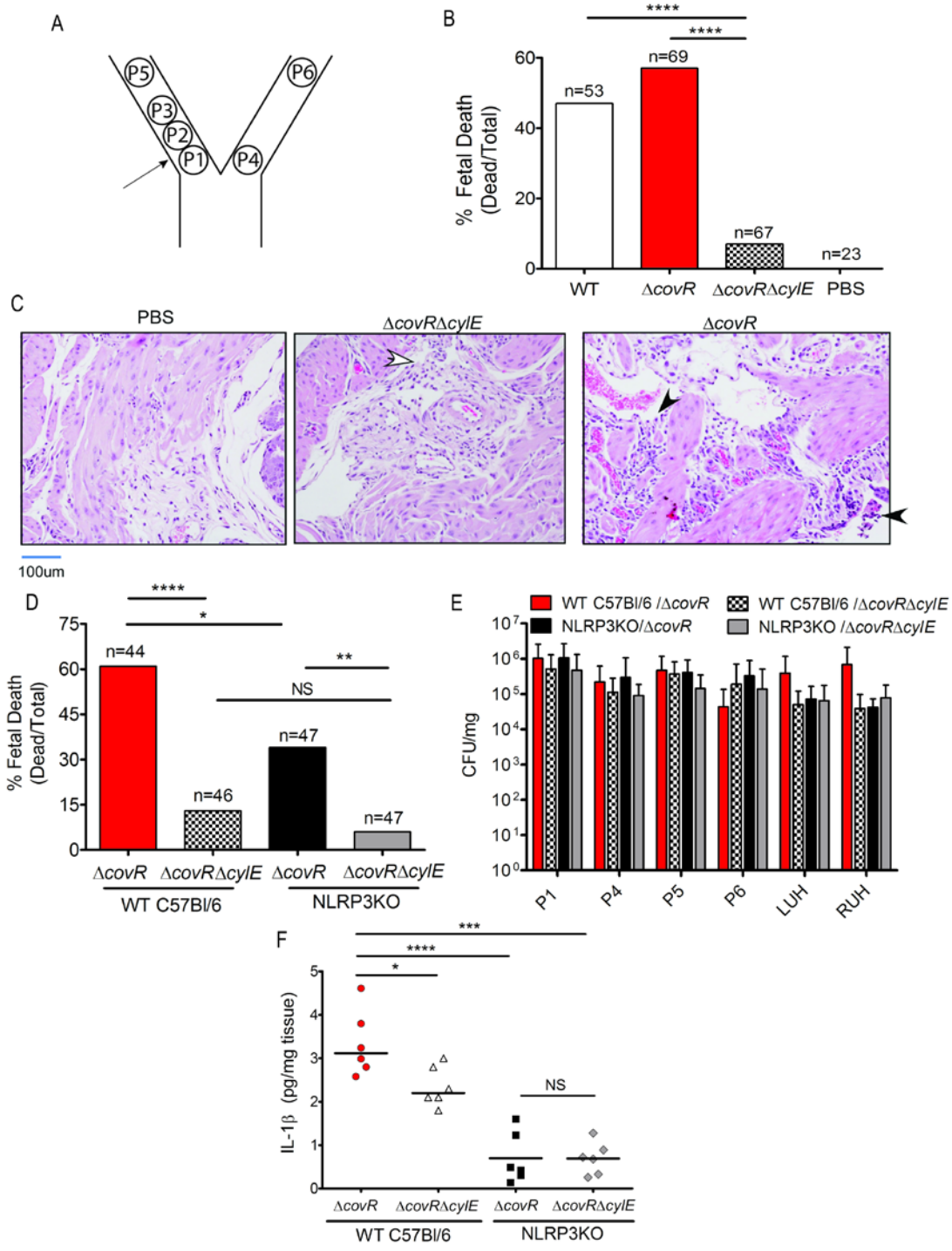

Figure 3-7. The GBS pigment causes fetal injury by NLRP3 inflammasome-dependent and -independent mechanisms.

Female pregnant wild-type (CD-1, C57BL/6) or NLRP3-deficient mice were injected *in utero* with 10^{6-7} CFU of GBS WT, Δ*covR*, or Δ*covR*Δ*cylE* and monitored for preterm birth; Surgery and GBS inoculation for each pregnant mouse was performed independently. Data shown are representative of experiments with 6 animals per group for each GBS strain and 2 animals were used for saline controls.

(A) Scheme of pup numbering *in utero* and injection site between fetuses P1 and P2 is shown.

(B) *In utero* fetal death in wild-type CD-1 mice due to infection with GBS WT, hyperhemolytic Δ*covR* and nonhemolytic Δ*covR*Δ*cylE*; Fetal death is represented by the number of dead fetuses /total number of fetuses obtained from 6 pregnant mice per group. '*n*' indicates total number of pups (both live and dead); **** $p < 0.0001$, Fisher's exact test.

(C) H and E staining of uterine tissue. Open arrow indicates the presence of few mononuclear cells whereas filled arrows indicate increased infiltration of inflammatory cells and necrotic debris.

(D) Fetal death due to infection with hyperhemolytic GBS Δ*covR* and nonhemolytic Δ*covR*Δ*cylE* in WT C57BL/6 and NLRP3 inflammasome-deficient mice; fetal death is represented by the number of dead fetuses /total number of fetuses obtained from 6 pregnant mice per group. '*n*' indicates total number of pups (both live and dead); * $p = 0.011$, ** $p = 0.0015$, **** $p < 0.0001$, Fisher's exact test. Fetal death due to Δ*covR*Δ*cylE* in WT C57BL/6 and NLRP3KO mice was not significant and is indicated as NS; $p = 0.31$, Fisher's exact test.

(E) Bacterial burden in fetal pups and uterine horns from mice infected with the various GBS strains (*n=6*/pup; of note pups that were delivered preterm were excluded from CFU enumeration. Scheme of pup numbering is shown in Fig. 7A. RUH and LUH indicate right uterine horn and left uterine horn, respectively. CFU are not significantly different between any groups (ANOVA, $p = 0.6$, error bars ± SEM).

(F) IL-1β levels in GBS-infected tissues (placenta & fetus, *n*=6/group) was measured by Luminex assay (*$p = 0.025$, *** $p = 0.0002$, **** $p < 0.0001$, Bonferroni's multiple comparison test following ANOVA). IL-1β levels was not significantly different in NLRP3KO mice infected with Δ*covR* compared to NLRP3KO mice infected with Δ*covR*Δ*cylE* mice and is indicated as NS; $p = 0.99$.

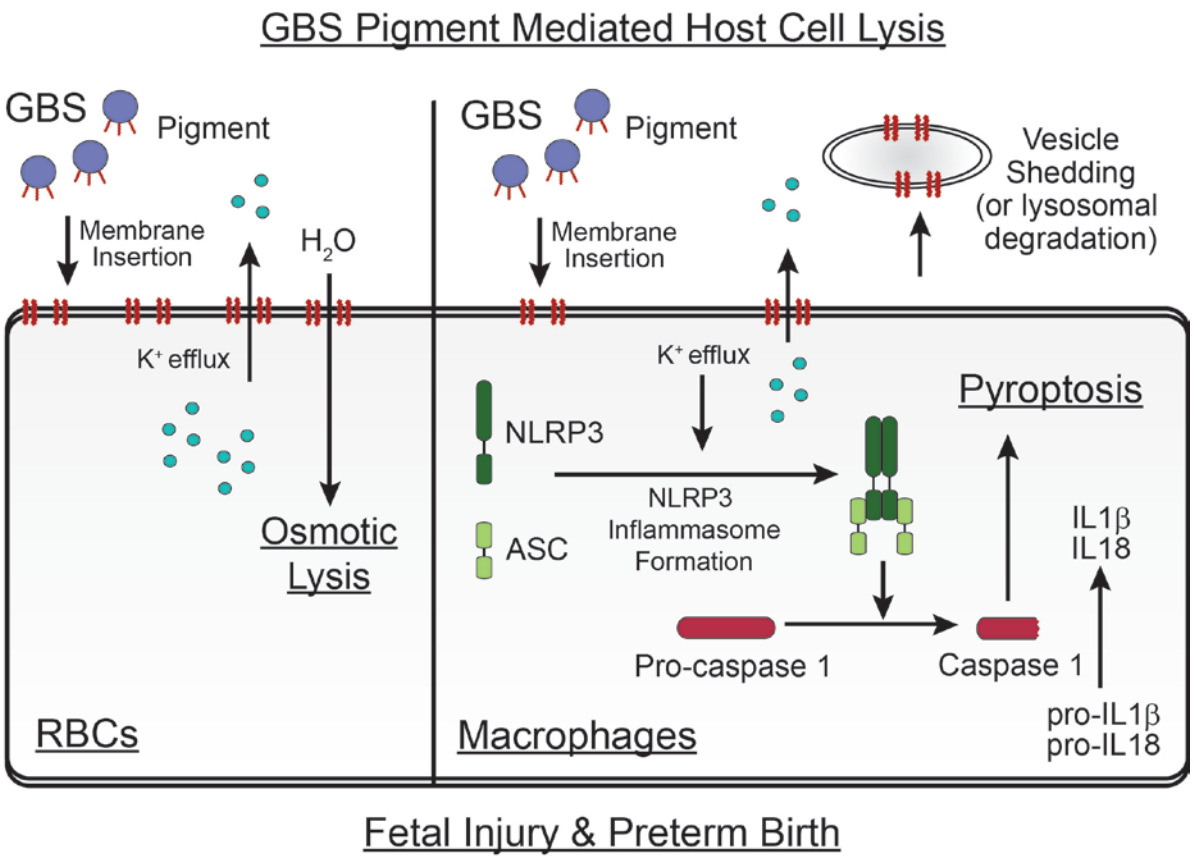

Figure 3-8. Proposed model on GBS pigment-mediated host cell lysis and preterm birth.

The GBS pigment intercalates into host cell membranes leading to membrane permeability and ion flux. In RBC, this leads to colloidal-osmotic lysis. In macrophages, the loss of intracellular potassium serves as a trigger for NLRP3 inflammasome formation. The activated inflammasome then activates caspase 1, which cleaves pro-IL-1β and pro-IL-18 to their active forms. Finally, caspase 1 activation causes cell death by pyroptosis. While NLRP3 dependent pyroptosis is the major form of cell death observed in macrophages exposed to purified pigment and hemolytic/pigmented GBS strains, hyperpigmented GBS strains induced low levels of cell death in NLRP3- and ASC-deficient macrophages that is independent of the inflammasome and caspase 3/7. In host cells that are either resistant or recover from pigment-induced membrane damage (*e.g.* NLRP3 deficient macrophages), we predict that lysosomal degradation of pigment or shedding of vesicles that contain pigment-membrane complexes and the turn-over of plasma membrane prevents cell death. The GBS pigment exacerbates fetal injury and preterm birth through the combined action of colloidal osmotic lysis and pyroptosis.

Supplementary Information

Supplementary Figures

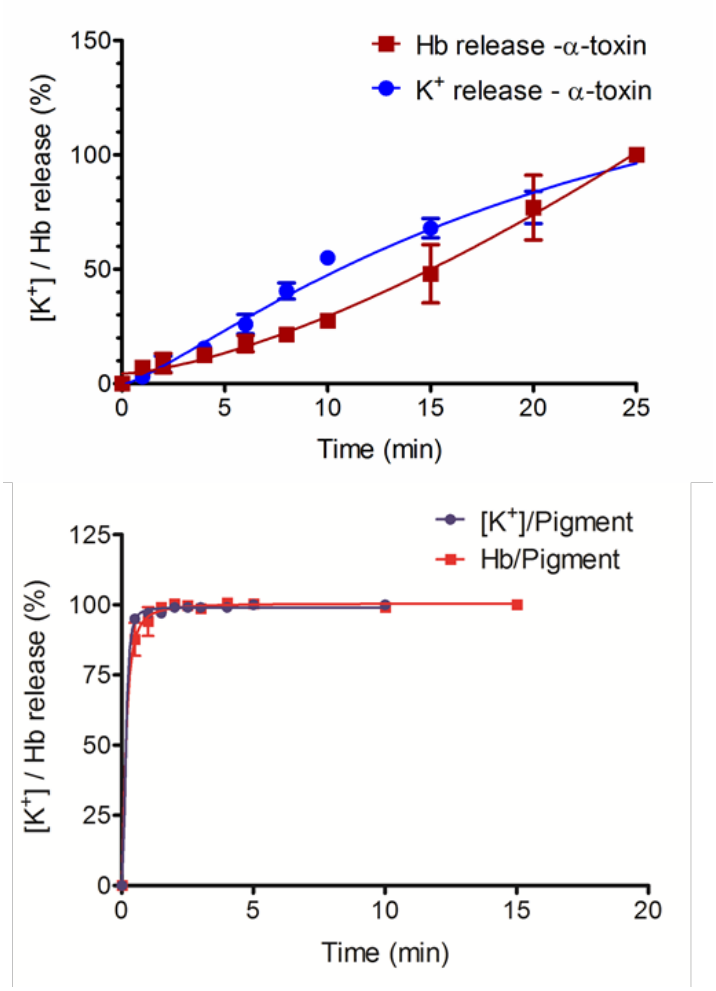

Figure 3-S1. Kinetics of K^+ and Hb efflux due to hemolysis induced by *Staphylococcus aureus* α-toxin and Triton X 100.

(A) Release of K^+ and Hb release was measured from RBC treated with 0.47µM *S. aureus* α-toxin. Efflux of K^+ occurred faster than Hb, as measured by time to 50% release (9.6min vs 13.3min, $p < 0.001$, extra sum-of-squares F test); this lag is similar to the lag observed for GBS pigment-mediated hemolysis (see Fig. 1B). Data are the average ± SEM of two independent experiments. (B) K^+ and Hb release was measured from RBC treated with 0.22µM Triton-X 100 and 100% release of K^+ and Hb occurred instantly.

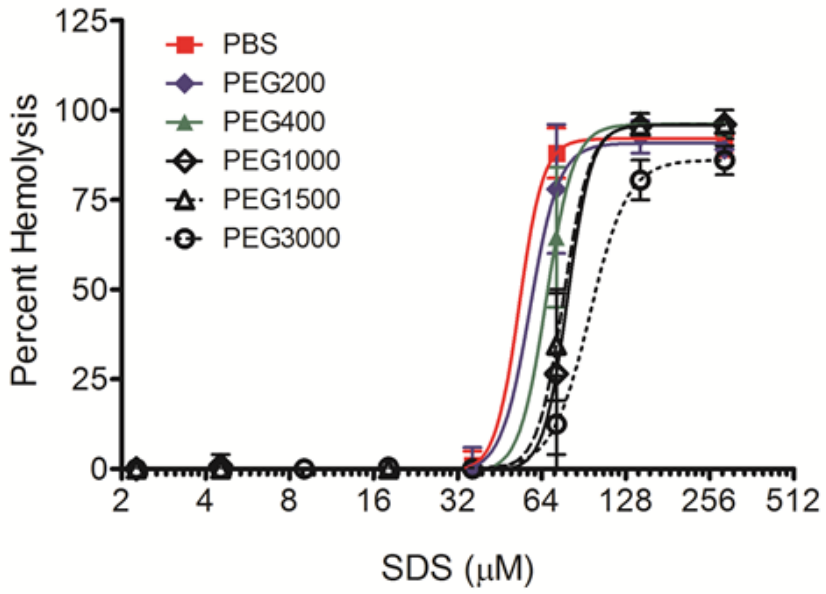

Figure 3-S2. Osmoprotectants do not protect from direct lysis.

Osmoprotectants provide minimal protection from hemolysis caused by SDS (a direct lysis mechanism). Notably, the osmoprotectants PEG1500 and PEG3000 provided complete protection to lysis induced by the GBS pigment, suggesting that the pigment induces hemolysis not via a direct lysis mechanism, but rather a colloidal-osmotic mechanism (see Fig. 1C). Data are the average ± SEM of two independent experiments.

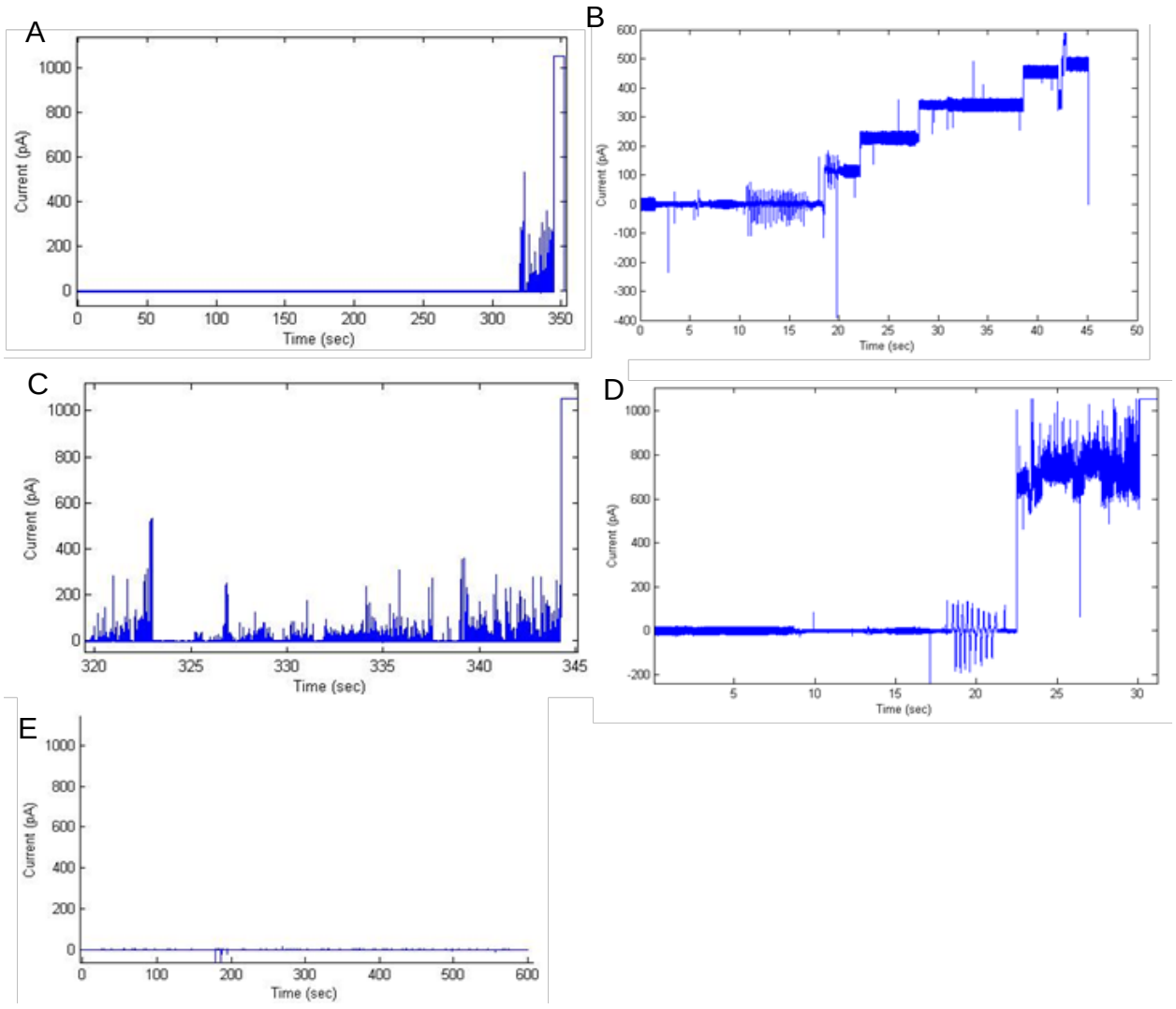

Figure 3-S3. Disruption of artificial lipid bilayers by GBS pigment (75nM), pore forming porin MspA of *Mycobacterium smegmatis* and detergent SDS.

(A, B) GBS pigment (75nM) induces membrane permeability in black lipid membranes (BLMs), see A & for detail *t* = 320-345s, see B. An equivalent volume of Δ*cylE* extract does not disrupt BLMs (see C). As controls, BLMs were incubated with MspA (0.51nM; D) or SDS (350µM; E). For MspA, protein was added at *t* = 0s, and mixed by pipetting from *t* =10-20s. Stepwise increase in current indicative of multiple pore formation is observed. For SDS, detergent was added at *t*=0s and mixed by pipetting from *t* =17-22s. A rapid and large increase in conductance is observed around 23s which is sustained for a few seconds before bilayer disruption, indicative of bilary solubilization.

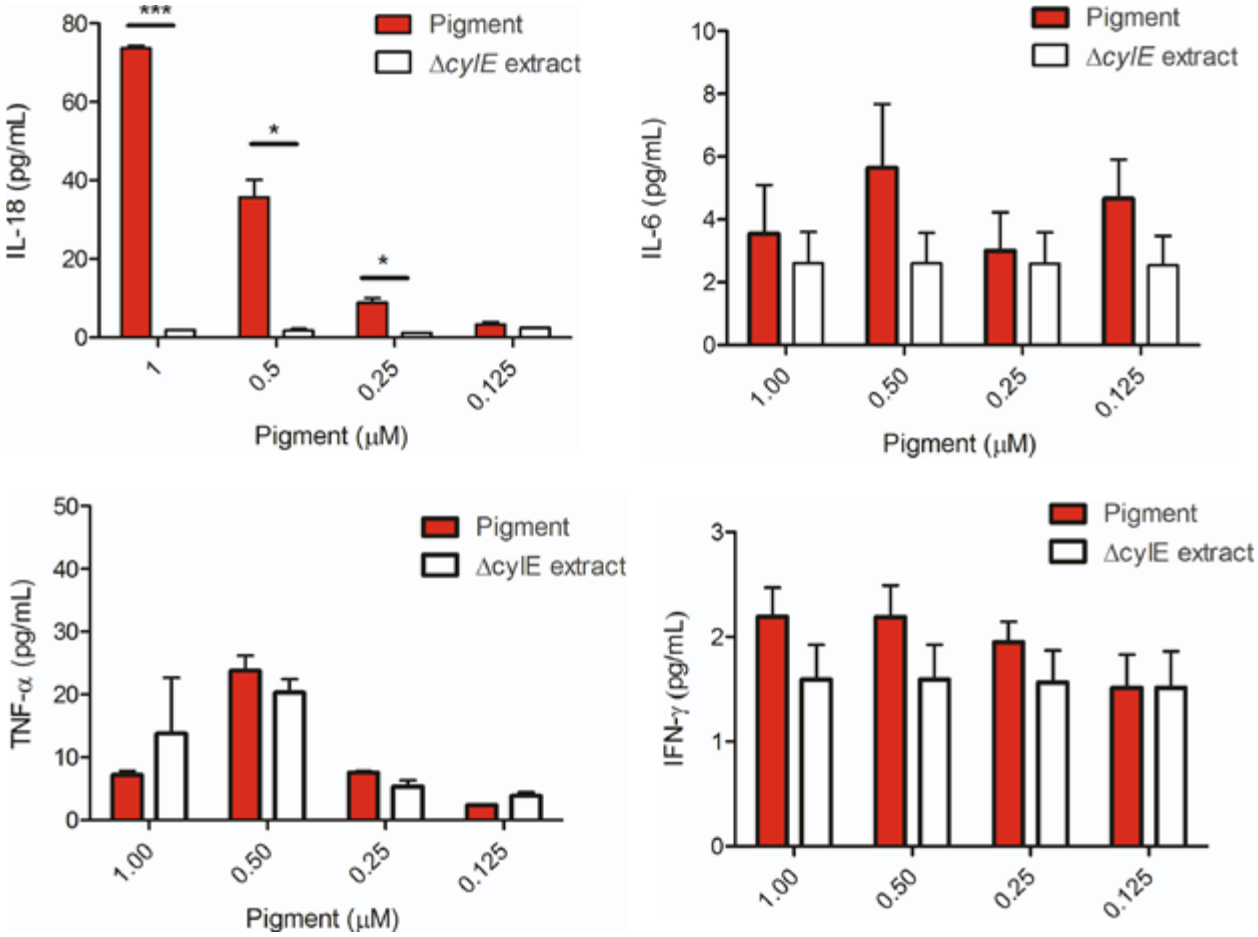

Figure 3-S4. The GBS pigment induces secretion of IL18 but not IL6, TNF- α and IFN-γ from THP-1 derived macrophages.

Levels of IL-6, TNF-α, and IFN-γ or IL-18 in the supernatant of pigment or Δ*cylE* extract treated THP-1 cells were measured. While secretion of IL-18 is significantly higher in pigment treated cells, there is no significant increase in IL-6, TNF-α, or IFN-γ in response to purified GBS pigment. This suggests that the purified pigment induces activation of the NLRP3 inflammasome, but it does not induce secretion of TLR-mediated cytokines ($n=3$, ***p = 0.0002, *p = 0.017 for 0.5 μM pigment, *p = 0.025; for 0.25μM pigment, Bonferroni's multiple comparison test following ANOVA; error bars ± SEM).

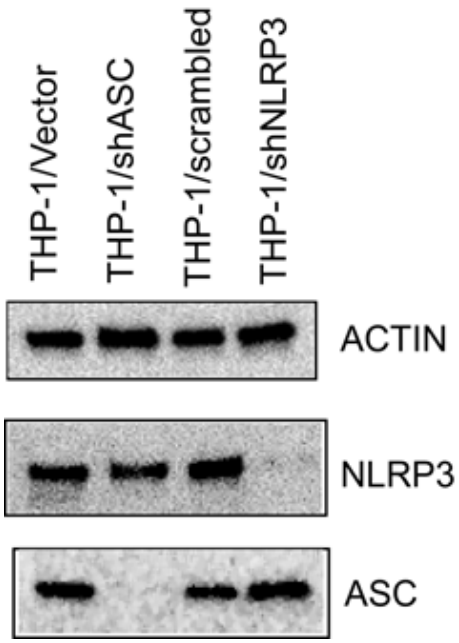

Figure 3-S5. Western blots of THP-1 ShRNA knockdown cell lines.

Western blots demonstrate the lack of ASC and NLRP3 in the shRNA knockdown THP-1/shASC, and THP-1/shNLRP3 cell lines, respectively. Briefly, equal amounts of whole cell lysates from $5x10^6$ cells of the PMA-differentiated THP-1 cell lines (THP-1/vector, THP-1/scrambled, THP-1/shASC, THP-1/shNLRP3) were resolved on SDS-PAGE and probed by western blotting for either ASC or NLRP3 using anti-ASC (1μg/ml; Enzo Life Science) and anti-NLRP3/NALP3 antibodies (1μg/ml; Adipogen), respectively. For comparison, equal amounts of protein on SDS-PAGE were also probed for actin using an anti-actin antibody (0.05μg/mL; GenScript). The results below indicate that unlike the THP-1/vector and THP-1/scrambled cell lines, signal corresponding to ASC and NLRP3 is significantly reduced if not completely absent in the THP-1/shASC cell line (lane 2) and THP-1/shNLRP3 cell line (lane 4), respectively.

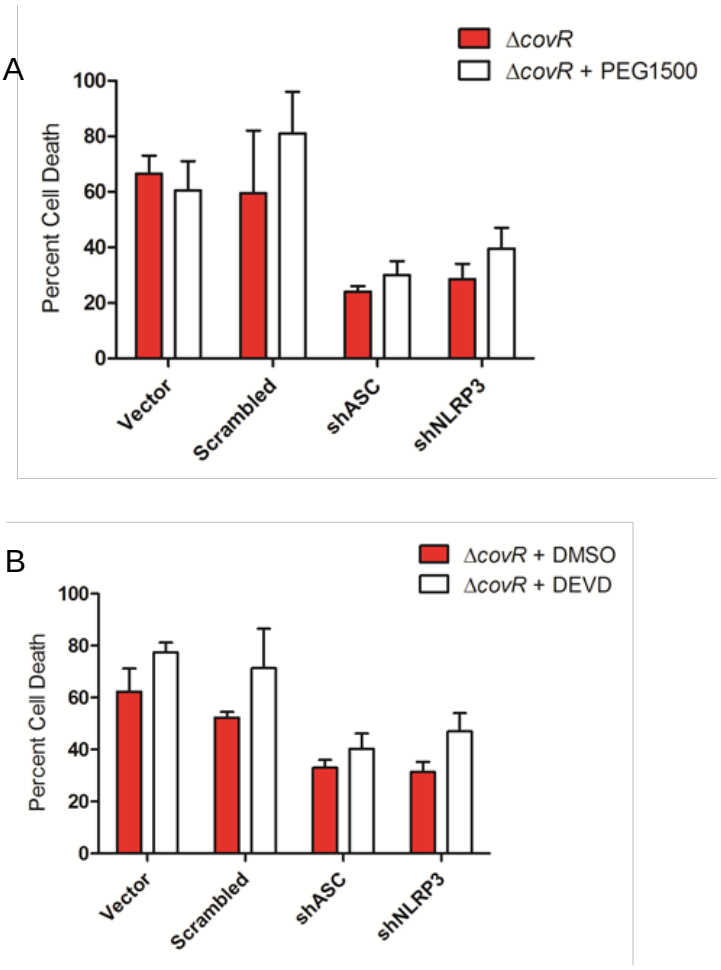

Figure 3-S6. Osmoprotectants or caspase 3/7 inhibiton do not provide protection from macrophage cell death observed with hyperpigmented GBS.

THP-1 cells transfected with empty vector, scrambled control, shASC or shNLRP3 were incubated with GBS Δ*covR* (MOI=1) for 4 hours in the presence or absence of 30mM PEG1500 (A) or 100μM caspase 3/7 inhibitor (Z-DEVD-FMK, shown as DEVD or with control DMSO (B). Percent cell death was then measured by LDH release. The addition of the osmoprotectant (PEG1500) or DEVD did not reduce the amount of cell death in THP-1-derived macrophages including shASC and shNLRP3 cells.

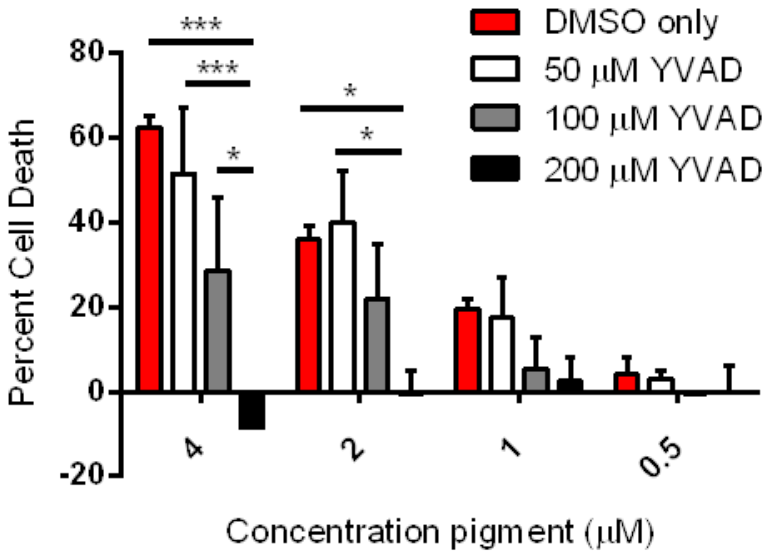

Figure 3-S7. Increasing amounts of the caspase I inhibitor Z-YVAD-FMK provided significant protection from GBS pigment mediated cell death in macrophages.

WT THP-1 macrophages were treated with increasing amounts of the the caspase 1 inhibitor Z-YVAD-FMK or control 'DMSO only' prior to treatment with the GBS pigment. At 200μM Z-YVAD-FMK, significant and essentially complete protection from GBS pigment mediated cell death was observed. Data are the average of two independent experiments with independent batches of purified pigment used in both experiments; error bars ± SEM. Bonferroni's multiple comparison test following ANOVA, (*n=2*, *** $p = 0.0001$, *$p = 0.044$ for 4μM pigment, 100 vs. 200 μM YVAD; *$p = 0.049$ for 2μM pigment, DMSO only vs. 200 μM YVAD; * $p = 0.023$ for 2μM pigment, 50 vs. 200 μM YVAD).

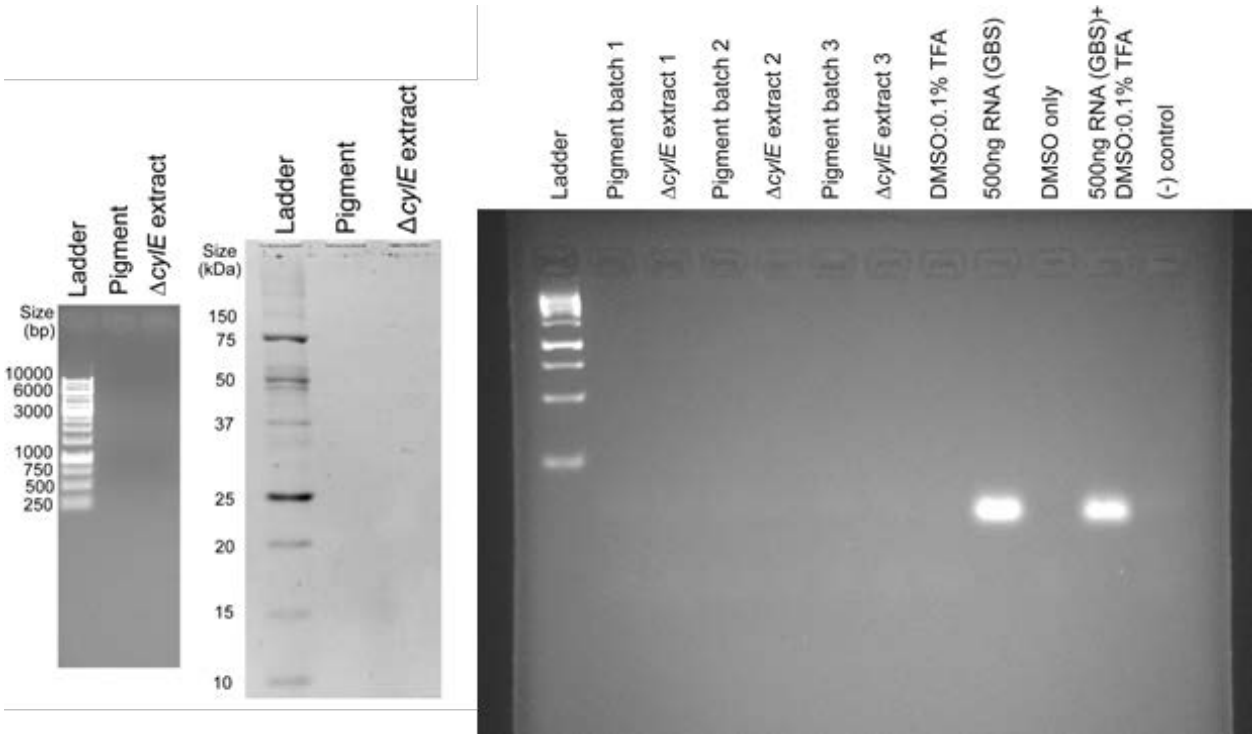

Figure 3-S8. Nucleic acid or proteins are absent from purified GBS pigment.

(Left Panel) Purified GBS pigment (1.6nmol) and an equivalent amount of control Δ*cylE* extract were resolved by agarose gel electrophoresis and stained with ethidium bromide for detection of nucleic acids (DNA or RNA).
(Middle Panel) Purified GBS pigment (9.3nmol) and an equivalent amount of control Δ*cylE* extract were resolved by SDS-PAGE followed by Sypro Ruby staining for detection of proteins.
(Right Panel) Three independently purified batches of GBS pigment (0.6nmol in 3µL) and Δ*cylE* extract were tested for the presence of GBS RNA using RT-PCR (Qiagen); reverse transcription and PCR for the housekeeping gene *rpsL* was performed as previously described (34). As a control, 500ng of RNA isolated from the GBS strain A909 were tested in the presence or absence of DMSO:0.1% TFA.

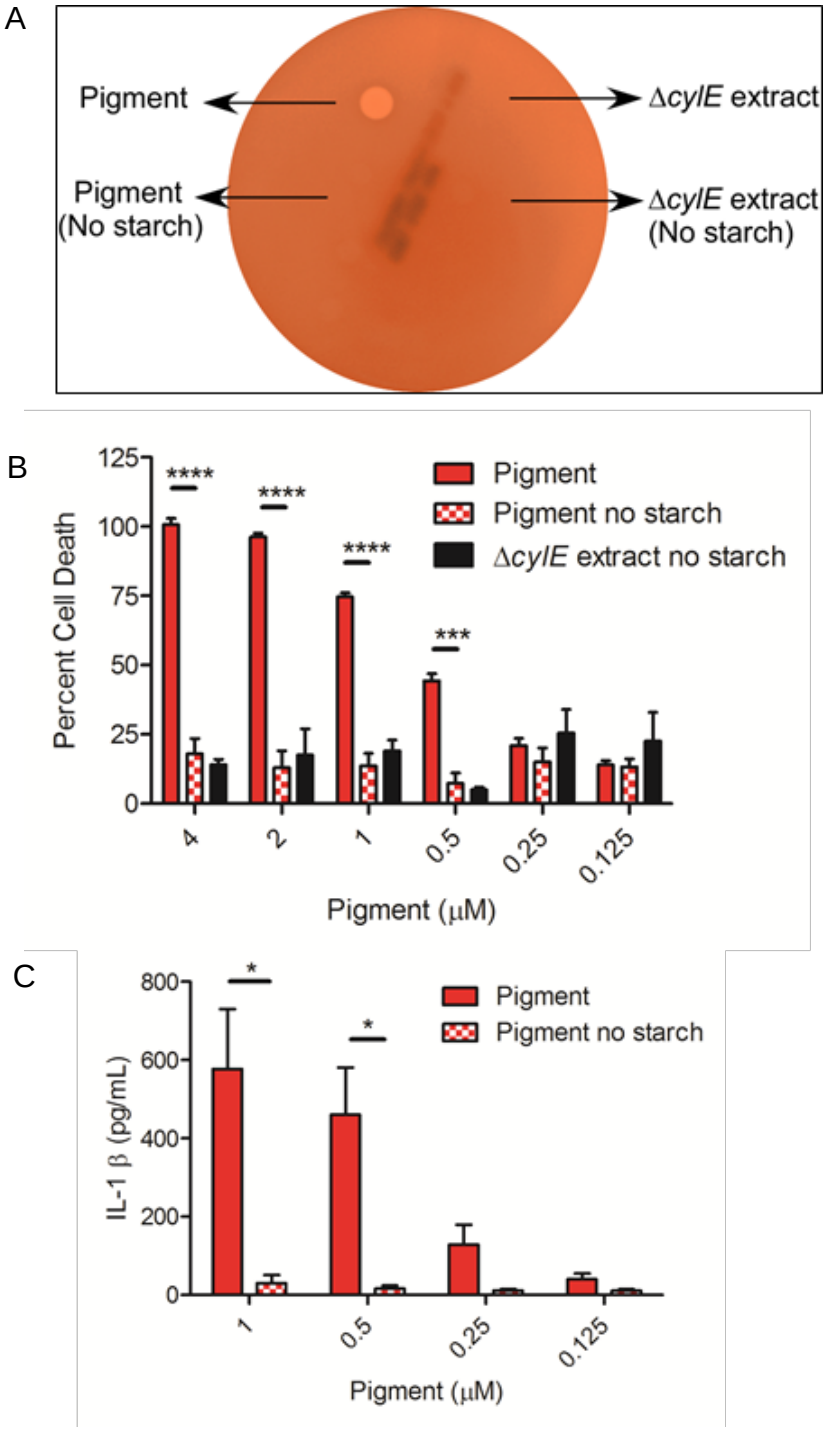

Figure 3-S9. Inactive GBS pigment is not hemolytic and does not induce cell death or IL-1β secretion in THP-1 macrophages.

(A) GBS pigment dissolved in DMSO:0.1%TFA:20% starch is hemolytic whereas GBS pigment dissolved only in DMSO:0.1%TFA (without starch) is not hemolytic.
(B, C) Inactive, nonhemolytic GBS pigment (due to the absence of starch) does not induce cell death (see B) or IL1β release (see C) in THP-1 macrophages. Data are the average of three independent experiments, error bars ± SEM (n=3, **** p = 0.0002, *** p = 0.001, *p = 0.035 for 1μM pigment, *p = 0.0097 for 0.5 μM pigment; Bonferroni's multiple comparison test following ANOVA).

Chapter 4 – Conclusions and Future Directions

Summary of findings

This dissertation addresses several key questions concerning mechanisms of GBS pathogenesis. These results provide insight into the molecular nature of the GBS hemolysin and its role in intrauterine GBS infection, fetal injury, and preterm birth.

The data presented in Chapter 2 demonstrate for the first time, that the GBS pigment is the hemolysin. In this chapter, we also demonstrated that hyperhemolytic/hyperpigmented GBS strains such as those lacking the *cyl* operon repressor CovR (Δ*covR*) penetrate human placental membranes *ex vivo*, in a hemolysin-dependent manner. Also, hyperhemolytic/hyperpigmented GBS strains with mutations in the *covRS* genes were isolated from the amniotic fluid and placental membranes of women in preterm labor. These data suggest that vaginal colonization by hyperpigmented GBS can increase the risk of ascending *in utero* infection and penetration of the placental membranes.

With the discovery that the GBS pigment is hemolytic, we then addressed how the pigment disrupts host cell membranes. In Chapter 3, we used purified toxin to show that the GBS pigment led to membrane disruption in artificial bilayers and red blood cells. This membrane disruption was unlike mechanisms of pore formation typically observed with protein toxins, but resembled lysis caused by smaller hemolytic peptides such as gramicidin S (148). In red blood cells, we observed that the GBS pigment induced membrane perturbations led to ion flux across the cell membrane, resulting in colloidal-osmotic lysis.

We were also able to identify the immune pathways that are activated by the GBS pigment. In THP-1 derived macrophages, pigment-mediated membrane damage leads to potassium efflux

from the cell. This potassium efflux activates the NLRP3 inflammasome, leading to IL-1β release and pyroptosis. This pathway was partially responsible for fetal injury during intrauterine infection with the hyperhemolytic GBS Δ*covR*. Significantly less fetal death was observed in NLRP3-deficient mice compared to WT mice. However, even in NLRP3-deficient mice, significantly more fetal injury was observed during intrauterine infection with hyperpigmented GBS Δ*covR* than with nonpigmented GBS Δ*covR*Δ*cylE*. This suggests that NLRP3-mediated inflammation is not the only factor leading to fetal injury. Further discussion of these findings and suggestions for future avenues of research are presented below.

The impact of *covRS* mutations on GBS population dynamics

The identification of strains with *covRS* mutations from women in preterm birth demonstrates that hyperhemolytic GBS strains occur naturally and may be associated with intrauterine infection. Interestingly, *covR* mutants are less fit than WT GBS in a mouse model of vaginal colonization, suggesting a dynamic relationship between GBS strains adapted to colonize the vaginal tract and those causing invasive disease (68). GBS population dynamics in these environments can be partially understood using a source-sink model, where the more favorable vaginal environment (source) serves as a reservoir for bacteria entering the less favorable uterus (sink) (164). In this model, GBS with *covRS* mutations may randomly arise during colonization in the vaginal tract. Mutant bacteria remaining in the vaginal tract will eventually be eliminated from the population, perhaps because they elicit a more potent host inflammatory response. However, *covRS* mutants may be more likely to cause ascending infection than WT strains or are better adapted to replicate in the uterus. The resulting intrauterine bacterial growth may trigger inflammation and lead to fetal injury or preterm birth. There are some gaps in this model,

reflecting the lack of a detailed understanding of GBS colonization and transmission. The vaginal tract itself may not be a stable source for GBS, as women can be intermittently or transiently colonized (165, 166). It may be more accurate to consider the lower GI tract as the source with the vaginal tract and uterus as sinks. However, little information is presently available regarding GBS colonization of the lower GI tract. This may represent a consistently colonized reservoir over the course of an individual's life, or individuals may be transiently colonized and infected from other sources. Transmission of GBS between individuals is also poorly understood. Recent work has suggested that GBS can be acquired by multiple routes of transmission including sexual contact or foodborne transmission (167). Interestingly, the odds ratios for GBS colonization and these potential transmission routes varied between capsular serotypes. Colonization with serotype Ia and Ib strains is associated with fish consumption but not sexual contact, while colonization with other serotypes is associated with sexual contact but not fish consumption. This suggests that serotype or sequence type differences may be important for GBS transmission. A better understanding of GBS colonization and transmission mechanisms can help to explain how potentially dangerous strains arise and aid in screening women at risk of intrauterine GBS infection.

The *cyl* gene products as drug targets

Hemolytic activity is a key GBS virulence factor, and an inhibitor of hemolysin/pigment production could serve as an anti-virulence drug for GBS (see (168) for a review on anti-virulence drugs). Anti-virulence factor drugs are chemicals designed to inhibit production or activity of a pathogen's virulence factor. It has been hypothesized that such drugs would be less prone to the development of resistance, especially in commensals that can become pathogens

such as GBS (169, 170). Since these drugs would only impact the survival of actively virulent bacteria instead of the whole population, there would be less selective pressure on the bacterial species. An anti-virulence drug may be effective for GBS disease, and hemolytic activity would be a good virulence factor to target. This would mean inhibition of enzymes required for pigment production – the *cyl* gene products. However, it is unclear which *cyl* genes are necessary for pigment production/hemolysis. Of the genes thought to be necessary for pigment biosynthesis, only *cylA* and *cylE* have been shown to be necessary by targeted deletion (see Table 4-1). *cylX* and *cylG* have never been tested, and *cylD*, *acpC*, and *cylZ* were only tested via transposon mutagenesis which can be confounded by polar effects.

Table 4-1. Predicted *cyl* gene functions and their role in hemolysis.

Gene	Function	Relation to hemolysis[a]	*fab* Homologue[b]	Reference
cylX	Acetyl CoA carboxylase	Unknown	*accA-D*	
cylD	Malonyl-CoA-ACP transacylase	Required (TN)*	*fabD*	(54)
cylG	3-ketoacyl-ACP reductase	Unknown	*fabG*	
acpC	Acyl carrier protein	Required (TN)*	*acpC*	(50)
cylZ	β-hydroxy-ACP dehydratase	Required (TN)*	*fabZ*	(50)
cylA	ABC transport (ATPase)	Required	n/a	(52)
cylB	ABC transport (Transmembrane)	Required/Δ reduces (TN)[c]	n/a	(51, 54)
cylE	N-acyltransferase	Required	n/a	(51)
cylF	Aminomethyltransferase	Δ reduces (TN)	n/a	(51, 54)
cylI	3-ketoacyl-ACP synthase	Δ reduces (TN)	*fabH*	(51, 54)
cylJ	Glycosyltransferase	Δ reduces	n/a	(45)
cylK	Phosphopantetheinyl transferase	Δ reduces	n/a	(45)

a (TN) indicates transposon mutagenesis study. 'Δ reduces' indicates that deletion of the gene only reduces hemolytic activity. * indicates that no pictures were shown, hemolytic activity was only mentioned in text.
b Homolog to fatty acid biosynthesis genes.
c Conflicting reports.

The lack of data concerning the importance of each *cyl* gene complicates design of an anti-virulence drug targeting these genes. Potentially, a type II fatty acid biosynthesis (FASII) inhibitor could be used to block pigment production. Many FASII inhibitors target enoyl-ACP reductases, which catalyze the reduction of a double bond to a single bond, but there is no gene with this function in the *cyl* operon (171). This limits FASII inhibitor targets to CylX, CylD, CylG, AcpC, CylZ, CylI, and CylK. With the exception of CylK, the necessity of these genes for pigment biosynthesis has only been tested by transposon mutagenesis, making it is difficult to predict whether an inhibitor would be effective. Even if an inhibitor were successful *in vitro*, GBS can scavenge host-derived lipids, which may impact inhibitor efficacy *in vivo*. Uptake of exogenous fatty acids from serum was shown to overcome deletion of the *fab* genes (fatty acid biosynthesis) in GBS (172). This seems less likely to impact pigment biosynthesis, as single bonds in exogenous lipids would need to be oxidized to *trans* double bonds before incorporation into the pigment. There is no enzyme with such activity in the *cyl* operon, though it may be present elsewhere in the GBS genome. More work is needed to determine if FASII inhibitors targeting *cylX, cylD, cylG, acpC, cylZ, cylI,* or *cylK* could serve as an anti-GBS virulence factor drug.

The other *cyl* genes appear to modify and export the pigment. Of the enzymes involved in modifying the pigment structure – CylE, CylJ, and CylF – only CylE appears to be essential for pigment production (45, 51). CylE likely catalyzes the transfer of the lipid chain from the AcpC carrier to the α-amine of ornithine (129). CylE is a good target for an anti-virulence factor drug; GBSΔ*cylE* strains are nonhemolytic and nonpigmented but still grow and are competent for colonization ((36, 50, 51) unpublished data). However, no inhibitor to this class of enzymes has

been described. CylF methylates the ε-amine of the ornithine, accounting for the presence of the methylated version of the pigment at 691 m/z in the mass spectra (see Figure 2-S2). However, CylF is not essential for hemolytic activity (51). At the other end of the lipid chain, the pigment is rhamnosylated by CylJ (45). GBSΔ*cylJ* strains indeed produce a pigment lacking the rhamnose (unpublished data), but are still slightly hemolytic (45). Thus, the rhamnose does not appear to be necessary for the GBS pigment to be active, although it is unclear if this is due to the molecule being less cytotoxic or simply a decrease in production/export. Nonetheless, the decrease in hemolytic activity suggests that CylJ may be an effective target. The final two *cyl* products are the ABC transporter CylAB that exports the pigment (52). CylA has been shown to be a functional ATPase while CylB is a predicted transmembrane channel. Catalytically active CylA is necessary for hemolytic activity, and conflicting reports exist about the necessity of CylB (51, 52). The strain used by Pritzlaff *et al.* to demonstrate that CylB was not essential had a transposon insertion late in the gene (codon 262 of 295), which may not have inactivated the protein (51, 52). A CylAB inhibitor may be an effective anti-virulence drug, although targeting an ABC transporter with enough specificity to avoid side effects or an impact on general bacterial fitness may be difficult. Nevertheless, the *cyl* gene products warrant further study as potential GBS drug targets.

Localization of the pigment

Gottschalk *et al.* showed that the ABC transporter CylAB secreted the hemolysin from the cytoplasm, and that secretion was required for hemolytic activity (52). However, what happens to the GBS pigment after export and where it goes in the bacterial cell are not understood. Starch, BSA, and Tween can stabilize the pigment *in vitro*, but the endogenous stabilizer in the

bacterial cell is unknown (46, 49, 55). The high hydrophobicity of the pigment suggests it would tightly associate with another hydrophobic molecule. As secretion is required, the associated molecule must be a cell membrane or envelope component. The GBS cell envelope consists of a thick peptidoglycan cell wall with incorporated teichoic acids and a thick polysaccharide capsule. It is likely that the pigment associates with one or more components of the capsule, the cell wall, or the cell membrane. Support for this conclusion stems from the observations that different classes of macromolecules can stabilize the pigment *in vitro* (i.e. the carbohydrate starch, the protein BSA, and the lipid Tween) suggesting that the pigment could associate with multiple components of the bacterial cell.

The pigment may associate with components of the GBS capsule. The capsule is the outermost structure of the envelope (173). Thus, it would be the first to contact host cells and would be exposed to the carrier molecules used to extract the pigment from the bacteria. However, acapsular mutants are still hemolytic and pigmented, indicating that the capsule is not necessary for pigment stabilization and GBS hemolysis (unpublished observation). It is possible that the pigment normally associates with the capsule, but in its absence the pigment is able to associate with other hydrophobic components. One way to test this hypothesis would to enzymatically isolate the GBS capsule and test for hemolytic activity/pigmentation. Alternatively, the GBS pigment may also associate with the cell wall or membrane. There is some evidence of cell wall components serving to stabilize the pigment. A study by Tasihong *et al.* reported that purified lipoteichoic acid was able to serve as a carrier molecule for hemolysin extraction (49). This association could be tested in the bacteria by enzymatically digesting and purifying the GBS cell wall and testing for hemolytic activity. However, it remains unclear

exactly how the pigment would be transported from CylAB to a teichoic acid acceptor without exposure to an aqueous environment. Solvent exposure could be avoided if CylAB releases the pigment directly into the cell membrane, and it is localized there. This would raise different questions, specifically about how the pigment could be extracted from the membrane by a carrier molecule. Further study in this area will help to resolve these key questions on the nature of the endogenous pigment stabilizer and transportation of pigment to the GBS cell surface, and help to gain a better understanding of how GBS utilizes a novel rhamnolipid pigment for pathogenesis.

The inflammasome and the immune response to GBS

Chapter 3 demonstrated that the GBS pigment activates the NLRP3 inflammasome, and that this activation is important *in vivo*. However, some fetal injury was still observed in NLRP3-deficient mice infected with the hyperhemolytic GBS Δ*covR*. This highlights the complex interplay between GBS and the innate immune system. While NLRP3-dependent pyroptosis did not occur in these mice, it is possible that either necrosis or another form of cell death led to fetal injury. This appears to be pigment dependent, as GBS Δ*covR* caused more fetal injury than GBS Δ*covR*Δ*cylE* even with a similar bacterial burden. In cell types that do not undergo pyroptosis, the immune response to purified pigment is unknown. Such cells may be able to repair membrane damage like THP-1 cells deficient in NLRP3 or ASC, undergo colloidal-osmotic lysis like red blood cells, or activate an alternative immune pathway that leads to a different from of programmed cell death.

The role of different inflammasomes in programmed cell death has been a topic of significant interest. The PAMPs (Pathogen-Associated Molecular Patterns) and DAMPs (Danger-Associated Molecular Patterns) sensed by different inflammasomes have been identified. AIM2

senses cytoplasmic dsDNA, NLRP1 senses muramyl dipeptide, and NLRC4 senses flagellin (174). Despite significant effort, the signal sensed by NLRP3 remains elusive. As this sensor protein can be activated by many different stimuli, the current model in the field hypothesizes that NLRP3 senses a disruption in cellular homeostasis (175). Intriguingly, NLRP3 seems to localize to the mitochondria upon activation, and some studies have proposed that mitochondrial reactive oxygen species or DNA aid activation of NLRP3 (175-177). Alternatively, changes in the concentration of cytoplasmic cations such as calcium or potassium have also been proposed as the activating signal. Recent work by Muñoz-Planillo *et al.* suggested that potassium flux and not calcium flux or mitochondrial perturbation was required for NLRP3 activation (139). It is also possible that NLRP3 is activated by multiple direct signals rather than by just one master signal that can be triggered by all activating compounds. Further studies will be needed to determine the upstream events leading to NLRP3 activation.

Events following NLRP3 activation are better defined. Upon recruitment of ASC, NLRP3 forms an inflammasome that leads to caspase 1 activation. Caspase 1 can then cleave the proinflammatory cytokines IL-1β and IL-18, activating other immune cells and amplifying the inflammatory response at the site of infection. In addition, caspase 1 activation can trigger the programmed cell death known as pyroptosis (141, 178). In contrast to apoptosis, in which cellular debris is packaged into vesicles in order to avoid release of DAMPs such as nucleic acid and ATP, pyroptosis leads to DAMP release into the surrounding environment. These DAMPs further activate local immune cells, increasing inflammation. This robust inflammation is both beneficial to the host by helping pathogen clearance, and potentially detrimental by damaging local tissue. Inflammation can be especially detrimental during pregnancy when an inflammatory

uterine environment can lead to fetal injury and preterm birth (6). As ascending and intrauterine infection become better understood it will be important to define the resulting immune responses responsible for pathology in our model of intrauterine infection.

Programmed cell death is a major component of the innate immune response. As described in chapter 3, hemolytic GBS can induce pyroptosis in macrophages. However, hyperhemolytic GBS strains also cause NLRP3 inflammasome-independent cytotoxicity in THP-1 cells. It is remains unclear whether this is simply necrosis due to the pigment or if a different cell death program is activated in the absence of pyroptosis. GBS have been shown to induce a form of programmed cell death with features of apoptosis (127, 179). Unlike apoptosis however, this form of cell death can not be inhibited by addition of the caspase 3/7 inhibitor z-DEVD-FMK or the pan-caspase inhibitor z-VAD-FMK. This suggests that GBS can also trigger a non-pyroptotic, non-apoptotic cell death. In addition to pyroptosis and apoptosis, other programs of cell death have been recently proposed (180, 181). These include programmed necrosis, necroptosis, pyronecrosis, and autophagy. Importantly, these classifications are based on morphological changes in the cell and dependence on certain proteins (181). This strategy for classifying types of cell death is useful but does have its shortcomings, such as potentially underestimating the diversity of cell death pathways. While both *Salmonella* and GBS pigment induce pyroptosis (cell death that requires caspase 1), they do so by activating different sensors (180, 182). These different sensors may activate other immune response pathways and result in a functionally different overall response to infection. To call both cell death events ‘pyroptosis’ potentially ignores this heterogeneity. This classification strategy is further complicated *in vivo*, where different cell types in the same tissue can differentially express the machinery required for

cell death (183). Because of this, it will be important to study how the GBS pigment interacts with lung epithelial cells, brain endothelial cells, cells in the placental membranes, and other immune cells like neutrophils and dendritic cells. The immune response in these cells may differ from the macrophage immune response in ways that impact pathogenesis. The use of purified pigment will help to guide study the of host-GBS interactions but must be ultimately be complemented by studies of the immune response to whole GBS bacteria. GBS infection has been shown to induce pro-inflammatory cytokines and chemokines including IL-1β, IL-6, IL-8, IL-12, IFNβ, and TNFα through activation of multiple PRRs including TLR2, TLR7, NLRP3, CD14, and a cytosolic DNA sensor (39, 150, 184-186). Identifying how these pathways contribute to intrauterine infection and preterm birth will be important to gaining a complete understanding of GBS pathogenesis.

Events preceding intrauterine infection

This dissertation presents work defining the role of the GBS pigment during intrauterine infection. While treatments for intrauterine infection are important, they require accurate and rapid diagnosis that may not be possible in resource-limited settings. Addressing intrauterine GBS infection will require developing prevention strategies, which in turn will require an accurate understanding of the events leading to intrauterine infection. How GBS enter the uterus from the lower genital tract – ascending infection – remains poorly understood. The current model of ascending infection is based on the hypothesis that lower genital tract organisms like GBS, upon sensing an as yet undefined signal, traffic from the vaginal tract, into the uterus. How GBS, which are non-motile and presumed to be extracellular pathogens, can accomplish this is unclear.

Treatment and prevention of intrauterine GBS infection

Intrauterine GBS infection leads to fetal injury and preterm birth. The importance of the NLRP3 inflammasome suggests that a caspase inhibitor could serve as a therapeutic. Indeed, a broad-spectrum caspase inhibitor was able to delay preterm birth in a mouse model of intraperitoneal infection with heat-killed GBS (130). However, caspase 1 is also activated during term labor and delivery and may be involved in a general parturition pathway (187, 188). Administration of a caspase 1 inhibitor in pregnant women may have severe repercussions. Moreover, drug-based intervention will likely face the same problems as IAP – drug resistance to antibiotics, no efficacy for intrauterine infection and LOD, and administration barriers in low- and middle-income countries. While drug-based interventions for GBS infection may help non-perinatal GBS infection, addressing perinatal GBS disease will require an effective vaccine.

A successful GBS vaccine will likely need to induce a strong antibody response to GBS. Natural antibodies to the GBS capsule occur, and high maternal titers are protective against neonatal GBS infection (189). However, the adaptive immune response to GBS is poorly defined, and serotype conversion may impact the effectiveness of an anti-capsule vaccine (22, 190, 191). Some effective bacterial vaccines, including anti-diphtheria and anti-tetanus vaccines, address this by targeting toxins rather than the bacteria themselves (192). These vaccines induce immunity to toxins by inoculating with a toxoid, a non-toxic derivative of the toxin. A toxoid vaccine inducing immunity against the GBS hemolysin could be an effective strategy for preventing GBS disease. Unfortunately, this is complicated by the fact that the GBS hemolysin is not a protein, but a rhamnolipid. Classically, lipids have been considered non-immunogenic. However, recent studies have shown that antibodies can be raised against oxidized lipids, and

antibodies against polyenes such as squalene, amphotericin B, and nystatin have been generated (193, 194). This typically requires either incorporation into liposomes or conjugation to an immunogenic protein carrier. The solubility requirement of the pigment (DMSO:0.1% TFA) imposes a major limitation on both liposome incorporation and the protein-conjugation reactions that could be used. One alternative approach to protein-conjugation may be isolation of AcpC from a GBSΔ*cylE* strain. If CylE is necessary for transfer of the pigment lipid chain from AcpC to ornithine, loss of CylE should lead to a build-up of AcpC connected to the pigment lipid chain (see Figure 2-6). If the AcpC could then be purified, it may be effective at generating antibodies to the GBS hemolysin.

Final thoughts

Perinatal GBS disease is a major burden worldwide, and a better understanding of GBS pathogenesis will help the design of new approaches to treatment. The work presented in this dissertation makes a small step toward this goal by identifying and characterizing a major GBS virulence factor, the host immune response to it, and its role in intrauterine infection. The discovery that the GBS hemolysin is the pigment will hopefully enable future studies to develop strategies to treat and ultimately prevent GBS infection.

References

1. **Liu, L., H. L. Johnson, S. Cousens, J. Perin, S. Scott, J. E. Lawn, I. Rudan, H. Campbell, R. Cibulskis, M. Li, C. Mathers, and R. E. Black.** 2012. Global, regional, and national causes of child mortality: an updated systematic analysis for 2010 with time trends since 2000. Lancet **379:**2151-2161.
2. **Romero, R., S. K. Dey, and S. J. Fisher.** 2014. Preterm labor: one syndrome, many causes. Science **345:**760-765.
3. **Blencowe, H., S. Cousens, M. Z. Oestergaard, D. Chou, A. B. Moller, R. Narwal, A. Adler, C. Vera Garcia, S. Rohde, L. Say, and J. E. Lawn.** 2012. National, regional, and worldwide estimates of preterm birth rates in the year 2010 with time trends since 1990 for selected countries: a systematic analysis and implications. Lancet **379:**2162-2172.
4. **Behrman, R. E., and A. S. Butler (ed.).** 2007. Preterm Birth: Causes, Consequences and Prevention. The National Academies Press, Washington, D.C.
5. **Mendz, G. L., N. O. Kaakoush, and J. A. Quinlivan.** 2013. Bacterial aetiological agents of intra-amniotic infections and preterm birth in pregnant women. Front. Cell. Infect. Microbiol. **3:**58.
6. **Kemp, M. W.** 2014. Preterm birth, intrauterine infection, and fetal inflammation. Front. Immunol. **5:**574.
7. **Romero, R., R. Gomez, T. Chaiworapongsa, G. Conoscenti, J. C. Kim, and Y. M. Kim.** 2001. The role of infection in preterm labour and delivery. Paediatr. Perinat. Epidemiol. **15 Suppl 2:**41-56.
8. **Baker, C. J.** 2013. The spectrum of perinatal group B streptococcal disease. Vaccine **31 Suppl 4:**D3-6.
9. **Baker, C. J., and M. S. Edwards.** 2001. Group B streptococcal infections, p. 1091-1156. *In* J. S. Remington and J. O. Klein (ed.), Infectious Diseases of the fetus and Newborn Infant. W.B. Saunders, Philadelphia, PA.
10. **Berardi, A., C. Rossi, L. Lugli, R. Creti, M. L. Bacchi Reggiani, M. Lanari, L. Memo, M. F. Pedna, C. Venturelli, E. Perrone, M. Ciccia, E. Tridapalli, M. Piepoli, R. Contiero, and F. Ferrari.** 2013. Group B *streptococcus* late-onset disease: 2003-2010. Pediatrics **131:**e361-368.
11. **Barbadoro, P., A. Marigliano, S. Savini, M. M. D'Errico, and E. Prospero.** 2011. Group B Streptococcal sepsis: an old or ongoing threat? Am. J. Infect. Control **39:**e45-48.
12. **Melin, P.** 2011. Neonatal group B streptococcal disease: from pathogenesis to preventive strategies. Clin. Microbiol. Infect.
13. **Libster, R., K. M. Edwards, F. Levent, M. S. Edwards, M. A. Rench, L. A. Castagnini, T. Cooper, R. C. Sparks, C. J. Baker, and P. E. Shah.** 2012. Long-term outcomes of group B streptococcal meningitis. Pediatrics **130:**e8-15.
14. **Thigpen, M. C., C. G. Whitney, N. E. Messonnier, E. R. Zell, R. Lynfield, J. L. Hadler, L. H. Harrison, M. M. Farley, A. Reingold, N. M. Bennett, A. S. Craig, W. Schaffner, A. Thomas, M. M. Lewis, E. Scallan, and A. Schuchat.** 2011. Bacterial meningitis in the United States, 1998-2007. N. Engl. J. Med. **364:**2016-2025.

15. **Edmond, K. M., C. Kortsalioudaki, S. Scott, S. J. Schrag, A. K. Zaidi, S. Cousens, and P. T. Heath.** 2012. Group B streptococcal disease in infants aged younger than 3 months: systematic review and meta-analysis. Lancet **379:**547-556.
16. **Johri, A. K., H. Lata, P. Yadav, M. Dua, Y. Yang, X. Xu, A. Homma, M. A. Barocchi, M. J. Bottomley, A. Saul, K. P. Klugman, and S. Black.** 2013. Epidemiology of Group B *Streptococcus* in developing countries. Vaccine **31 Suppl 4:**D43-45.
17. **Le Doare, K., and P. T. Heath.** 2013. An overview of global GBS epidemiology. Vaccine **31 Suppl 4:**D7-12.
18. **Lin, F. Y., L. E. Weisman, J. Troendle, and K. Adams.** 2003. Prematurity is the major risk factor for late-onset group B *streptococcus* disease. J. Infect. Dis. **188:**267-271.
19. **Deutscher, M., M. Lewis, E. R. Zell, T. H. Taylor, Jr., C. Van Beneden, and S. Schrag.** 2011. Incidence and severity of invasive *Streptococcus pneumoniae,* group A *Streptococcus,* and group B *Streptococcus* infections among pregnant and postpartum women. Clin. Infect. Dis. **53:**114-123.
20. **McDonald, H. M., and H. M. Chambers.** 2000. Intrauterine infection and spontaneous midgestation abortion: is the spectrum of microorganisms similar to that in preterm labor? Infect. Dis. Obstet. Gynecol. **8:**220-227.
21. **Oster, G., J. Edelsberg, K. Hennegan, C. Lewin, V. Narasimhan, K. Slobod, M. S. Edwards, and C. J. Baker.** 2014. Prevention of group B streptococcal disease in the first 3 months of life: would routine maternal immunization during pregnancy be cost-effective? Vaccine **32:**4778-4785.
22. **Bellais, S., A. Six, A. Fouet, M. Longo, N. Dmytruk, P. Glaser, P. Trieu-Cuot, and C. Poyart.** 2012. Capsular switching in group B *Streptococcus* CC17 hypervirulent clone: a future challenge for polysaccharide vaccine development. J. Infect. Dis. **206:**1745-1752.
23. **Gynecology, A. C. o. O. a.** 2011. ACOG Committee Opinion No. 485: Prevention of early-onset group B streptococcal disease in newborns. Obstet. Gynecol. **117:**1019-1027.
24. **Schrag, S. J., S. Zywicki, M. M. Farley, A. L. Reingold, L. H. Harrison, L. B. Lefkowitz, J. L. Hadler, R. Danila, P. R. Cieslak, and A. Schuchat.** 2000. Group B streptococcal disease in the era of intrapartum antibiotic prophylaxis. N. Engl. J. Med. **342:**15-20.
25. **Kimura, K., S. Suzuki, J. Wachino, H. Kurokawa, K. Yamane, N. Shibata, N. Nagano, H. Kato, K. Shibayama, and Y. Arakawa.** 2008. First molecular characterization of group B streptococci with reduced penicillin susceptibility. Antimicrob. Agents Chemother. **52:**2890-2897.
26. **Banno, H., K. Kimura, Y. Tanaka, H. Kitanaka, W. Jin, J. Wachino, K. Yamada, K. Shibayama, and Y. Arakawa.** 2014. Characterization of multidrug-resistant group B streptococci with reduced penicillin susceptibility forming small non-Beta-hemolytic colonies on sheep blood agar plates. J. Clin. Microbiol. **52:**2169-2171.
27. **Back, E. E., E. J. O'Grady, and J. D. Back.** 2012. High rates of perinatal group B *Streptococcus* clindamycin and erythromycin resistance in an upstate New York hospital. Antimicrob. Agents Chemother. **56:**739-742.

28. **Heelan, J. S., M. E. Hasenbein, and A. J. McAdam.** 2004. Resistance of group B *streptococcus* to selected antibiotics, including erythromycin and clindamycin. J. Clin. Microbiol. **42:**1263-1264.
29. **Lukacs, S. L., K. C. Schoendorf, and A. Schuchat.** 2004. Trends in sepsis-related neonatal mortality in the United States, 1985-1998. Pediatr. Infect. Dis. J. **23:**599-603.
30. **Hensler, M. E., G. Y. Liu, S. Sobczak, K. Benirschke, V. Nizet, and G. P. Heldt.** 2005. Virulence role of group B *Streptococcus* beta-hemolysin/cytolysin in a neonatal rabbit model of early-onset pulmonary infection. J. Infect. Dis. **191:**1287-1291.
31. **Nizet, V., K. S. Kim, M. Stins, M. Jonas, E. Y. Chi, D. Nguyen, and C. E. Rubens.** 1997. Invasion of brain microvascular endothelial cells by group B streptococci. Infect. Immun. **65:**5074-5081.
32. **Nizet, V., R. L. Gibson, and C. E. Rubens.** 1997. The role of group B streptococci beta-hemolysin expression in newborn lung injury. Adv. Exp. Med. Biol. **418:**627-630.
33. **Ring, A., J. S. Braun, J. Pohl, V. Nizet, W. Stremmel, and J. L. Shenep.** 2002. Group B streptococcal beta-hemolysin induces mortality and liver injury in experimental sepsis. J. Infect. Dis. **185:**1745-1753.
34. **Lembo, A., M. A. Gurney, K. Burnside, A. Banerjee, M. de los Reyes, J. E. Connelly, W. J. Lin, K. A. Jewell, A. Vo, C. W. Renken, K. S. Doran, and L. Rajagopal.** 2010. Regulation of CovR expression in Group B *Streptococcus* impacts blood-brain barrier penetration. Mol. Microbiol. **77:**431-443.
35. **Gibson, R. L., V. Nizet, and C. E. Rubens.** 1999. Group B streptococcal beta-hemolysin promotes injury of lung microvascular endothelial cells. Pediatr. Res. **45:**626-634.
36. **Liu, G. Y., K. S. Doran, T. Lawrence, N. Turkson, M. Puliti, L. Tissi, and V. Nizet.** 2004. Sword and shield: linked group B streptococcal beta-hemolysin/cytolysin and carotenoid pigment function to subvert host phagocyte defense. Proc. Natl. Acad. Sci. U. S. A. **101:**14491-14496.
37. **Fettucciari, K., E. Rosati, L. Scaringi, P. Cornacchione, G. Migliorati, R. Sabatini, I. Fetriconi, R. Rossi, and P. Marconi.** 2000. Group B *Streptococcus* induces apoptosis in macrophages. J. Immunol. **165:**3923-3933.
38. **Doran, K. S., G. Y. Liu, and V. Nizet.** 2003. Group B streptococcal beta-hemolysin/cytolysin activates neutrophil signaling pathways in brain endothelium and contributes to development of meningitis. J. Clin. Invest. **112:**736-744.
39. **Costa, A., R. Gupta, G. Signorino, A. Malara, F. Cardile, C. Biondo, A. Midiri, R. Galbo, P. Trieu-Cuot, S. Papasergi, G. Teti, P. Henneke, G. Mancuso, D. T. Golenbock, and C. Beninati.** 2012. Activation of the NLRP3 inflammasome by group B streptococci. J. Immunol. **188:**1953-1960.
40. **Romero, R., D. T. Brody, E. Oyarzun, M. Mazor, Y. K. Wu, J. C. Hobbins, and S. K. Durum.** 1989. Infection and labor. III. Interleukin-1: a signal for the onset of parturition. Am. J. Obstet. Gynecol. **160:**1117-1123.
41. **Hirsch, E., Y. Filipovich, and M. Mahendroo.** 2006. Signaling via the type I IL-1 and TNF receptors is necessary for bacterially induced preterm labor in a murine model. Am. J. Obstet. Gynecol. **194:**1334-1340.

42. **Sadowsky, D. W., K. M. Adams, M. G. Gravett, S. S. Witkin, and M. J. Novy.** 2006. Preterm labor is induced by intraamniotic infusions of interleukin-1beta and tumor necrosis factor-alpha but not by interleukin-6 or interleukin-8 in a nonhuman primate model. Am. J. Obstet. Gynecol. **195:**1578-1589.
43. **Suzuki, Y., T. Yamamoto, K. Kojima, M. Tanemura, H. Tateyama, and K. Suzumori.** 2006. Evaluation levels of cytokines in amniotic fluid of women with intrauterine infection in the early second trimester. Fetal Diagn. Ther. **21:**45-50.
44. **Saji, F., Y. Samejima, S. Kamiura, K. Sawai, K. Shimoya, and T. Kimura.** 2000. Cytokine production in chorioamnionitis. J. Reprod. Immunol. **47:**185-196.
45. **Forquin, M. P., A. Tazi, M. Rosa-Fraile, C. Poyart, P. Trieu-Cuot, and S. Dramsi.** 2007. The putative glycosyltransferase-encoding gene *cylJ* and the group B *Streptococcus* (GBS)-specific gene *cylK* modulate hemolysin production and virulence of GBS. Infect. Immun. **75:**2063-2066.
46. **Marchlewicz, B. A., and J. L. Duncan.** 1981. Lysis of erythrocytes by a hemolysin produced by a group B *Streptococcus sp*. Infect. Immun. **34:**787-794.
47. **Tapsall, J. W.** 1987. Relationship between pigment production and haemolysin formation by Lancefield group B streptococci. J. Med. Microbiol. **24:**83-87.
48. **Marchlewicz, B. A., and J. L. Duncan.** 1980. Properties of a hemolysin produced by group B streptococci. Infect. Immun. **30:**805-813.
49. **Tsaihong, J. C. W.-D. E.** 1983. Effect of carrier molecules on production and properties of extracellular hemolysin produced by *Streptococcus agalactiae*. Curr. Microbiol. **9:**333-338.
50. **Spellerberg, B., B. Pohl, G. Haase, S. Martin, J. Weber-Heynemann, and R. Lutticken.** 1999. Identification of genetic determinants for the hemolytic activity of *Streptococcus agalactiae* by ISS1 transposition. J. Bacteriol. **181:**3212-3219.
51. **Pritzlaff, C. A., J. C. Chang, S. P. Kuo, G. S. Tamura, C. E. Rubens, and V. Nizet.** 2001. Genetic basis for the beta-haemolytic/cytolytic activity of group B *Streptococcus*. Mol. Microbiol. **39:**236-247.
52. **Gottschalk, B., G. Broker, M. Kuhn, S. Aymanns, U. Gleich-Theurer, and B. Spellerberg.** 2006. Transport of multidrug resistance substrates by the *Streptococcus agalactiae* hemolysin transporter. J. Bacteriol. **188:**5984-5992.
53. **Nizet, V.** 2002. Streptococcal beta-hemolysins: genetics and role in disease pathogenesis. Trends Microbiol. **10:**575-580.
54. **Spellerberg, B., S. Martin, C. Brandt, and R. Lutticken.** 2000. The *cyl* genes of *Streptococcus agalactiae* are involved in the production of pigment. FEMS Microbiol. Lett. **188:**125-128.
55. **Tapsall, J. W.** 1986. Pigment production by Lancefield-group-B streptococci (*Streptococcus agalactiae*). J. Med. Microbiol. **21:**75-81.
56. **de la Rosa, M., M. Perez, C. Carazo, L. Pareja, J. I. Peis, and F. Hernandez.** 1992. New Granada Medium for detection and identification of group B streptococci. J. Clin. Microbiol. **30:**1019-1021.
57. **Church, D. L., H. Baxter, T. Lloyd, B. Miller, and S. Elsayed.** 2008. Evaluation of StrepB carrot broth versus Lim broth for detection of group B *Streptococcus* colonization status of near-term pregnant women. J. Clin. Microbiol. **46:**2780-2782.

58. **Rosa-Fraile, M., J. Rodriguez-Granger, A. Haidour-Benamin, J. M. Cuerva, and A. Sampedro.** 2006. Granadaene: proposed structure of the group B *Streptococcus* polyenic pigment. Appl. Environ. Microbiol. **72:**6367-6370.
59. **Kawai, Y., and I. Yano.** 1983. Ornithine-containing lipid of *Bordetella pertussis*, a new type of hemagglutinin. Eur. J. Biochem. **136:**531-538.
60. **Sanchez, M., F. J. Aranda, J. A. Teruel, M. J. Espuny, A. Marques, A. Manresa, and A. Ortiz.** 2010. Permeabilization of biological and artificial membranes by a bacterial dirhamnolipid produced by *Pseudomonas aeruginosa*. J. Colloid Interface Sci. **341:**240-247.
61. **Knopik-Skrocka, A., and J. Bielawski.** 2002. The mechanism of the hemolytic activity of polyene antibiotics. Cell Mol Biol Lett **7:**31-48.
62. **Rajagopal, L.** 2009. Understanding the regulation of Group B Streptococcal virulence factors. Future Microbiology **4:**201-221.
63. **Lamy, M. C., M. Zouine, J. Fert, M. Vergassola, E. Couve, E. Pellegrini, P. Glaser, F. Kunst, T. Msadek, P. Trieu-Cuot, and C. Poyart.** 2004. CovS/CovR of group B *streptococcus*: a two-component global regulatory system involved in virulence. Mol. Microbiol. **54:**1250-1268.
64. **Jiang, S. M., M. J. Cieslewicz, D. L. Kasper, and M. R. Wessels.** 2005. Regulation of virulence by a two-component system in group B *streptococcus*. J. Bacteriol. **187:**1105-1113.
65. **Santi, I., R. Grifantini, S. M. Jiang, C. Brettoni, G. Grandi, M. R. Wessels, and M. Soriani.** 2009. CsrRS regulates group B *Streptococcus* virulence gene expression in response to environmental pH: a new perspective on vaccine development. J. Bacteriol. **191:**5387-5397.
66. **Gryllos, I., J. C. Levin, and M. R. Wessels.** 2003. The CsrR/CsrS two-component system of group A *Streptococcus* responds to environmental Mg2+. Proc. Natl. Acad. Sci. U. S. A. **100:**4227-4232.
67. **Lin, W. J., D. Walthers, J. E. Connelly, K. Burnside, K. A. Jewell, L. J. Kenney, and L. Rajagopal.** 2009. Threonine phosphorylation prevents promoter DNA binding of the Group B *Streptococcus* response regulator CovR. Mol. Microbiol. **71:**1477-1495.
68. **Patras, K. A., N. Y. Wang, E. M. Fletcher, C. K. Cavaco, A. Jimenez, M. Garg, J. Fierer, T. R. Sheen, L. Rajagopal, and K. S. Doran.** 2013. Group B *Streptococcus* CovR regulation modulates host immune signalling pathways to promote vaginal colonization. Cell Microbiol **15:**1154-1167.
69. **Federle, M. J., K. S. McIver, and J. R. Scott.** 1999. A response regulator that represses transcription of several virulence operons in the group A *streptococcus*. J. Bacteriol. **181:**3649-3657.
70. **Graham, M. R., L. M. Smoot, C. A. Migliaccio, K. Virtaneva, D. E. Sturdevant, S. F. Porcella, M. J. Federle, G. J. Adams, J. R. Scott, and J. M. Musser.** 2002. Virulence control in group A *Streptococcus* by a two-component gene regulatory system: global expression profiling and in vivo infection modeling. Proc. Natl. Acad. Sci. U. S. A. **99:**13855-13860.
71. **Horstmann, N., P. Sahasrabhojane, B. Suber, M. Kumaraswami, R. J. Olsen, A. Flores, J. M. Musser, R. G. Brennan, and S. A. Shelburne, 3rd.** 2011. Distinct single

amino acid replacements in the control of virulence regulator protein differentially impact streptococcal pathogenesis. PLoS Pathog **7:**e1002311.

72. **Engleberg, N. C., A. Heath, A. Miller, C. Rivera, and V. J. DiRita.** 2001. Spontaneous mutations in the CsrRS two-component regulatory system of *Streptococcus pyogenes* result in enhanced virulence in a murine model of skin and soft tissue infection. J. Infect. Dis. **183:**1043-1054.
73. **Goldenberg, R. L., J. C. Hauth, and W. W. Andrews.** 2000. Intrauterine infection and preterm delivery. N. Engl. J. Med. **342:**1500-1507.
74. **Watts, D. H., M. A. Krohn, S. L. Hillier, and D. A. Eschenbach.** 1992. The association of occult amniotic fluid infection with gestational age and neonatal outcome among women in preterm labor. Obstet. Gynecol. **79:**351-357.
75. **Yoon, B. H., R. Romero, J. S. Park, C. J. Kim, S. H. Kim, J. H. Choi, and T. R. Han.** 2000. Fetal exposure to an intra-amniotic inflammation and the development of cerebral palsy at the age of three years. Am. J. Obstet. Gynecol. **182:**675-681.
76. **Gravett, M. G., C. E. Rubens, and T. M. Nunes.** 2010. Global report on preterm birth and stillbirth (2 of 7): discovery science. BMC Pregnancy Childbirth **10 Suppl 1:**S2.
77. **Verani, J. R., L. McGee, and S. J. Schrag.** 2010. Prevention of perinatal group B streptococcal disease--revised guidelines from CDC, 2010. MMWR Recomm Rep **59:**1-36.
78. **Puopolo, K. M.** 2008. Epidemiology of Neonatal Early-onset Sepsis. NeoReviews **9:** e571-e579.
79. **Hillier, S. L., J. Martius, M. Krohn, N. Kiviat, K. K. Holmes, and D. A. Eschenbach.** 1988. A case-control study of chorioamnionic infection and histologic chorioamnionitis in prematurity. N. Engl. J. Med. **319:**972-978.
80. **Romero, R., M. Sirtori, E. Oyarzun, C. Avila, M. Mazor, R. Callahan, V. Sabo, A. P. Athanassiadis, and J. C. Hobbins.** 1989. Infection and labor. V. Prevalence, microbiology, and clinical significance of intraamniotic infection in women with preterm labor and intact membranes. Am. J. Obstet. Gynecol. **161:**817-824.
81. **Hillier, S. L., M. A. Krohn, N. B. Kiviat, D. H. Watts, and D. A. Eschenbach.** 1991. Microbiologic causes and neonatal outcomes associated with chorioamnion infection. Am. J. Obstet. Gynecol. **165:**955-961.
82. **Ledger, W. J.** 2008. Perinatal infections and fetal/neonatal brain injury. Curr. Opin. Obstet. Gynecol. **20:**120-124.
83. **Weston, E. J., T. Pondo, M. M. Lewis, P. Martell-Cleary, C. Morin, B. Jewell, P. Daily, M. Apostol, S. Petit, M. Farley, R. Lynfield, A. Reingold, N. I. Hansen, B. J. Stoll, A. J. Shane, E. Zell, and S. J. Schrag.** 2011. The Burden of Invasive Early-onset Neonatal Sepsis in the United States, 2005-2008. Pediatr. Infect. Dis. J. **30:**937-941.
84. **Hutson, J. R., F. Garcia-Bournissen, A. Davis, and G. Koren.** 2011. The human placental perfusion model: a systematic review and development of a model to predict in vivo transfer of therapeutic drugs. Clin. Pharmacol. Ther. **90:**67-76.
85. **Ala-Kokko, T. I., P. Myllynen, and K. Vahakangas.** 2000. Ex vivo perfusion of the human placental cotyledon:implications for anesthetic pharmacology. International Journal of Obstetric Anesthesia **9:**26-38.

86. **Bourne, G. L.** 1960. The microscopic anatomy of the human amnion and chorion. Am. J. Obstet. Gynecol. **79:**1070-1073.
87. **Winram, S. B., M. Jonas, E. Chi, and C. E. Rubens.** 1998. Characterization of group B streptococcal invasion of human chorion and amnion epithelial cells In vitro. Infect. Immun. **66:**4932-4941.
88. **Naeye, R. L., and E. C. Peters.** 1978. Amniotic fluid infections with intact membranes leading to perinatal death: a prospective study. Pediatrics **61:**171-177.
89. **Bobitt, J. R., and W. J. Ledger.** 1977. Unrecognized amnionitis and prematurity: a preliminary report. J. Reprod. Med. **19:**8-12.
90. **Rajagopal, L., A. Vo, A. Silvestroni, and C. E. Rubens.** 2006. Regulation of cytotoxin expression by converging eukaryotic-type and two-component signalling mechanisms in *Streptococcus agalactiae*. Mol. Microbiol. **62:**941-957.
91. **Doran, K. S., E. J. Engelson, A. Khosravi, H. C. Maisey, I. Fedtke, O. Equils, K. S. Michelsen, M. Arditi, A. Peschel, and V. Nizet.** 2005. Blood-brain barrier invasion by group B *Streptococcus* depends upon proper cell-surface anchoring of lipoteichoic acid. J. Clin. Invest. **115:**2499-2507.
92. **Doran, K. S., J. C. Chang, V. M. Benoit, L. Eckmann, and V. Nizet.** 2002. Group B streptococcal beta-hemolysin/cytolysin promotes invasion of human lung epithelial cells and the release of interleukin-8. J. Infect. Dis. **185:**196-203.
93. **Kawai, Y., A. Moribayashi, and I. Yano.** 1982. Ornithine-containing lipid of *Bordetella pertussis* that carries hemagglutinating activity. J. Bacteriol. **152:**907-910.
94. **Gonzalez, M. R., M. Bischofberger, L. Pernot, F. G. van der Goot, and B. Freche.** 2008. Bacterial pore-forming toxins: the (w)hole story? Cell. Mol. Life Sci. **65:**493-507.
95. **Giaever, I., and C. R. Keese.** 1993. A morphological biosensor for mammalian cells. Nature **366:**591-592.
96. **Romero, R., C. Avila, U. Santhanam, and P. B. Sehgal.** 1990. Amniotic fluid interleukin 6 in preterm labor. Association with infection. J. Clin. Invest. **85:**1392-1400.
97. **Romero, R., M. Ceska, C. Avila, M. Mazor, E. Behnke, and I. Lindley.** 1991. Neutrophil attractant/activating peptide-1/interleukin-8 in term and preterm parturition. Am. J. Obstet. Gynecol. **165:**813-820.
98. **Romero, R., K. R. Manogue, M. D. Mitchell, Y. K. Wu, E. Oyarzun, J. C. Hobbins, and A. Cerami.** 1989. Infection and labor. IV. Cachectin-tumor necrosis factor in the amniotic fluid of women with intraamniotic infection and preterm labor. Am. J. Obstet. Gynecol. **161:**336-341.
99. **Gotsch, F., R. Romero, J. P. Kusanovic, S. Mazaki-Tovi, B. L. Pineles, O. Erez, J. Espinoza, and S. S. Hassan.** 2007. The fetal inflammatory response syndrome. Clin. Obstet. Gynecol. **50:**652-683.
100. **Zaga-Clavellina, V., G. Garcia-Lopez, H. Flores-Herrera, A. Espejel-Nunez, A. Flores-Pliego, D. Soriano-Becerril, R. Maida-Claros, H. Merchant-Larios, and F. Vadillo-Ortega.** 2007. In vitro secretion profiles of interleukin (IL)-1beta, IL-6, IL-8, IL-10, and TNF alpha after selective infection with *Escherichia coli* in human fetal membranes. Reprod Biol Endocrinol **5:**46.
101. **Stevens, A. M., and J. D. Bancroft.** 1977. Theory and Practice of Histological Techniques. Churchill Livingstone, Edinburgh.

102. **Hitti, J., M. A. Krohn, D. L. Patton, P. Tarczy-Hornoch, S. L. Hillier, E. M. Cassen, and D. A. Eschenbach.** 1997. Amniotic fluid tumor necrosis factor-alpha and the risk of respiratory distress syndrome among preterm infants. Am. J. Obstet. Gynecol. **177:**50-56.
103. **Tettelin, H., V. Masignani, M. J. Cieslewicz, C. Donati, D. Medini, N. L. Ward, S. V. Angiuoli, J. Crabtree, A. L. Jones, A. S. Durkin, R. T. Deboy, T. M. Davidsen, M. Mora, M. Scarselli, I. Margarit y Ros, J. D. Peterson, C. R. Hauser, J. P. Sundaram, W. C. Nelson, R. Madupu, L. M. Brinkac, R. J. Dodson, M. J. Rosovitz, S. A. Sullivan, S. C. Daugherty, D. H. Haft, J. Selengut, M. L. Gwinn, L. Zhou, N. Zafar, H. Khouri, D. Radune, G. Dimitrov, K. Watkins, K. J. O'Connor, S. Smith, T. R. Utterback, O. White, C. E. Rubens, G. Grandi, L. C. Madoff, D. L. Kasper, J. L. Telford, M. R. Wessels, R. Rappuoli, and C. M. Fraser.** 2005. Genome analysis of multiple pathogenic isolates of *Streptococcus agalactiae*: implications for the microbial "pan-genome". Proc. Natl. Acad. Sci. U. S. A. **102:**13950-13955.
104. **Jiang, S. M., N. Ishmael, J. D. Hotopp, M. Puliti, L. Tissi, N. Kumar, M. J. Cieslewicz, H. Tettelin, and M. R. Wessels.** 2008. Variation in the group B *Streptococcus* CsrRS regulon and effects on pathogenicity. J. Bacteriol. **190:**1956-1965.
105. **Nizet, V., R. L. Gibson, E. Y. Chi, P. E. Framson, M. Hulse, and C. E. Rubens.** 1996. Group B streptococcal beta-hemolysin expression is associated with injury of lung epithelial cells. Infect. Immun. **64:**3818-3826.
106. **Tapsall, J. W., and E. A. Phillips.** 1991. The hemolytic and cytolytic activity of group B streptococcal hemolysin and its possible role in early onset group B streptococcal disease. Pathology (Phila). **23:**139-144.
107. **Vanberg, C., B. F. Lutnaes, T. Langsrud, I. F. Nes, and H. Holo.** 2007. *Propionibacterium jensenii* produces the polyene pigment granadaene and has hemolytic properties similar to those of *Streptococcus agalactiae*. Appl. Environ. Microbiol. **73:**5501-5506.
108. **Kawai, Y., and A. Moribayashi.** 1982. Characteristic lipids of *Bordetella pertussis*: simple fatty acid composition, hydroxy fatty acids, and an ornithine-containing lipid. J. Bacteriol. **151:**996-1005.
109. **Glaser, P., C. Rusniok, C. Buchrieser, F. Chevalier, L. Frangeul, T. Msadek, M. Zouine, E. Couve, L. Lalioui, C. Poyart, P. Trieu-Cuot, and F. Kunst.** 2002. Genome sequence of *Streptococcus agalactiae*, a pathogen causing invasive neonatal disease. Mol. Microbiol. **45:**1499-1513.
110. **Henneke, P., O. Takeuchi, R. Malley, E. Lien, R. R. Ingalls, M. W. Freeman, T. Mayadas, V. Nizet, S. Akira, D. L. Kasper, and D. T. Golenbock.** 2002. Cellular activation, phagocytosis, and bactericidal activity against group B *streptococcus* involve parallel myeloid differentiation factor 88-dependent and independent signaling pathways. J. Immunol. **169:**3970-3977.
111. **Bebien, M., M. E. Hensler, S. Davanture, L. C. Hsu, M. Karin, J. M. Park, L. Alexopoulou, G. Y. Liu, V. Nizet, and T. Lawrence.** 2012. The pore-forming toxin beta hemolysin/cytolysin triggers p38 MAPK-dependent IL-10 production in macrophages and inhibits innate immunity. PLoS Pathog **8:**e1002812.
112. **Maione, D., I. Margarit, C. D. Rinaudo, V. Masignani, M. Mora, M. Scarselli, H. Tettelin, C. Brettoni, E. T. Iacobini, R. Rosini, N. D'Agostino, L. Miorin, S. Buccato,**

M. Mariani, G. Galli, R. Nogarotto, V. Nardi Dei, F. Vegni, C. Fraser, G. Mancuso, G. Teti, L. C. Madoff, L. C. Paoletti, R. Rappuoli, D. L. Kasper, J. L. Telford, and G. Grandi. 2005. Identification of a universal Group B *streptococcus* vaccine by multiple genome screen. Science **309:**148-150.

113. **Krogh, A., B. Larsson, G. von Heijne, and E. L. Sonnhammer.** 2001. Predicting transmembrane protein topology with a hidden Markov model: application to complete genomes. J. Mol. Biol. **305:**567-580.
114. **Geiger, O., N. Gonzalez-Silva, I. M. Lopez-Lara, and C. Sohlenkamp.** 2010. Amino acid-containing membrane lipids in bacteria. Prog. Lipid Res. **49:**46-60.
115. **Haussler, S., M. Nimtz, T. Domke, V. Wray, and I. Steinmetz.** 1998. Purification and characterization of a cytotoxic exolipid of *Burkholderia pseudomallei*. Infect. Immun. **66:**1588-1593.
116. **Lancefield, R. C., M. McCarty, and W. N. Everly.** 1975. Multiple mouse-protective antibodies directed against group B streptococci. Special reference to antibodies effective against protein antigens. J. Exp. Med. **142:**165-179.
117. **Martin, T. R., C. E. Rubens, and C. B. Wilson.** 1988. Lung antibacterial defense mechanisms in infant and adult rats: implications for the pathogenesis of group B streptococcal infections in neonatal lung. J. Infect. Dis. **157:**91-100.
118. **Musser, J. M., S. J. Mattingly, R. Quentin, A. Goudeau, and R. K. Selander.** 1989. Identification of a high-virulence clone of type III *Streptococcus agalactiae* (group B *Streptococcus*) causing invasive neonatal disease. Proc. Natl. Acad. Sci. U. S. A. **86:**4731-4735.
119. **Okada, N., R. T. Geist, and M. G. Caparon.** 1993. Positive transcriptional control of mry regulates virulence in the group A *streptococcus*. Mol. Microbiol. **7:**893-903.
120. **Horton, R. M.** 1995. PCR-mediated recombination and mutagenesis. SOEing together tailor-made genes. Mol. Biotechnol. **3:**93-99.
121. **Chaffin, D. O., S. B. Beres, H. H. Yim, and C. E. Rubens.** 2000. The serotype of type Ia and III group B streptococci is determined by the polymerase gene within the polycistronic capsule operon. J. Bacteriol. **182:**4466-4477.
122. **Rajagopal, L., A. Clancy, and C. E. Rubens.** 2003. A eukaryotic type serine/threonine kinase and phosphatase in *Streptococcus agalactiae* reversibly phosphorylate an inorganic pyrophosphatase and affect growth, cell segregation, and virulence. J. Biol. Chem. **278:**14429-14441.
123. **Chaffin, D. O., and C. E. Rubens.** 1998. Blue/white screening of recombinant plasmids in Gram-positive bacteria by interruption of alkaline phosphatase gene (phoZ) expression. Gene **219:**91-99.
124. **Sun, K., R. Ma, X. Cui, B. Campos, R. Webster, D. Brockman, and L. Myatt.** 2003. Glucocorticoids induce cytosolic phospholipase A2 and prostaglandin H synthase type 2 but not microsomal prostaglandin E synthase (PGES) and cytosolic PGES expression in cultured primary human amnion cells. J. Clin. Endocrinol. Metab. **88:**5564-5571.
125. **Giaever, I., and C. R. Keese.** 1991. Micromotion of mammalian cells measured electrically. Proc. Natl. Acad. Sci. U. S. A. **88:**7896-7900.

126. **Matorras, R., A. Garcia Perea, F. Omenaca, J. A. Usandizaga, A. Nieto, and R. Herruzo.** 1989. Group B *streptococcus* and premature rupture of membranes and preterm delivery. Gynecol. Obstet. Invest. **27:**14-18.
127. **Fettucciari, K., I. Fetriconi, R. Mannucci, I. Nicoletti, A. Bartoli, S. Coaccioli, and P. Marconi.** 2006. Group B *Streptococcus* induces macrophage apoptosis by calpain activation. J. Immunol. **176:**7542-7556.
128. **Sendi, P., L. Johansson, S. Dahesh, N. M. Van-Sorge, J. Darenberg, M. Norgren, J. Sjolin, V. Nizet, and A. Norrby-Teglund.** 2009. Bacterial phenotype variants in group B streptococcal toxic shock syndrome. Emerg. Infect. Dis. **15:**223-232.
129. **Whidbey, C., M. I. Harrell, K. Burnside, L. Ngo, A. K. Becraft, L. M. Iyer, L. Aravind, J. Hitti, K. M. Waldorf, and L. Rajagopal.** 2013. A hemolytic pigment of Group B *Streptococcus* allows bacterial penetration of human placenta. J. Exp. Med. **210:**1265-1281.
130. **Equils, O., C. Moffatt-Blue, T. O. Ishikawa, C. F. Simmons, V. Ilievski, and E. Hirsch.** 2009. Pretreatment with pancaspase inhibitor (Z-VAD-FMK) delays but does not prevent intraperitoneal heat-killed group B *Streptococcus*-induced preterm delivery in a pregnant mouse model. Infect. Dis. Obstet. Gynecol. **2009:**749432.
131. **Elovitz, M. A., and C. Mrinalini.** 2004. Animal models of preterm birth. Trends Endocrinol Metab **15:**479-487.
132. **Vanderhoeven, J. P., C. J. Bierle, R. P. Kapur, R. M. McAdams, R. P. Beyer, T. K. Bammler, F. M. Farin, A. Bansal, M. Spencer, M. Deng, M. G. Gravett, C. E. Rubens, L. Rajagopal, and K. M. Adams Waldorf.** 2014. Group B streptococcal infection of the choriodecidua induces dysfunction of the cytokeratin network in amniotic epithelium: a pathway to membrane weakening. PLoS Pathog **10:**e1003920.
133. **Gupta, R., S. Ghosh, B. Monks, R. Deoliveira, T. Tzeng, P. Kalantari, A. Nandy, B. Bhattacharjee, J. Chan, F. Ferreira, V. Rathinam, S. Sharma, E. Lien, N. Silverman, K. Fitzgerald, A. Firon, P. Trieu-Cuot, P. Henneke, and D. Golenbock.** 2014. RNA and beta-hemolysin of Group B *streptococcus* induce IL-1beta by activating NLRP3 inflammasomes in mouse macrophages. J. Biol. Chem.
134. **Butler, T. Z., M. Pavlenok, I. M. Derrington, M. Niederweis, and J. H. Gundlach.** 2008. Single-molecule DNA detection with an engineered MspA protein nanopore. Proc. Natl. Acad. Sci. U. S. A. **105:**20647-20652.
135. **Keyel, P. A., L. Loultcheva, R. Roth, R. D. Salter, S. C. Watkins, W. M. Yokoyama, and J. E. Heuser.** 2011. Streptolysin O clearance through sequestration into blebs that bud passively from the plasma membrane. J. Cell Sci. **124:**2414-2423.
136. **Taxman, D. J., M. T. Huang, and J. P. Ting.** 2010. Inflammasome inhibition as a pathogenic stealth mechanism. Cell Host Microbe **8:**7-11.
137. **Willingham, S. B., D. T. Bergstralh, W. O'Connor, A. C. Morrison, D. J. Taxman, J. A. Duncan, S. Barnoy, M. M. Venkatesan, R. A. Flavell, M. Deshmukh, H. M. Hoffman, and J. P. Ting.** 2007. Microbial pathogen-induced necrotic cell death mediated by the inflammasome components CIAS1/cryopyrin/NLRP3 and ASC. Cell Host Microbe **2:**147-159.
138. **McNeela, E. A., A. Burke, D. R. Neill, C. Baxter, V. E. Fernandes, D. Ferreira, S. Smeaton, R. El-Rachkidy, R. M. McLoughlin, A. Mori, B. Moran, K. A. Fitzgerald,**

J. Tschopp, V. Petrilli, P. W. Andrew, A. Kadioglu, and E. C. Lavelle. 2010. Pneumolysin activates the NLRP3 inflammasome and promotes proinflammatory cytokines independently of TLR4. PLoS Pathog **6:**e1001191.

139. **Munoz-Planillo, R., P. Kuffa, G. Martinez-Colon, B. L. Smith, T. M. Rajendiran, and G. Nunez.** 2013. K(+) efflux is the common trigger of NLRP3 inflammasome activation by bacterial toxins and particulate matter. Immunity **38:**1142-1153.
140. **Davis, B. K., H. Wen, and J. P. Ting.** 2011. The inflammasome NLRs in immunity, inflammation, and associated diseases. Annu. Rev. Immunol. **29:**707-735.
141. **LaRock, C. N., and B. T. Cookson.** 2013. Burning down the house: cellular actions during pyroptosis. PLoS Pathog **9:**e1003793.
142. **Elovitz, M. A., Z. Wang, E. K. Chien, D. F. Rychlik, and M. Phillippe.** 2003. A new model for inflammation-induced preterm birth: the role of platelet-activating factor and Toll-like receptor-4. Am. J. Pathol. **163:**2103-2111.
143. **Hirsch, E., I. Saotome, and D. Hirsh.** 1995. A model of intrauterine infection and preterm delivery in mice. Am. J. Obstet. Gynecol. **172:**1598-1603.
144. **Sitkiewicz, I., N. M. Green, N. Guo, A. M. Bongiovanni, S. S. Witkin, and J. M. Musser.** 2009. Transcriptome adaptation of group B *Streptococcus* to growth in human amniotic fluid. PLoS ONE **4:**e6114.
145. **Brydges, S. D., J. L. Mueller, M. D. McGeough, C. A. Pena, A. Misaghi, C. Gandhi, C. D. Putnam, D. L. Boyle, G. S. Firestein, A. A. Horner, P. Soroosh, W. T. Watford, J. J. O'Shea, D. L. Kastner, and H. M. Hoffman.** 2009. Inflammasome-mediated disease animal models reveal roles for innate but not adaptive immunity. Immunity **30:**875-887.
146. **Kovarova, M., P. R. Hesker, L. Jania, M. Nguyen, J. N. Snouwaert, Z. Xiang, S. E. Lommatzsch, M. T. Huang, J. P. Ting, and B. H. Koller.** 2012. NLRP1-dependent pyroptosis leads to acute lung injury and morbidity in mice. J. Immunol. **189:**2006-2016.
147. **Brown, J. H.** 1920. The Cultural Differentiation of Beta Hemolytic Streptococci of Human and Bovine Origin. J. Exp. Med. **31:**35-47.
148. **Semrau, S., M. W. Monster, M. van der Knaap, B. I. Florea, T. Schmidt, and M. Overhand.** 2010. Membrane lysis by gramicidin S visualized in red blood cells and giant vesicles. Biochim. Biophys. Acta **1798:**2033-2039.
149. **Schrodinger, LLC.** 2010. The PyMOL Molecular Graphics System, Version 1.3r1.
150. **Henneke, P., and R. Berner.** 2006. Interaction of neonatal phagocytes with group B *streptococcus*: recognition and response. Infect. Immun. **74:**3085-3095.
151. **Furtig, B., C. Richter, J. Wohnert, and H. Schwalbe.** 2003. NMR spectroscopy of RNA. Chembiochem **4:**936-962.
152. **Jaiswal, M. K., V. Agrawal, T. Mallers, A. Gilman-Sachs, E. Hirsch, and K. D. Beaman.** 2013. Regulation of apoptosis and innate immune stimuli in inflammation-induced preterm labor. J. Immunol. **191:**5702-5713.
153. **Flores-Herrera, H., G. Garcia-Lopez, N. F. Diaz, A. Molina-Hernandez, M. Osorio-Caballero, D. Soriano-Becerril, and V. Zaga-Clavellina.** 2012. An experimental mixed bacterial infection induced differential secretion of proinflammatory cytokines (IL-1beta, TNFalpha) and proMMP-9 in human fetal membranes. Placenta **33:**271-277.

154. **Robertson, S. A., R. J. Skinner, and A. S. Care.** 2006. Essential role for IL-10 in resistance to lipopolysaccharide-induced preterm labor in mice. J. Immunol. **177:**4888-4896.
155. **Breen, K., A. Brown, I. Burd, J. Chai, A. Friedman, and M. A. Elovitz.** 2012. TLR-4-dependent and -independent mechanisms of fetal brain injury in the setting of preterm birth. Reprod Sci **19:**839-850.
156. **Filipovich, Y., S. J. Lu, S. Akira, and E. Hirsch.** 2009. The adaptor protein MyD88 is essential for *E coli*-induced preterm delivery in mice. Am. J. Obstet. Gynecol. **200:**93 e91-98.
157. **Kallapur, S. G., P. Presicce, P. Senthamaraikannan, M. Alvarez, A. F. Tarantal, L. M. Miller, A. H. Jobe, and C. A. Chougnet.** 2013. Intra-amniotic IL-1beta induces fetal inflammation in rhesus monkeys and alters the regulatory T cell/IL-17 balance. J. Immunol. **191:**1102-1109.
158. **Randis, T. M., S. E. Gelber, T. A. Hooven, R. G. Abellar, L. H. Akabas, E. L. Lewis, L. B. Walker, L. M. Byland, V. Nizet, and A. J. Ratner.** 2014. Group B *Streptococcus* beta-hemolysin/cytolysin breaches maternal-fetal barriers to cause preterm birth and intrauterine fetal demise in vivo. J. Infect. Dis.
159. **Zulianello, L., C. Canard, T. Kohler, D. Caille, J. S. Lacroix, and P. Meda.** 2006. Rhamnolipids are virulence factors that promote early infiltration of primary human airway epithelia by *Pseudomonas aeruginosa*. Infect. Immun. **74:**3134-3147.
160. **Kebaier, C., R. R. Chamberland, I. C. Allen, X. Gao, P. M. Broglie, J. D. Hall, C. Jania, C. M. Doerschuk, S. L. Tilley, and J. A. Duncan.** 2012. *Staphylococcus aureus* alpha-hemolysin mediates virulence in a murine model of severe pneumonia through activation of the NLRP3 inflammasome. J. Infect. Dis. **205:**807-817.
161. **Kuga, S.** 1981. Pore size distribution of gel substances by size exclusion chromatography. J. Chromatogr. **206:**449-461.
162. **Hornung, V., F. Bauernfeind, A. Halle, E. O. Samstad, H. Kono, K. L. Rock, K. A. Fitzgerald, and E. Latz.** 2008. Silica crystals and aluminum salts activate the NALP3 inflammasome through phagosomal destabilization. Nat Immunol **9:**847-856.
163. **Holzinger, D., L. Gieldon, V. Mysore, N. Nippe, D. J. Taxman, J. A. Duncan, P. M. Broglie, K. Marketon, J. Austermann, T. Vogl, D. Foell, S. Niemann, G. Peters, J. Roth, and B. Loffler.** 2012. *Staphylococcus aureus* Panton-Valentine leukocidin induces an inflammatory response in human phagocytes via the NLRP3 inflammasome. J. Leukoc. Biol. **92:**1069-1081.
164. **Sokurenko, E. V., R. Gomulkiewicz, and D. E. Dykhuizen.** 2006. Source-sink dynamics of virulence evolution. Nat Rev Microbiol **4:**548-555.
165. **Hansen, S. M., N. Uldbjerg, M. Kilian, and U. B. Sorensen.** 2004. Dynamics of *Streptococcus agalactiae* colonization in women during and after pregnancy and in their infants. J. Clin. Microbiol. **42:**83-89.
166. **Kwatra, G., P. V. Adrian, T. Shiri, E. J. Buchmann, C. L. Cutland, and S. A. Madhi.** 2014. Serotype-specific acquisition and loss of group B *streptococcus* recto-vaginal colonization in late pregnancy. PLoS ONE **9:**e98778.

167. **Foxman, B., B. W. Gillespie, S. D. Manning, and C. F. Marrs.** 2007. Risk factors for group B streptococcal colonization: potential for different transmission systems by capsular type. Ann. Epidemiol. **17:**854-862.
168. **Rasko, D. A., and V. Sperandio.** 2010. Anti-virulence strategies to combat bacteria-mediated disease. Nat Rev Drug Discov **9:**117-128.
169. **Allen, R. C., R. Popat, S. P. Diggle, and S. P. Brown.** 2014. Targeting virulence: can we make evolution-proof drugs? Nat Rev Microbiol **12:**300-308.
170. **Brown, S. P., D. M. Cornforth, and N. Mideo.** 2012. Evolution of virulence in opportunistic pathogens: generalism, plasticity, and control. Trends Microbiol. **20:**336-342.
171. **Zhang, Y. M., S. W. White, and C. O. Rock.** 2006. Inhibiting bacterial fatty acid synthesis. J. Biol. Chem. **281:**17541-17544.
172. **Brinster, S., G. Lamberet, B. Staels, P. Trieu-Cuot, A. Gruss, and C. Poyart.** 2009. Type II fatty acid synthesis is not a suitable antibiotic target for Gram-positive pathogens. Nature **458:**83-86.
173. **Maisey, H. C., K. S. Doran, and V. Nizet.** 2008. Recent advances in understanding the molecular basis of group B *Streptococcus* virulence. Expert Rev Mol Med **10:**e27.
174. **Broz, P., and D. M. Monack.** 2011. Molecular mechanisms of inflammasome activation during microbial infections. Immunol. Rev. **243:**174-190.
175. **Wen, H., E. A. Miao, and J. P. Ting.** 2013. Mechanisms of NOD-like receptor-associated inflammasome activation. Immunity **39:**432-441.
176. **Zhou, R., A. S. Yazdi, P. Menu, and J. Tschopp.** 2011. A role for mitochondria in NLRP3 inflammasome activation. Nature **469:**221-225.
177. **Subramanian, N., K. Natarajan, M. R. Clatworthy, Z. Wang, and R. N. Germain.** 2013. The adaptor MAVS promotes NLRP3 mitochondrial localization and inflammasome activation. Cell **153:**348-361.
178. **Bergsbaken, T., S. L. Fink, and B. T. Cookson.** 2009. Pyroptosis: host cell death and inflammation. Nat Rev Microbiol **7:**99-109.
179. **Reiss, A., J. S. Braun, K. Jager, D. Freyer, G. Laube, C. Buhrer, U. Felderhoff-Muser, C. Stadelmann, V. Nizet, and J. R. Weber.** 2011. Bacterial pore-forming cytolysins induce neuronal damage in a rat model of neonatal meningitis. J. Infect. Dis. **203:**393-400.
180. **Ting, J. P., S. B. Willingham, and D. T. Bergstralh.** 2008. NLRs at the intersection of cell death and immunity. Nat Rev Immunol **8:**372-379.
181. **Galluzzi, L., I. Vitale, J. M. Abrams, E. S. Alnemri, E. H. Baehrecke, M. V. Blagosklonny, T. M. Dawson, V. L. Dawson, W. S. El-Deiry, S. Fulda, E. Gottlieb, D. R. Green, M. O. Hengartner, O. Kepp, R. A. Knight, S. Kumar, S. A. Lipton, X. Lu, F. Madeo, W. Malorni, P. Mehlen, G. Nunez, M. E. Peter, M. Piacentini, D. C. Rubinsztein, Y. Shi, H. U. Simon, P. Vandenabeele, E. White, J. Yuan, B. Zhivotovsky, G. Melino, and G. Kroemer.** 2012. Molecular definitions of cell death subroutines: recommendations of the Nomenclature Committee on Cell Death 2012. Cell Death Differ. **19:**107-120.
182. **Brennan, M. A., and B. T. Cookson.** 2000. *Salmonella* induces macrophage death by caspase-1-dependent necrosis. Mol. Microbiol. **38:**31-40.

183. **Kroemer, G., L. Galluzzi, P. Vandenabeele, J. Abrams, E. S. Alnemri, E. H. Baehrecke, M. V. Blagosklonny, W. S. El-Deiry, P. Golstein, D. R. Green, M. Hengartner, R. A. Knight, S. Kumar, S. A. Lipton, W. Malorni, G. Nunez, M. E. Peter, J. Tschopp, J. Yuan, M. Piacentini, B. Zhivotovsky, and G. Melino.** 2009. Classification of cell death: recommendations of the Nomenclature Committee on Cell Death 2009. Cell Death Differ. **16:**3-11.
184. **Draper, D. W., H. N. Bethea, and Y. W. He.** 2006. Toll-like receptor 2-dependent and -independent activation of macrophages by group B streptococci. Immunol. Lett. **102:**202-214.
185. **Charrel-Dennis, M., E. Latz, K. A. Halmen, P. Trieu-Cuot, K. A. Fitzgerald, D. L. Kasper, and D. T. Golenbock.** 2008. TLR-independent type I interferon induction in response to an extracellular bacterial pathogen via intracellular recognition of its DNA. Cell Host Microbe **4:**543-554.
186. **Henneke, P., O. Takeuchi, J. A. van Strijp, H. K. Guttormsen, J. A. Smith, A. B. Schromm, T. A. Espevik, S. Akira, V. Nizet, D. L. Kasper, and D. T. Golenbock.** 2001. Novel engagement of CD14 and multiple toll-like receptors by group B streptococci. J. Immunol. **167:**7069-7076.
187. **Gotsch, F., R. Romero, T. Chaiworapongsa, O. Erez, E. Vaisbuch, J. Espinoza, J. P. Kusanovic, P. Mittal, S. Mazaki-Tovi, C. J. Kim, J. S. Kim, S. Edwin, C. L. Nhan-Chang, N. Hamill, L. Friel, N. G. Than, M. Mazor, B. H. Yoon, and S. S. Hassan.** 2008. Evidence of the involvement of caspase-1 under physiologic and pathologic cellular stress during human pregnancy: a link between the inflammasome and parturition. J Matern Fetal Neonatal Med **21:**605-616.
188. **Lappas, M.** 2014. Caspase-1 activation is increased with human labour in foetal membranes and myometrium and mediates infection-induced interleukin-1beta secretion. Am. J. Reprod. Immunol. **71:**189-201.
189. **Baker, C. J., V. J. Carey, M. A. Rench, M. S. Edwards, S. L. Hillier, D. L. Kasper, and R. Platt.** 2014. Maternal antibody at delivery protects neonates from early onset group B streptococcal disease. J. Infect. Dis. **209:**781-788.
190. **Meehan, M., R. Cunney, and M. Cafferkey.** 2014. Molecular epidemiology of group B streptococci in Ireland reveals a diverse population with evidence of capsular switching. Eur. J. Clin. Microbiol. Infect. Dis. **33:**1155-1162.
191. **Tan, T. Q.** 2012. Pediatric invasive pneumococcal disease in the United States in the era of pneumococcal conjugate vaccines. Clin. Microbiol. Rev. **25:**409-419.
192. **Keller-Stanislawski, B., J. A. Englund, G. Kang, P. Mangtani, K. Neuzil, H. Nohynek, R. Pless, P. Lambach, and P. Zuber.** 2014. Safety of immunization during pregnancy: A review of the evidence of selected inactivated and live attenuated vaccines. Vaccine **32:**7057-7064.
193. **Walker-Caprioglio, H. M., J. M. MacKenzie, and L. W. Parks.** 1989. Antibodies to nystatin demonstrate polyene sterol specificity and allow immunolabeling of sterols in Saccharomyces cerevisiae. Antimicrob. Agents Chemother. **33:**2092-2095.
194. **Matyas, G. R., N. M. Wassef, M. Rao, and C. R. Alving.** 2000. Induction and detection of antibodies to squalene. J. Immunol. Methods **245:**1-14.